

# EPSC2018

## **OPS3 abstracts**

## Observing the Potential for a Diversity of Metabolic Pathways in the Ocean of Enceladus

**J. Hunter Waite** (1), Christine Ray (2,1), Chris Glein (1), Sascha Kempf (3), Frank Postberg (4,5) and Jonathan Lunine (6)

(1) Southwest Research Institute, San Antonio, USA ([hwaite@swri.edu](mailto:hwaite@swri.edu)), (2) The University of Texas at San Antonio, San Antonio, USA ([christine.ray@swri.org](mailto:christine.ray@swri.org)), (3) Laboratory for Atmospheric and Space Physics, Boulder, USA ([sascha.kempf@colorado.edu](mailto:sascha.kempf@colorado.edu)), (4) Institut für Geowissenschaften, Heidelberg, Germany ([frank.postberg@geow.uni-heidelberg.de](mailto:frank.postberg@geow.uni-heidelberg.de)), (5) Klaus-Tschira-Labor für Kosmochemie, Heidelberg, Germany ([frank.postberg@geow.uni-heidelberg.de](mailto:frank.postberg@geow.uni-heidelberg.de)), (6) Department of Astronomy and Carl Sagan Institute, Ithaca, USA ([jlunine@astro.cornell.edu](mailto:jlunine@astro.cornell.edu))

### Abstract

The Cassini Ion Neutral Mass Spectrometer (INMS) and the Cosmic Dust Analyzer (CDA) revealed a salty ocean<sup>a</sup> environment at Enceladus with a pH of  $\sim 9^{b,a}$  and an abundance of molecular hydrogen<sup>c</sup> in the ocean to support a methanogenic metabolism. The measurements also suggested that the ocean may be fed by extant hydrothermal systems found at the interior rocky interface with the ocean<sup>c,d</sup>. These environmental attributes suggest that the interior ocean of Enceladus is habitable. However, methanogenesis is not the only possible metabolism in this environment. Oxidants produced on the ice surface layer by electron bombardment can penetrate the ice layer and produce additional oxidized species that may well support alternative metabolic pathways<sup>e</sup>. In this presentation we review the observations provided by Cassini INMS and CDA in terms of metabolic pathways at Enceladus, and we explore measurements that might be provided by a future mission to Enceladus that would revolutionize our knowledge of potential metabolic pathways in the interior ocean of Enceladus.

### References

- <sup>a</sup> Postberg, F., Schmidt, J., Hillier, J., Kempf, S., Srama, R., Nature 474, 620–622, 2011.
- <sup>b</sup> Glein, C., Baross, J., Waite Jr., J., Geochim. Cosmochim. Acta 162, 202–219, 2015.
- <sup>c</sup> Waite et al., Science 356, 155–159, 2017.
- <sup>d</sup> Hsu, H-W. et al., Nature 519, 207–210 2015.
- <sup>e</sup> Ray et al., Abstract submitted to this session, 2018.

# Dehydration kinetics of hydrohalite under UV irradiation

**Bernhard Jost**, Robert Hodyss and Paul V. Johnson

Jet Propulsion Laboratory, California Institute of Technology, USA (bernhard.jost@jpl.nasa.gov)

## Abstract

We will present first results of a study characterizing the dehydration rate of fine grained hydrohalite as a function of temperature under UV irradiation. These results will help to infer the surface history of Europa by comparing remote sensing data from future Europa Clipper instruments to a systematic catalog of laboratory analogs.

## 1. Introduction

The investigation of ocean materials expressed on the surface of airless icy bodies, such as Europa or Enceladus, when exposed to surface temperature, vacuum, photolysis and radiolysis may bring light in the understanding of subsurface processes and corresponding timescales.

Hydrated salt minerals are one species of surface materials found by former space instruments. We selected hydrohalite as candidate material for systematic dehydration studies since it is the only stable hydration state of sodium chloride under Europa conditions compared to other materials which have numerous stable hydration states.

This work will provide the means to interpret the data acquired by future missions to icy worlds such as Europa Clipper and JUICE. Sodium chloride on Europa's surface may be directly and unambiguously identified if the characteristic spectral features of hydrohalite are observed because the spectrum of anhydrous NaCl is flat and indistinct [1] If features of hydrohalite are found they would indicate a relatively young terrain.

## 2. Methods

To analyze the hydration state of hydrohalite samples we use a combination of two different, but complementary techniques: 1. Passive near-infrared reflectance spectroscopy in the 1.4-7.0 $\mu$ m spectral

range (Thermo Nicolet 6700 FTIR; Pike Tech DiffusIR) 2. Raman spectroscopy (Horiba Jobin-Yvon LabRam HR). The sample is irradiated using a krypton arc lamp primarily emitting at 116.5 and 123.6nm, however the 116.5nm line is cutoff by the MgF<sub>2</sub> window.

## 3. Sample material

Hydrohalite forms in saturated NaCl solution below 268K. To ensure reproducible samples and particle size distribution we adapted a sample production protocol developed at Technical University of Braunschweig [2] and previously used for photometric studies [3]. A PARI Vios PRO Nebulizer System for medical applications is used to spray a saturated brine directly in liquid nitrogen using a 3bar compressor. The resulting particle radii were measured as 1.47+0.96-0.58 $\mu$ m [3].

## 4. Expected results

It is expected that lower temperatures will slow down the chemical reaction rates. The NIR-spectrum of water ice is known to be very sensitive to particles size, where smaller grains show more pronounced absorption features but are more reflective on inter-bands.

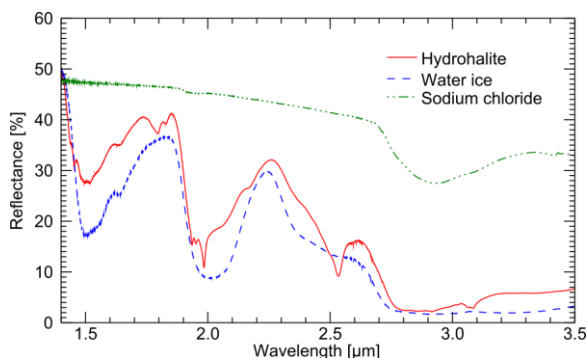


Figure 1: Preliminary NIR-spectra of hydrohalite, sodium chloride and water ice, all samples were crushed by a mortar and sieved with a 200 $\mu$ m mesh size.

It has to be investigated how particle-sintering at higher temperatures, where the total surface area is decreased, which should decrease reaction rates, influences the dehydration kinetics. This could potentially lead to non-linear effects.

## Acknowledgements

This research was carried out at the Jet Propulsion Laboratory, California Institute of Technology, under a contract with the National Aeronautics and Space Administration (NASA). Bernhard Jost is founded by the NASA Postdoctoral Program Administered by the Universities Space Research Association (USRA)

## References

- [1] Thomas, E. C., Hodyss, R., Vu, T. H., Johnson, P. V., Choukroun, M. Composition and Evolution of Frozen Chloride Brines under the Surface Conditions of Europa, *Earth and Space Chemistry*, 2017.
- [2] Gundlach, B., Kilius, S., Beitz, E., Blum, J.: Micrometer-sized ice particles for planetary-science experiments – 1. Preparation, critical rolling friction force, and specific surface energy. *Icarus* 214, p. 717-723, 2011.
- [3] Jost, B., Gundlach, B., Pommerol, A., Oesert, J., Gorb, S.N., Blum, J., Thomas, N.: Micrometer-sized ice particles for planetary-science experiments - II Bidirectional reflectance. *Icarus* 225, p. 352-366, 2013.



# Polarimetry of water ice particles providing insights on grain size and degree of sintering on icy planetary surfaces

R. Cerubini (1), O. Poch (2) A. Pommerol (1), H. M. Schmid (3), B. Jost (4), Y. Brouet (1), N. Thomas (1)

(1) Physikalisches Institut, University of Bern, Switzerland. ([romain.cerubini@space.unibe.ch](mailto:romain.cerubini@space.unibe.ch))

(2) Univ. Grenoble Alpes, CNRS, CNES, IPAG, 38000 Grenoble France

(3) NCCR PlanetS, Institute for Astronomy, ETH Zurich, Switzerland

(4) NASA JPL, 4800 Oak Grove Drive, Pasadena, CA 91109, USA

## 1. Context

The polarimetry of the light scattered by planetary surfaces is a powerful tool to complement observations performed in total light intensity, such as reflectance studies, providing additional constraints to interpret remote sensing observations of bodies in the Solar System and beyond [1]. For atmosphereless bodies, the unpolarized sunlight acquires its polarization when scattered by the first micrometer of their surfaces. The degree of polarization of the scattered light is particularly sensitive to the morphology (eg. size, shape, structure) and the chemistry (eg. composition, mixture) of the grains constituting the surface.

The fine characterization of the surface of icy bodies such as the Galilean moons (Europa, Ganymede and Callisto) is of major interest for future ESA (JUICE) and NASA (Europa Clipper) missions. Ground-based polarimetric observations of the icy satellites, conducted since many years [2, 3], provide a very precious dataset to prepare and complement the observations of these future missions. However, the interpretation of these polarimetric data is made difficult by the lack of good reference measurements, especially on surfaces made of ice. It is thus essential to build a database of polarimetric data on well-characterized samples of ice measured in the laboratory.

For this purpose, we have developed the POLarimeter for ICE Samples (POLICES) at the University of Bern, allowing measurement of the degree of polarization of the light scattered by surfaces in the visible range of wavelength (400 to 800 nm) and for  $1.5^\circ$  to  $30^\circ$  of phase angle. The setup uses a high precision photomultiplier tube coupled with two Photoelastics modulators (PEM) (Hinds Instruments) to measures the Q, U and V Stoke's parameters to describe the polarization of the scattered light.

## 2. Measurements and first results

We have prepared in the laboratory several surfaces made of pure water ice particles having well-controlled size and shape. We have measured the polarimetric phase curves of these surfaces and their temporal evolution, as the ice sinters. We noticed that the amplitude and the shape of the polarimetric phase curves are extremely dependent on the particles sizes and the degree of metamorphism of the ice.

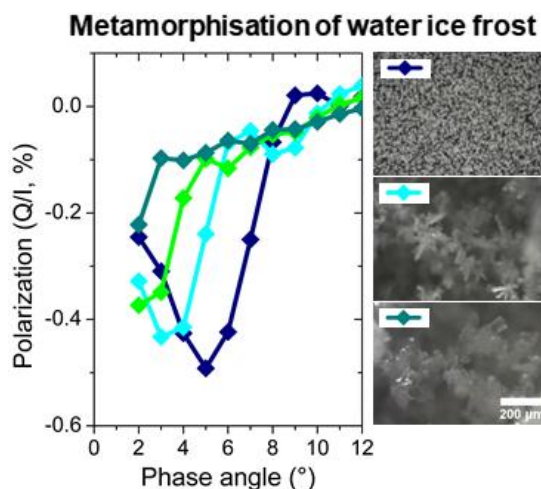


Figure 1: Polarimetric phase curves of an icy surface covered by frost growing and metamorphosing with time.

As an example, Figure 1 shows the phase curves measured during the nucleation, growth and metamorphism of water ice frost. Polarimetric phase curves of fresh frost nuclei exhibit strong oscillations typical of the Mie scattering by micrometric spherical particles (glory effect) [4]. As the spheres grow and the frost forms spikes and dendrites, the glory shifts to smaller phase angles. After few minutes, the frost evolves toward coarser irregular grains, leading to

flatter phase curves and lower absolute degree of polarization.

We observed this significant change of the phase curve with time due to thermal sintering for all our ice samples. Sintering, which is driven by the reduction of the total surface energy of the system, acts more rapidly on smaller particles [6]. This phenomenon modifies the shape of particles by making bridges between them, modifying the way the light is scattered and therefore changing the polarization of the surface.

We have also measured well-controlled larger ice grains of  $70 \pm 30 \mu\text{m}$ , characterized by shallower negative branch of polarization than fresh frost nuclei which do not exceed  $10 \mu\text{m}$  large (Fig.2).

Figure 2 shows a comparison of some of our laboratory measurements with average disk-integrated polarimetric phase curves of icy satellites. These data suggest that the surface of Europa is covered by relatively coarser grains ( $\sim 40\text{--}400 \mu\text{m}$ ) than those of the surfaces of Enceladus, Rhea or the trailing hemisphere of Iapetus. These surfaces are more consistent with finer frost. We note that these conclusions, obtained from polarimetric data in the visible domain, are in line with those obtained from mid-infrared spectroscopy [6, 7].

**Polarimetric phase curves of icy satellites**

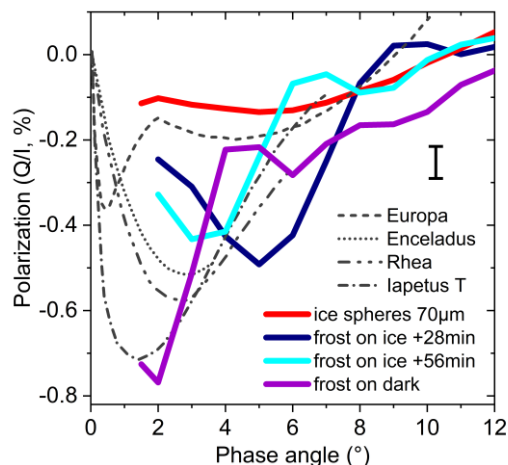


Figure 2: Comparison of our laboratory measurements [5] with disk-integrated polarimetric observations of icy satellites [3]

### 3. Summary and Perspectives

These measurements demonstrate the high sensitivity of polarization to the grain size and degree of sintering of ice particles. Therefore, polarimetry could be used to detect hints of ongoing processes on icy planetary surfaces, such as cryovolcanism or sputtering, producing coarse (via warming) or fine (fresh) ice grains. These first results open the way to further measurements with ice particles containing chemical impurities. We foresee to extend the measurements to icy mixtures consisting of water ice and colored chemical compound, such as sulphur, in order to investigate their polarimetric signal and constrain their possible identification by ground-based polarimetry observations of Europa's surface. The presence of salts could also influence the polarization of the light by modifying the morphology of the ice grains as well as its color.

### Acknowledgements

The team from the University of Bern is supported by the Swiss National National Science Foundation and through the NCCR PlanetS. Poch, O. acknowledges a postdoctoral research fellowship from CNES.

### References

- [1] Kolokolova, L., Hough, J., Levasseur-Regourd, A-C., (2015), *Polarimetry of stars and planetary systems*, Cambridge University Press.
- [2] Kiselev, N., et al., (2009). Polarimetry of the Galilean satellites and Jupiter near opposition. *Journal of Quantitative Spectroscopy and Radiative Transfer*, 110, 1713–1718
- [3] Rosenbush, V., Kiselev, N., Afanasiev, V., (2015). Icy moons of the outer planets. *Polarimetry of Stars and Planetary Systems*, 340.
- [4] Jost, B., et al., (2016), Experimental Characterization of the opposition surge in fine-grained water-ice and high albedo ice analogs, *Icarus* 264, 109–131
- [5] Poch, O., (2018) *Article in prep.*
- [6] Ligier, N., et al., (2016), VLT/SINFONI Observations of Europa: New insights into the surface composition, *The Astronomical Journal*, 151-153
- [7] Jaumann, R., et al., (2008), Distribution of icy particles across Enceladus' surface as derived from Cassini-VIMS measurements, *Icarus* 193, 407-419

# Laboratory reflectance measurements of water ice/salt mixture irradiated by electrons

**R. Cerubini** (1), A. Pommerol (1), A. Galli (1), Z. Yoldi (1), O. Poch (2), A. Oza (1), P. Wurz (1), N. Thomas (1),  
(1) Physikalisches Institut, University of Bern, Switzerland. ([romain.cerubini@space.unibe.ch](mailto:romain.cerubini@space.unibe.ch))  
(2) Univ. Grenoble Alpes, CNRS, CNES, IPAG, 38000 Grenoble France

## 1. Context

The Near Infrared Mapping Spectrometer (NIMS) observed Galilean moons during the Galileo mission in the nineties. Reflectance measurements revealed strong signatures of water ice almost everywhere at the surface of three of the four Galilean moons of Jupiter. The resolution of these data is sufficient to detect as well the presence of non-water ice components mostly present for example on the trailing side of Europa, or more homogeneously distributed at the surface of Ganymede. For several decades now, the exact nature of the compounds has remained unclear and is still a subject of debates in the scientific community. The non-ice components seem highly hydrated and probably contain sulphurs and chlorides [1-3].

In the case of Europa, several species in addition to water ice are proposed, such as magnesium salt epsomite ( $\text{MgSO}_4 \cdot 7\text{H}_2\text{O}$ ) or higher hydrated states, hydrated forms of sulphuric acid ( $\text{H}_2\text{SO}_4 \cdot n\text{H}_2\text{O}$ ) or sodium chloride ( $\text{NaCl}$ ). These salts are subject to intense irradiation by the electrons and ions from Jupiter's magnetosphere [4]. These irradiation processes have already been proposed as inputs for the sulphur exogenous component of Europa [5]. They also induce chemical reactions in the ice and eject particles via sputtering, thus creating the neutral atmosphere of Europa [6]. The non-icy compounds present at the surface of Europa could differ from those at Ganymede or Callisto because the plasma flux precipitating onto the surface decreases with distance from Io [7]. Moreover, the intrinsic magnetic field of Ganymede modifies the spatial distribution of energetic particles than can reach its surface.

The MEFISTO facility at the University of Bern contains a vacuum chamber where icy surfaces can be irradiated with ions and electrons [as described by 9]. To complement this facility, a VIS-NIR

hyperspectral imaging system developed by the Planetary Imaging Group (PIG) was adapted to the chamber. It consists of two cameras (visible and infrared) taking pictures of an illuminated sample. The light sent onto the sample through an optic fibre is spectrally selected by a monochromator ranging from 0.38 to 2.4 micrometres. Hyperspectral cubes are acquired by recording images at different wavelengths. Averaged reflectance spectra are then obtained by defining Regions of Interest (ROIs) in the cubes and averaging the signal inside.

## 2. Measurements and first results

Here we present results of irradiation of pure and salty water ices (produced by our Setup for Production of Icy Planetary Analogs, SPIPA) by electrons at energies of 0.5 eV to 5 keV and currents from 0.5 to 5  $\mu\text{A}$ . The purposes of these measurement were *i*) to know if we can detect a modification of temperature related to electron irradiations and *ii*) to extend the understanding of the process of coloration which happens during irradiation of salty ices. This irradiation has been done previously on  $\text{NaCl}$  by others [1, 10], with different energies and with UV irradiation, to mimic and explain the colored double/triple bands at the surface of Europa.

We observed the appearance of dark spots at the surface of the salty samples irradiated by electrons. The reflectance of these spots exhibits the F (460nm) and M (705nm) centers coloration of the  $\text{NaCl}$  crystal reacting to electron irradiation. The disorder induced by electrons perturbing manifests itself by visible coloration. This effect was already observed by Hand and Carlson (2015) [11] for higher energies (10keV), suggesting also the reversibility of this phenomena for lower energies (see fig.1 the difference between “fresh” and “old” samples).

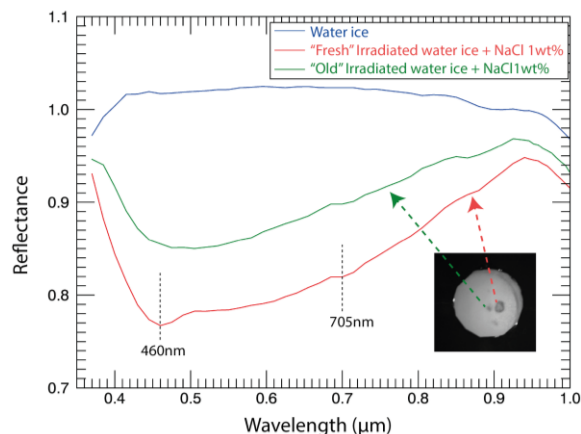


Figure 1: Reflectance measurements of pure water ice and irradiated mixture of water ice + 1 wt% of NaCl. The irradiation was stopped on the “old” spot almost 1 hour before the measurements of the “fresh” spot.

We manually modified the temperature of the sample and recorded the reflectance (figure2). The depth of the absorption band at  $1.65\mu\text{m}$  is highly sensitive to the temperature of the few uppermost micrometres of the sample surface, as it has already been demonstrated by Grundy et al., [12, 13]. Since it is complicated to make a direct measurement of the surface temperature of an icy sample, the possibility of doing it by remote sensing with good confidence is of major interest. We tried to fit a reflectance model on this band specifically. We will show first determinations of temperature on our samples, the quality and the potential applications of such a tool to reflectance measurements.

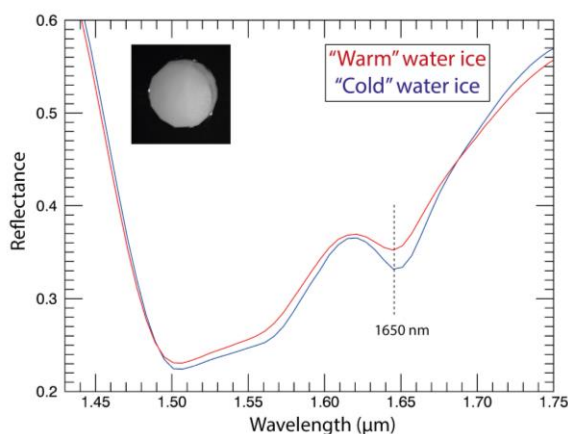


Figure 2: Reflectance measurements of warm water ice at 119K and cold-water ice at 100K. These temperatures are those of the sensors in contact with the sample holder. We expect these temperatures to be different from those of the ice’s surface

## Acknowledgements

The team from the University of Bern is supported by the Swiss National National Science Foundation and through the NCCR PlanetS.

## References

- [1] Thomas, E.C., et al., (2017), Composition and Evolution of Frozen Chloride Brines under the Surface Conditions of Europa, *ACS Earth and Space Chemistry*, 14 – 23
- [2] Carlson, R., et al., (2005), Distribution of hydrate on Europa: Further evidence for sulfuric acid hydrate, *Icarus* 177, 461 – 471
- [3] McCord, T., et al., (2010), Hydrated minerals on Europa’s surface: An improved look from the Galileo NIMS investigation, *Icarus* 209, 639 – 650
- [4] Paranicas, C., et al., (2002), The ion environment near Europa and its role in surface energetics, *Geophysical Research Letters* 29.
- [5] Johnson, R.E., et al., (2004), *Radiation Effects on the Surface of the Galilean Satellites*, Jupiter, Cambridge University Press
- [6] Plainaki, C., et al., (2018), Towards a Global Unified Model of Europa’s Tenuous Atmosphere, *Space Science Review*
- [7] Cooper et al., (2001) Energetic Ion and Electron Irradiation of the Icy Galilean Satellites, *Icarus* 149, 133 - 159
- [8] Galli, A., et al., (2016), Surface charging of thick porous water ice layers relevant for ion sputtering experiments, *Planetary and Space Science* 126, 63 - 71
- [9] Galli, A., et al., (2017), 0.2 to 10 keV electrons interacting with water ice: Radiolysis, sputtering, and sublimation, *Planetary and Space Science*
- [10] Galli, A., et al., (2018), First experimental data of sulphur sputtering water ice, *Icarus*
- [11] Hand, K.P., Carlson, R.W., (2015) Europa’s surface color suggests an ocean rich with sodium chloride, *Geophysical Research Letter*, 3174 – 3178
- [12] Grundy, W.M., Schmitt, B., (1998), The temperature dependent near-infrared absorption spectrum of hexagonal  $\text{H}_2\text{O}$  ice, *JGR* 103, 25’809 – 25’822
- [13] Grundy, W.M., et al., (1999), Near-infrared Spectra of Icy Outer Solar System Surfaces: Remote Determination of  $\text{H}_2\text{O}$  Ice Temperatures, *Icarus* 142, 536 – 549

## Exploring Oxidative Chemistry and Metabolic Pathways in Enceladus' Ocean

Christine Ray (1,2), Chris Glein (2), J. Hunter Waite (2,1), Ben Teolis (2), Julie Huber (3)

(1) The University of Texas at San Antonio, Department of Physics and Astronomy, San Antonio, TX 78249, (2) Southwest Research Institute, San Antonio, TX 78228, (3) Josephine Bay Paul Center, Marine Biological Laboratory, Woods Hole, MA 02543

(christine.ray@swri.org)

### 1. Introduction

The detection of molecular hydrogen in the plume of Saturn's icy moon Enceladus implies that there is positive chemical affinity (i.e., free energy available) for methanogenesis, the metabolic reaction of hydrogen with carbon dioxide to form methane and water [1]. Methanogenesis, however, is just one of many possible metabolic pathways that could be utilized by putative microorganisms. While reduced species are abundant in the plume, CO<sub>2</sub> was the only oxidant observed. To constrain the amount of other metabolically important oxidants including sulfate (SO<sub>4</sub><sup>2-</sup>), molecular oxygen (O<sub>2</sub>), hydrogen peroxide (H<sub>2</sub>O<sub>2</sub>) and ferric iron (for which we choose FeOOH (goethite) as representative of ferric oxyhydroxide solids) in Enceladus' ocean, we present a geochemical model of the ocean based on detections made by the Cassini INMS instrument [1] and likely equilibrium mineralogies of Enceladus' core.

### 1. Methods

#### 2.1 Production of O<sub>2</sub> and H<sub>2</sub>O<sub>2</sub>:

We use a model of water ice radiolysis on the surface of Enceladus to estimate the amount of molecular oxygen and hydrogen peroxide contained in the ice, and calculate the delivery rate of oxidants from the surface ice to the ocean using previous estimates of the rate of ice plume particle deposition on the south polar region [2]. We also consider O<sub>2</sub> and H<sub>2</sub>O<sub>2</sub> produced radiolytically in the ocean from electrons and gamma rays released by the decay of <sup>40</sup>K atoms, from the inferred <sup>40</sup>K concentration in Enceladus' ocean (based on [3] and [4]) and rate equations for radiolytic reactions in primitive ocean waters from [5].

#### 2.1 Production of SO<sub>4</sub><sup>2-</sup> and FeOOH:

The oxygen and peroxide that is produced can react with sulfides and ferrous iron dissolved in the ocean to produce SO<sub>4</sub><sup>2-</sup> and FeOOH, respectively. We set upper limits on the concentrations of these species from the equilibrium solubilities of different possible ocean floor minerals, calculated using the Geochemist's Workbench [6]. We then determine the final concentrations of SO<sub>4</sub><sup>2-</sup> and FeOOH in the ocean using oxidation reaction rate laws in natural waters from [7-10].

### 3. Results and Discussion:

We calculate the amount of chemical energy that could be available from a wide range of alternate metabolic pathways over time. We consider reactions involving O<sub>2</sub>, H<sub>2</sub>O<sub>2</sub>, SO<sub>4</sub><sup>2-</sup> and FeOOH reacting with reductants such as molecular hydrogen, sulfides, ferrous iron, ammonia and hydrocarbons, and compare it with the energy available from methanogenesis reported in [1], and the maintenance energy requirements to sustain microbial life on Earth. Finally, we consider how the production of oxidants from radiolysis of pore water in the core, and how the abiotic hydrothermal consumption of oxidants by reduced minerals in the core, could affect the reported results.

### 4. References

- [1] Waite et al., Cassini finds molecular hydrogen in the enceladus plume: Evidence for hydrothermal processes, *Science*, 356(6334), 155–159 (2017)
- [2] Kempf, S., Beckmann, U. and J. Schmidt, J, How the enceladus dust plume feeds saturns e ring, *Icarus*, 206(2), 446–457 (2010)

[3] Postberg et al., Sodium salts in e-ring ice grains from an ocean below the surface of Enceladus, *Nature*, 459(7250), 1098–1101 (2009)

[4] Lodders, K., Solar system abundances and condensation temperatures of the elements, *The Astrophysical Journal*, 591(2), 1220 (2003)

[5] Draganic et al., Decomposition of ocean waters by potassium-40 radiation 3800 Ma ago as a source of oxygen and oxidizing species, *Precambrian Research*, 52(3-4), 337–345 (1991)

[6] Bethke, C. M. and Yeakel, S., *Geochemist's Workbench Essentials Guide*, Aqueous Solutions, LLC, Champaign, Illinois (2018).

[7] Millero, F. J., Sotolongo, S. and Izaguirre, M., The oxidation kinetics of Fe(II) in seawater, *Geochimica et Cosmochimica Acta*, 51(4), 793–801 (1987a)

[8] Millero et al., Oxidation of H<sub>2</sub>S in seawater as a function of temperature, pH, and ionic strength, *Environmental science & technology*, 21(5), 439–443 (1987b)

[9] Millero, F. and Sotolongo, S. The oxidation of Fe(II) with H<sub>2</sub>O<sub>2</sub> in seawater, *Geochimica et Cosmochimica Acta*, 53, 1867–1873 (1989a)

[10] Millero et al., Oxidation of H<sub>2</sub>S with H<sub>2</sub>O<sub>2</sub> in Natural Waters, *Environmental science & technology*, 23, 209–213 (1989b)



# Observational constraints on the distribution and temperature dependence of $\text{H}_2\text{O}_2$ on the surface of Europa

**S. K. Trumbo** (1), M. E. Brown (1), K. P. Hand (2), and K. de Kleer (1)

(1) Division of Geological and Planetary Sciences, California Institute of Technology, Pasadena, CA, 91125, USA  
(strumbo@caltech.edu) (2) Jet Propulsion Laboratory, California Institute of Technology, Pasadena, CA, 91109, USA

## Abstract

We present L-band Keck NIRSPAO and NASA IRTF SpeX observations of hydrogen peroxide ( $\text{H}_2\text{O}_2$ ) on the surface of Europa. We map  $\text{H}_2\text{O}_2$  across the surface at a spatial resolution of  $\sim 300$  km and investigate the geographic variability in its abundance. We find elevated concentrations at low-latitudes, potentially correlated with chaos terrain, and relative depletions toward the cold poles. We also examine the temperature effects on Europa's  $\text{H}_2\text{O}_2$  abundance by examining changes in the  $\text{H}_2\text{O}_2$  band strength before and after eclipse.

## 1. Introduction

Hydrogen peroxide ( $\text{H}_2\text{O}_2$ ) is part of an important radiolytic cycle on Europa. The bombardment of surface water ice by magnetospheric ions and electrons converts  $\text{H}_2\text{O}$  to  $\text{H}_2\text{O}_2$ , losing  $\text{H}_2$  in the process and creating an oxidizing surface [1, 2, 4]. Understanding this cycle is not only important to our knowledge of the chemical composition of Europa's surface and to the study of surface-magnetosphere interactions throughout the solar system, but it is also critical for our understanding of the potential chemical energy sources to Europa's ocean [3, 6]. Water-rock interactions at the seafloor can be a source of reductants, but the energy available for redox chemistry will likely depend on the supply of oxidants, such as  $\text{H}_2\text{O}_2$ , from the radiolytically processed surface environment [3, 6].

Spectroscopic observations of potentially endogenous salts suggest that low-latitude chaos regions on the leading and anti-Jovian hemispheres may be important sites of exchange between the surface and subsurface environments [5]. However, laboratory experiments [8, 9] and disk-integrated spectroscopic observations of

Europa's surface [7] suggest that the local  $\text{H}_2\text{O}_2$  concentrations are controlled by the local temperature and availability of water ice, leading to the prediction that the highest  $\text{H}_2\text{O}_2$  concentrations would lie at the cold, icy high-latitudes of the leading hemisphere, rather than the warm, salty equatorial regions. If these predictions are correct, such a spatial separation of  $\text{H}_2\text{O}_2$  and the most likely locations of surface-subsurface exchange could limit the delivery of oxidants to the subsurface ocean. A definitive understanding of the distribution and controls of  $\text{H}_2\text{O}_2$  across the surface of Europa is therefore crucial for understanding its potential habitability.

## 2. Observations and results

We present L-band observations of Europa taken with the near-infrared spectrograph NIRSPEC and adaptive optics (AO) system (hereby combined to NIRSPAO) on the Keck II telescope, as well as with the near-infrared spectrograph SpeX of the NASA Infrared Telescope Facility (IRTF). Our NIRSPAO observations map the  $3.5\ \mu\text{m}$   $\text{H}_2\text{O}_2$  feature across the surface of Europa at a nominal spatial resolution of  $\sim 300$  km, thereby testing the expectation that  $\text{H}_2\text{O}_2$  is concentrated in the coldest, iciest regions. Figure 1 shows representative NIRSPAO spectra of the high- and low- latitudes on the leading hemisphere. Contrary to expectations, our NIRSPAO data exhibit a depletion of  $\text{H}_2\text{O}_2$  at the high latitudes and higher abundances near the warm equator. Intriguingly, as demonstrated in the mapped slit of Figure 2, these data also suggest a potential concentration of  $\text{H}_2\text{O}_2$  within the salty chaos terrains, which may imply a compositional control on abundance.

Our SpeX data examine the strength of the  $3.5\ \mu\text{m}$   $\text{H}_2\text{O}_2$  feature in disk-integrated spectra taken before and after Europa's daily eclipse and are therefore sensitive to temperature controls that are independent

of geographic location. A simple thermal model of Europa's surface [10] predicts a temperature drop of 10–20 K during eclipse. Comparison of  $\text{H}_2\text{O}_2$  band strengths before and after this temperature change will investigate the importance of temperature in the equilibrium concentrations of  $\text{H}_2\text{O}_2$  on Europa.

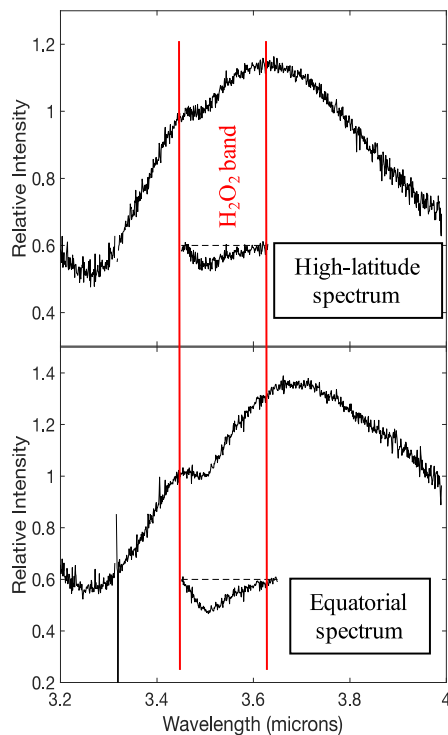


Figure 1: Two representative spectra from a NIRSPAO N/S slit across Europa. The high-latitude spectrum exhibits a smaller  $\text{H}_2\text{O}_2$  absorption than the equatorial spectrum. This observation is contrary to the expectation that  $\text{H}_2\text{O}_2$  be concentrated in the coldest and iciest regions on Europa's surface.

## Acknowledgements

S. K. Trumbo is supported through a NASA Earth and Space Sciences Fellowship (NESSF). K. de Kleer is supported via the *51 Pegasi b* Fellowship Program.

## References

[1] Carlson, R. W., Anderson, M. S., Johnson, R. E., Smythe, W. D., Hendrix, A. R., Barth, C. A., Soderblom, L. A., Hansen, G. B., McCord, T. B., Dalton, J. B., Clark, R. N., Shirley, J. H., Ocampo, A. C., and Matson, D. L.: Hydrogen Peroxide on the Surface of Europa, *Science*, Vol. 283, pp. 2062–2064, 1999.

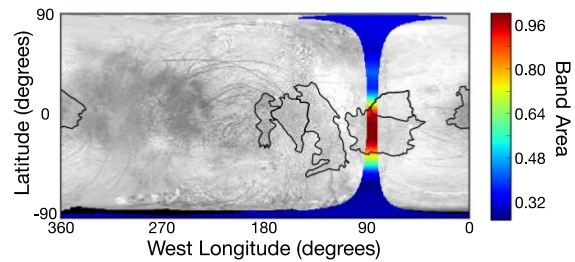


Figure 2: A NIRSPAO N/S slit across the leading hemisphere of Europa. The  $\text{H}_2\text{O}_2$  abundance appears to be lowest at high latitudes and most concentrated in the salty chaos region, Tara Regio. This implies a potential compositional, rather than temperature, control on  $\text{H}_2\text{O}_2$  abundance.

[2] Carlson, R. W., Calvin, W. M., Dalton, J. B., Hansen, G. B., Hudson, R. L., Johnson, R. E., McCord, T. B., and Moore, M. H.: in *Europa*, University of Arizona Press, 2009.

[3] Chyba, C. F. : Energy for microbial life on Europa, *Nature*, Vol. 403, pp. 381–382, 2000.

[4] Cooper, P. D., Johnson, R. E., Quickenden, T. I.: Hydrogen peroxide dimers and the production of  $\text{O}_2$  in icy satellite surfaces, *Icarus*, Vol. 162, pp. 444–446, 2003.

[5] Fischer, P. D., Brown, M. E., Hand, K. P.: Spatially resolved spectroscopy of Europa: the distinct spectrum of large-scale chaos, *AJ*, Vol. 150, pp. 164.

[6] Hand, K. P., Chyba, C. F., Priscu, J. C., Carlson, R. W., and Nealson, K. H.: in *Europa*, University of Arizona Press, 2009.

[7] Hand, K. P. and Brown, M. E.: Keck II observations of hemispherical differences in  $\text{H}_2\text{O}_2$  on Europa, *ApJ Letters*, Vol. 766, pp. L21.

[8] Hand, K. P. and Carlson, R. W.:  $\text{H}_2\text{O}_2$  production by high-energy electrons on icy satellites as a function of surface temperature and electron flux, *Icarus*, Vol. 215, pp. 226–233.

[9] Loeffler, M. J., Raut, U., Vidal, R. A., Baragiola, R. A., and Carlson, R. W.: Synthesis of hydrogen peroxide in water ice by ion irradiation, *Icarus*, Vol. 180, pp. 265–273.

[10] Trumbo, S. K., Brown, M. E., and Butler, B. J.: ALMA thermal observations of a proposed plume source region on Europa, *AJ*, Vol. 154, pp. 148.



# Layer formation in Europa's subsurface ocean by double-diffusive convection

**Teresa Wong** (1), Ulrich Hansen (1), Thomas Wiesehöfer (1), and William B. McKinnon (2)

(1) Institut für Geophysik, Westfälische Wilhelms-Universität Münster, Germany (2) Washington University in St. Louis, USA (t.wong@uni-muenster.de)

## Abstract

Double-diffusive convection could occur in Europa's subsurface ocean in the presence of dissolved salts. We demonstrate with numerical models that layers can form in the ocean. The stability of these layers lower the efficiency of heat and material transport. We explore the evolution of these layers, and whether plumes originating from the seafloor can reach the bottom of the icy shell.

## 1. Introduction

The existence of Europa's subsurface ocean is suggested by the induced magnetic fields by *Galileo* and recent images by Hubble Space Telescope. Colored bands and disrupted terrains on the surface are enhanced in hydrated minerals, potentially indicative of the composition of the subsurface ocean. These observations invoke various hypotheses of how materials are being transported from the seafloor to the surface by hydrothermal plumes, and raise questions on heat transfer. Previous studies assessed the occurrence of double-diffusive convection as a possible mechanism affect heat and material transport by analyzing the stability of the subsurface ocean mainly based on linear stability [1, 2]. However the onset of convection predicted by linear theory has been shown to be inadequate for the non-linear behaviour of the fluid from laboratory and numerical experiments [3, 4].

We perform numerical simulations of double-diffusive convection to test the hypothesis that the heat and material can be transported from the interior through the subsurface ocean to the base of the icy shell, and ultimately expressed and posited on the surface. We observe layer formation and its subsequent evolution in the subsurface ocean.

## 2. Double-diffusive convection

Double-diffusive convection is a mixing process driven by the difference in thermal and chemical diffusivities when two chemical constituents are present. The chemical diffusivity is usually orders of magnitude smaller than the thermal diffusivity, which means temperature of the perturbed fluid is adjusted much more rapidly to its surroundings than the concentration, such that the small diffusivity acts to preserve the concentration of the fluid. The compositional density difference may provide an additional driving or restoring force to thermal convection, depending on their distribution. The different combinations of driving and restoring forces with different diffusive timescales give rise to very different dynamics in the convecting layer.

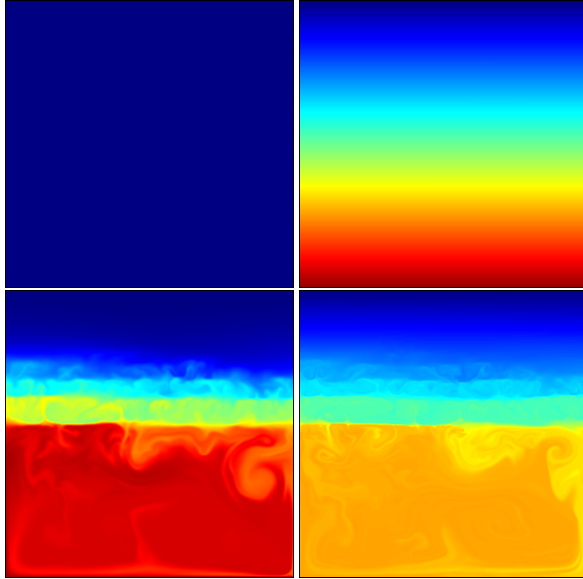
We model this subsurface water layer in Europa subjected to a destabilizing temperature gradient (warm at the bottom, cold on top) and simultaneously to a stabilizing compositional (salt) distribution. This configuration favours the formation layers, which form in a self-organized manner as they can evolve from a gradient without imposing a prior stratification of material or temperature [5, 6]. Layers can buffer heat transport through the ocean. Depending on initial conditions and material properties as represented by the Rayleigh numbers, different numbers of layers will evolve. We test three possible initial conditions: (1) uniformly cold with a smooth compositional gradient; (2) uniformly warm with a smooth compositional gradient; (3) in both temperature and compositional gradients.

Numerical calculations are performed with a finite volume code for double-diffusive convection in finite Prandtl number, where the chemical constituent (salt or other hydrated minerals) is treated in a field approach, meaning a further advection/diffusion equation for the constituent is solved. The temperature and compositional differences across the depth of the layer

are fixed.

### 3. Layer formation in the subsurface ocean

The figure panel below presents an example system that is initially cold, compositionally light on top and heavy at the bottom. Top figures show the initial temperature (left) and concentration (right) field (red=high, blue=low). Layers develop in a self-organized manner from a concentration gradient, as shown in the bottom figures.



The dynamics of the double-diffusive system is governed by three dimensionless parameters: (1) the buoyancy ratio  $R\rho = Ra_c/Ra$ , the ratio of compositional Rayleigh number  $Ra_c = \frac{\beta\rho g\Delta C d^3}{\kappa_C\eta}$ , to that of the thermal  $Ra = \frac{\alpha\rho g\Delta T d^3}{\kappa_T\eta}$ , both of which are dimensionless measures of the driving or restoring forces, (2) Lewis number  $Le = \kappa_T/\kappa_C$ , the ratio of thermal diffusivity to chemical diffusivity, and (3) Prandtl number  $Pr = \nu/\kappa_T$ , the ratio of momentum diffusivity  $\nu = \eta/\rho$  to thermal diffusivity. Other variables are the density  $\rho$ , gravity  $g$ , coefficient of thermal expansion  $\alpha$ , and coefficient of compositional expansion or saline contraction  $\beta$ . Parameters of the system for this figure panel are  $R\rho=3$ ,  $Le=100$ ,  $Pr=7$ .

The dynamics of layering is known to often exhibit intermittent behaviour. Individual layers can suddenly merge, increasing overall transport substantially. These intermittent changes in the layer pattern can potentially induce sudden large motion in the icy shell.

Layers can buffer heat transport through the ocean. By quantifying the transport of heat and material from numerical experiments, we measure the influence of layering on the overlying icy shell. In this study we observe the evolution of the ocean and discuss its impact on the icy shell.

### References

- [1] Vance, S., and Brown, J.: Layering and double-diffusion style convection in Europa's ocean, *Icarus*, 177(2):506–514, 2005.
- [2] Vance, S., and Goodman, J.: Oceanography of an ice-covered moon. In Pappalardo, R. T., McKinnon, W. B., and Khurana, K. K., editors, *Europa*, pages 459–482, The University of Arizona Press, 2009.
- [3] Huppert, H. E., and Moore, D. R.: Nonlinear double-diffusive convection. *Journal of Fluid Mechanics*, 78(4):821–854, 1976.
- [4] Fernando, H. J. S.: Buoyancy transfer across a diffusive interface, *Journal of Fluid Mechanics*, 209:1–34, 1989.
- [5] Hansen, U., and Yuen, D. A.: Formation of layered structures in double-diffusive convection as applied to the geosciences, in *Double-Diffusive Convection*, edited by Brandt, A. and Fernando, H., American Geophysical Union, Washington, D. C., 1995.
- [6] Radko, T.: *Double-Diffusive Convection*, Cambridge University Press, Cambridge, UK, 2013.

# Ice World Oceans, Salt Grains and Hypervelocity Impacts

Callum R. Fisher (1), Mark C. Price (1), James New (1), Anna L. Butterworth (2), Richard A. Mathies (2) and **Mark J. Burchell** (1)

(1) Centre for Astrophysics and Planetary Science, School of Physical Science, University of Kent, Canterbury, Kent, United Kingdom CT2 7NH ([m.j.burchell@kent.ac.uk](mailto:m.j.burchell@kent.ac.uk)). (2) Space Sciences Laboratory, University of California at Berkeley, Berkeley CA 94720, USA.

## Abstract

We report on studies of residues from salt projectiles fired into aluminium foil at speeds up to  $7 \text{ km s}^{-1}$ . The results show that we can find identifiable residue in craters after impact, with shock pressures up to 77 GPa. This has implications for analysis of samples obtained by flying through the plumes of sub-surface oceans on icy satellites e.g. [1-3], i.e. substantial amounts of residue are captured at speeds likely for impacts on a passing spacecraft.

## 1. Introduction

The presence of sub-surface oceans on various icy satellites of Jupiter and Saturn holds great interest for those interested in the development of minerals and organic chemistry on such bodies [4-7]. They are also of great interest to astrobiology. The water in the oceans is not however totally inaccessible – in some cases (e.g. Europa and Enceladus) it vents naturally from the satellites as plumes. The Cassini mission showed that a spacecraft can successfully traverse such plumes, and sample material from them. In the case of the Cosmic Dust Analyser on Cassini, small grains of salt were reported associated with the plumes [8]. Here we investigate in the laboratory what happens to salt grains when impacting a target at speeds from 2 to  $7 \text{ km s}^{-1}$ . Such speeds exceed those of a craft orbiting the body, but are typical of those for one in orbit around the parent planet and which makes a flyby of the body of interest.

## 2. Method

In this work we use four types of salt: sodium chloride (NaCl), sodium bicarbonate ( $\text{NaHCO}_3$ ), and magnesium sulfate ( $\text{MgSO}_4$ ), the latter in both hydrous (kieserite,  $\text{MgSO}_4 \cdot \text{H}_2\text{O}$ ) and anhydrous forms. Grain size was from  $10 \text{ }\mu\text{m}$  up to 100s of  $\mu\text{m}$ . Small amounts ( $\mu\text{g}$ ) of each salt were fired at aluminium targets using the University of Kent two stage light gas gun [9]. After a shot, the foil were

examined using a combination of SEM-EDX and Raman spectroscopy. There have been 17 shots so far. The impact speed was measured in each shot and ranged from 2 to  $7 \text{ km s}^{-1}$ .

## 3. Results

A typical impact crater is shown in Fig. 1. The rubble like debris in the lower part of the crater image shows strong Na and Cl EDX signals.

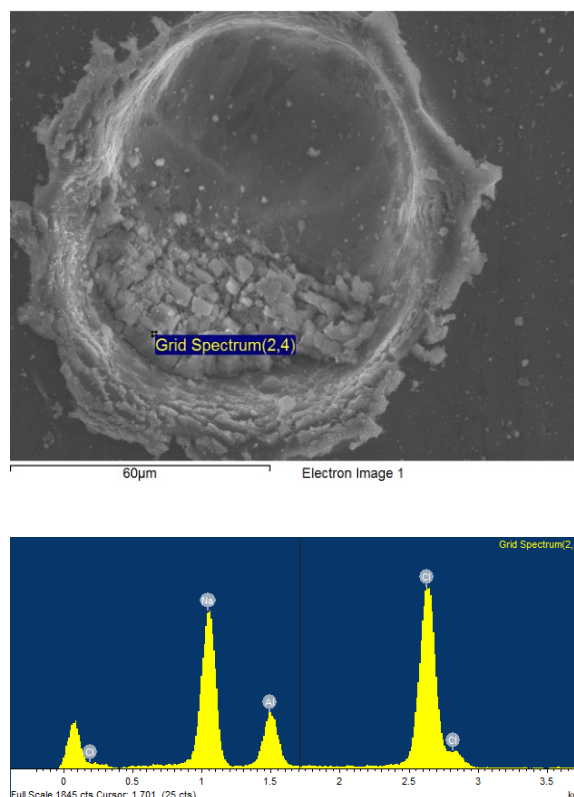


Figure 1: Impact of a NaCl grain at  $1.94 \text{ km s}^{-1}$ . (Top) The resulting impact crater. (Bottom) SEM-EDX spectrum showing peaks for Na and Cl, which are coincident with the rubble like residue visible in the lower region of the image of the crater.

The individual foil targets show a range of crater sizes due to the polydisperse size distribution of the raw samples. Therefore, when examined under the SEM, a range of crater sizes down to 10  $\mu\text{m}$  diam. has been studied. Projectile residue is found in all four types of salt, at all crater sizes and at all speeds used.

Peak pressures were calculated using the Planar Impact Approximation [10] and linear wave speed coefficients derived from the LANL database for single crystal NaCl salt. At the impact speeds here, peak shock pressures range from 14 to 77 GPa.

Using the EDX analysis it is possible to distinguish NaCl from the other salt types. Sodium bicarbonate is flagged by the presence of C and O peaks, and magnesium sulfate by Mg, S and O peaks. However, based on EDX alone we cannot currently distinguish hydrous from anhydrous.

The texture of the residue on the craters does vary with impact speed and salt type. In some cases we found what appeared to be salt crystals in the residues, but these may have recrystallised after impact when exposed to the damp atmosphere. Accordingly, we are testing recovery after impact and storage under inert  $\text{N}_2$  atmospheres to investigate this further.

## 4. Summary and Conclusions

The results so far are supportive that, despite capture via a high speed impact, a significant amount of identifiable residue is present in the resultant impact craters. We are currently doing the Raman spectrometry and testing to see if it has retained its original crystal structure as well as composition. To a degree this is not a surprise. The NASA Stardust mission to comet 81P/Wild-2 captured significant amounts of small particle residues after high speed impacts on foils [11-12], some of which retained significant crystallinity after capture [13]. Here we are demonstrating that this also applies to salt crystals, such as may be found in the plumes of Europa and Enceladus.

## Acknowledgements

We thank STFC for funding the light gas gun work reported here. CF also thanks STFC for a PhD scholarship. We thank M.J. Cole for operation of the Kent light gas gun.

## References

- [1] J. H. Waite, *et al.*, Cassini Ion and Neutral Mass Spectrometer: Enceladus Plume Composition and Structure. *Science* 311(5766), 1419–1422 (2006).
- [2] C. Hansen, L. Esposito, A.I.F. Stewart, J. Colwell, A. Hendrix, W. Pryor, D. Shemansky, R. West, Enceladus' water vapor plume. *Science* 311(5766), 1422 – 1426, (2006).
- [3] W. B. Sparks, K. P. Hand, M. A. McGrath, E. Bergeron, M. Cracraft, S. E. Deustua, Probing For Evidence of Plumes on Europa with HST/STIS. *The Astrophysical Journal* 829, 121(21 pages) (2016).
- [4] M.H. Carr, *et al.*, Evidence for a subsurface ocean on Europa. *Nature* 391(6665), 363 – 365 (1998).
- [5] R.T. Pappalardo, *et al.*, Does Europa have a subsurface ocean? Evaluation of the geological evidence. *Journal of Geophysical Research-Planets* 104(E10), 24015-24055 (1999).
- [6] O. Cadek, *et al.*, Enceladus's internal ocean and ice shell constrained from Cassini gravity, shape, and libration data. *Geophysical Research Letters* 43(11), 5653-5660 (2016).
- [7] K. K. Khurana, *et al.*, Induced magnetic fields as evidence for subsurface oceans in Europa and Callisto. *Nature* 395(6704), 777 – 780 (1998).
- [8] F. Postberg, *et al.*, A salt-water reservoir as the source of a compositionally stratified plume on Enceladus. *Nature* 474, 620 – 622, 2011.
- [9] M.J. Burchell, *et al.*, Hypervelocity Impact Studies Using the 2 MV Van de Graaff Dust Accelerator and Two Stage Light Gas Gun of the University of Kent at Canterbury. *Meas. Sci. Tech.* 10, 41-50 (1999).
- [10] H. J. Melosh, *Impact Cratering: A Geological Process*, pub. Oxford, 1988
- [11] A. T. Kearsley, *et al.*, Dust from comet Wild 2: Interpreting particle size, shape, structure and composition from impact features on the Stardust aluminium foils. *Meteoritics and Planetary Science* 43, 41 – 74, 2008.
- [12] M. C. Price, *et al.*, Comet 81P/Wild 2: The size distribution of finer (sub 10 micrometre) dust collected by the Stardust Spacecraft. *Meteoritics and Planetary Science* 45(9), 1409 – 1428, 2010.
- [13] P.J. Wozniakiewicz, *et al.*, The Origin of Crystalline Residues in Stardust Al Foils: Surviving Cometary Dust or Crystallized impact Melts? *Meteoritics and Planetary Science* 47, 660 – 670, 2012.

# Spectral properties of fresh impact craters in the Saturnian and Jovian system

**K. Stephan** (1), R. Jaumann (1,2), C. M. Dalle Ore (3,4), G. Filacchione (5), M. Ciarniello (5), D. P. Cruikshank (3).

(1) Institute of Planetary Research, German Aerospace Center (DLR), Berlin, Germany; (2) Freie Universität Berlin, 12249 Berlin, Germany; (3) NASA Ames, Moffett Field, CA 94035; (4) SETI Institute, Mountain View, CA; (5) INAF-IAPS Istituto di Astrofisica e Planetologia Spaziali, I-00133 Rome, Italy ([Katrin.Steph@dlr.de](mailto:Katrin.Steph@dlr.de)).

## Abstract

We investigated the spectral properties of fresh (more or less un-weathered) impact craters on the icy satellites of Saturn, which were observed by the Cassini spacecraft. In addition, Galileo SSI and NIMS observations of the Jovian satellite Ganymede have been included in the investigation in order to compare the spectral properties of fresh impact craters on icy bodies in two different planetary systems. Although, the surfaces of the icy satellites in the Saturnian system are known to be dominated by H<sub>2</sub>O ice, the spectral properties of fresh impact craters provide compositional information of the satellites' upper crustal material but also reveal information about the impact event itself and/or the surface temperature at the crater's location.

## 1. Introduction

The imaging instruments onboard the Cassini spacecraft detected the icy satellites of Saturn allowing the study of their geological and spectral surface properties. Especially Cassini ISS and VIMS data acquired during few targeted flybys at relatively low latitudes enable a detailed investigation of individual impact craters on Dione, Rhea and Tethys such as the prominent impact craters Creusa and Inktomi. In addition, several sufficiently resolved Galileo SSI and NIMS observations of the Jovian satellite Ganymede covering numerous morphologically fresh impact craters, are available.

The investigated impact craters have been chosen based on their morphological surface characteristics. The investigation of their spectral properties focused on the analysis of the spectral signature of H<sub>2</sub>O ice in comparison with H<sub>2</sub>O ice model spectra (1-3) including the numerous absorptions of H<sub>2</sub>O ice, which are known to be an indicator for the abundance as well as the sizes of the individual H<sub>2</sub>O ice particles (4-6).

## 2. Results

All investigated impact craters exhibit a high visible albedo and are composed of relatively pure H<sub>2</sub>O ice confirming an uppermost layer of the studied satellites dominated by H<sub>2</sub>O ice. The sizes of the H<sub>2</sub>O ice particles, however, vary dramatically and have been found rather to be an indicator for the environmental conditions. The fresh impact craters on the Saturnian satellites exhibit relatively small (~5 – 40 µm) H<sub>2</sub>O ice particle sizes. In contrast, the H<sub>2</sub>O ice particle sizes of fresh impact craters on Ganymede partly increase up to ~1mm. The comparison of the H<sub>2</sub>O-ice particle sizes with the maximum surface temperatures at the approximate location of the impact site (7-9) reveals a direct correlation between the H<sub>2</sub>O ice particle sizes and surface temperature. The smallest H<sub>2</sub>O ice particle sizes (~5 µm) are confined to Creusa located on Dione at ~50°N and a surface temperature of ~80 K (7, 9). At similar surface temperatures the H<sub>2</sub>O ice particle sizes on Ganymede and the Saturnian satellites are quite similar. Nevertheless, impact crater Tammuz located close to Ganymede' equator (~13°N), where the surface temperature can reach least 150 K (8), exhibits H<sub>2</sub>O ice particle sizes up to ~1mm. Thus, the derived particles sizes rather reflect the surface environment than the crustal properties.

## References

- [1] Hansen et al. (2009): *Icarus*, 203, 2, 672-676; [2] Dalle Ore et al. (2015): *Icarus*, 261, 80-90; [3] Ciarniello et al. (2011): *Icarus*, 214, 541-555; [4] Stephan et al. (2017): EPSC abstracts, 11, EPSC2017-350-2; [5] Jaumann et al. (2008): *Icarus*, 193, 2, 407-419; [6] Stephan et al. (2009): EPSC abstracts, 4, #EPSC2009-2633; [7] Howett et al. (2010): *Icarus*, 206, 573-593; [8] Squyres (1980): *Icarus*, 44, 502-510; [9] Filacchione et al. (2016): *Icarus*, 271, 292-313.

# Time scales of cryomagma eruptions on Europa

**E. Lesage (1)**, H. Massol (1) and F. Schmidt (1)

(1) GEOPS, Univ. Paris-Sud, CNRS, Université Paris-Saclay, Rue du Belvédère, Bât. 504-509, 91405 Orsay, France  
 (elodie.lesage@@u-psud.fr)

## Abstract

Smooth plains and lobate features are identified on Europa's surface, and seem to involve sub-surface liquid water reservoirs at shallow depth. Our study aims at modeling the ascent of liquid composed of pure or briny water from a freezing chamber to the surface, producing cryovolcanic eruptions. We show that if this kind of liquid flow takes place on Europa, the eruptions happen in a short time scale (tens of seconds to tens of hours), and the cryolavas travel to the surface at high speed (few tens of m/s) as a turbulent flow. For chamber radius varying between 10 and few hundred meters, the freezing time-scale varies between  $10^2$  to  $10^3$  years for a pure water cryomagma and from  $10^2$  to  $10^4$  years for a briny cryomagma.

## 1. Introduction

Data acquired by the Galileo spacecraft between 1995 and 2001 show smooth plains cover parts of the surface, and their morphologies and relationship to the surrounding terrains suggest that they result from viscous liquid extrusions [1]. Recent literature involves the presence of liquid reservoirs beneath the surface to explain the emplacement of common features, such as double ridges [2], lenticulae [3] and chaos [4].

We model the ascent of liquid water through a dike or a pipe-like conduit, from a sub-surface reservoir to Europa's surface and derive the eruption time-scale and the total volume extruded at the end of the eruption, depending on the chamber volume and depth. We also estimate the freezing time of the sub-surface reservoir necessary to trigger an eruption. Considering available data for density and eutectic temperature of salt impurities recently proposed for Europa [5], we discuss their effect on the cryomagma freezing time and ascent.

## 2. Model

Based on the work by Fagents [6], we consider the following mechanism summarized in Fig. 1: a liquid water pocket is present in the subsurface and the cryomagma contained in the chamber freezes and pressurizes over the time. When the stress applied on the chamber walls reaches the critical value, the walls break, and a fracture may propagate to the surface. The remaining fluid flows out at the surface through a dike or a pipe-like conduit. A numerical model calculates the evolution of flow velocity and chamber pressure with time.

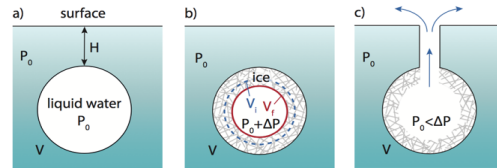


Fig. 1: Model used in this study. a) A hot liquid water lens is at isostatic pressure  $P_0$  and depth  $H$ . b) The cryomagma freezes and the liquid is compressed from a volume  $V_i$  to a volume  $V_f$ , generating an overpressure  $\Delta P$ . c) The eruption begins when the pressure reaches a critical value and ends when the chamber is back at isostatic pressure.

The pressure increase generated by the cryomagma freezing is related to the liquid volume decrease through the water compressibility  $\chi$ . The critical fraction of liquid  $n_c$  that has to freeze to generate the critical overpressure  $\Delta P_c$  and begin an eruption is given by:

$$n_c = \frac{\exp(\chi \Delta P_c) - 1}{\frac{\rho_l}{\rho_s} \exp(\chi \Delta P_c) - 1} \quad (1)$$

where  $\rho_l$  is the liquid density and  $\rho_s$  is the solid density.

In order to get an order of magnitude of the freezing time of the chamber and to evaluate the time necessary to reach the critical overpressure, we solve



the Stefan problem in 1D using cartesian coordinates [7]. The freezing time scale  $\tau_c$  is:

$$\tau_c = \left( \frac{n_c^{1/3} R_{chamber}}{2\lambda\sqrt{\kappa_s}} \right)^2 \quad (2)$$

where  $R_{chamber}$  is the chamber radius,  $\lambda$  is a parameter computed from the temperature gradient between the chamber and the surrounding ice and the solidification latent heat, and  $\kappa_s$  is the thermal diffusivity in the solid part of the cryomagma.

These calculations are derived in two cases: 1. a pure water composed cryomagma and 2. a briny cryomagma. As suggested by recent studies [8], a plausible composition for the Europa's ices and cryomagma is a mixture of  $H_2O$ ,  $MgSO_4$  and  $Na_2SO_4$ . In that second case, we modify accordingly the densities  $\rho_l$  and  $\rho_s$  in Eq. (1).

### 3. Results

For plausible volumes and depths varying between  $0.1km^3 < V < 10km^3$  and  $100m < H < 10km$ , the total extruded cryolava volume ranges from  $10^5$  to  $10^8 m^3$ , and the time scale of the eruptions varies from few minutes to few tens of hours. The freezing time-scale of the cryomagma pocket varies with the cryomagma composition: as shown in Fig. 2, it differs of few percent for a briny or a pure water cryomagma. The freezing time-scale varies between  $10^2$  to  $10^3$  years for a pure water cryomagma and from  $10^2$  to  $10^4$  years for a briny cryomagma [8]. The freezing timescale, within the life-time of putative liquid water lenses which varies from  $10^3$  to  $10^5$  years [3], indicates that eruption should be possible.

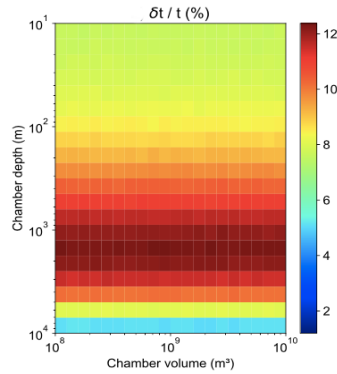


Fig. 2: Modification of the eruption duration between the case with a pure liquid water composed cryomagma and a mixture of  $H_2O$ ,  $MgSO_4$  and  $Na_2SO_4$ .

We plan to compare these results with the Galileo observations by carrying out a stereoscopic study of some lobate features in order to define plausible locations of cryovolcanic active areas on Europa. These results could be useful for the two missions JUICE (ESA) and Europa Clipper (NASA).

### Acknowledgements

We acknowledge support from the "Institut National des Sciences de l'Univers" (INSU), the "Centre National de la Recherche Scientifique" (CNRS) and "Centre National d'Etudes Spatiales" (CNES) through the "Programme National de Planétologie". We also thanks the "Institut Pierre Simon Laplace" (IPSL).

### References

- [1] Miyamoto, H., Mitri, G., Showman, A. P., Dohm, J. M., oct 2005. Putative ice flows on europa: Geometric patterns and relation to topography collectively constrain material properties and effusion rates. *Icarus* 177 (2), 413–424.
- [2] Craft, Kathleen L., Patterson, G. Wes, Lowell, Robert P., & Germanovich, Leonid. 2016. Fracturing and flow : Investigations on the formation of shallow water sills on Europa. *Icarus*, 274(aug), 297–313.
- [3] Manga, M. & Michaut, C. 2017. Formation of lenticulae on Europa by saucer-shaped sills. *Icarus*, 286(apr), 261–269.
- [4] Schmidt, B. E., Blankenship, D. D., Patterson, G. W., & Schenk, P. M. 2011. Active formation of 'chaos terrain' over shallow subsurface water on Europa. *Nature*, 479 (7374), 502–505.
- [5] Quick, L. C., Marsh, B. D., jun 2016. Heat transfer of ascending cryomagma on europa. *Journal of Volcanology and Geothermal Research* 319, 66–77.
- [6] Fagents, S. A., dec 2003. Considerations for effusive cryovolcanism on Europa : The post-Galileo perspective. *J.-Geophys.-Res.* 108 (E12).
- [7] Quick, L. C., Marsh, B. D., jun 2015. Constraining the thickness of europa's water-ice shell: Insights from tidal dissipation and conductive cooling. *Icarus* 253, 16–24.
- [8] Lesage, E., Massol, H., Schmidt, F. 2018. Cryomagma ascent on Europa, submitted to *Icarus*.
- [9] Kalousová, K., Souček, O., Tobie, G., Choblet, G., Čadež, O., mar 2014. Ice melting and downward transport of meltwater by two-phase flow in europa's ice shell. *Journal of Geophysical Research: Planets* 119 (3), 532–549.

# Radar sounding of Jovian icy moons : a simulation approach to active and passive sounding scenarios

C. Gerekos, L. Bruzzone  
Department of Information Engineering and Computer Science, University of Trento, Italy

## Abstract

We present an approach aimed at comprehensively simulating passive and active radar acquisitions from orbit in the noisy radio environment of the Jovian system. By comparing how a given representative target area on the icy moons appears in both cases, we expect to be able to extract valuable informations with regard both to the feasibility and value of passive sounding. Examples of simulations of Europa-like terrains are shown and discussed.

## 1. Introduction

Europa, Ganymede and Callisto, the three Jovian icy moons, are targets of two upcoming planetary science missions, both having a radar sounder included in their payload: ESA's Jupiter Icy Moons explorer (JUICE), carrying the RIME instrument, and NASA's Europa Clipper, carrying the REASON instrument. RIME operates at a central frequency of 9 MHz with a bandwidth of 1 or 2.8 MHz, while REASON is a dual-frequency instrument, with a mode at 9 MHz with a bandwidth of 1 MHz and another at 60 MHz a bandwidth of 10 MHz.

The Jovian radio environment in the HF band is very challenging. At frequencies below 40 MHz, it is characterised sporadic cyclotron emissions about five orders of magnitudes more intense than the galactic background [1]. The duration of those emissions can vary from hours to milliseconds. This limits the possibility to have standard active radio acquisitions, which in presence of this noise would have a very low SNR. However, recent research has suggested that those Jovian emissions could be used to perform passive sounding [2]. This may enhance the scientific value of the instrument, enabling data acquisitions in presence of Jovian noise. In [3], passive and active sounding are compared through their respective signal-to-noise (SNR) and signal-to-clutter (SCR).

In [3] the surface roughness is considered through a spreading factor in the SCR equation, but the roughness-induced loss of coherence was neglected. In [4], the influence of the ionosphere on the phase, amplitude, and harmonic content of considered signal was thoroughly examined. However, no comparative study of radar acquisitions in active and passive mode

that takes all those effects into account simultaneously has yet been carried out.

In this paper, we propose to generalise to passive sounding scenarios the 3D scattering simulation method presented in [5] for active sounding. For a given target area, the proposed method can thus provide simulated data for (i) active sounding with no noise to provide context, (ii) active sounding with Jovian noise, and (iii) passive sounding. This will allow to compare the simulated radargrams obtained with active and passive sounding and to bring further insight into identifying conditions where passive sounding can provide additional scientific value to active sounding. Preliminary simulations obtained with band-limited white noise confirm that passive sounding is possible, and is able to reveal surface and subsurface echoes otherwise invisible in active sounding in presence of Jupiter radio noise, but at the price of increased clutter.

## 2. Proposed simulation technique

The simulation method relies on the Stratton-Chu formula and on the linear phase approximation. It is able to compute radar echoes coming from target areas with an arbitrary number of rough geological layers [5]. The simulated data thus contains both the surface and the subsurface response. The noise is modelled as a plane wave, with a constant wavevector that depends on the relative position of Jupiter and the sounder. The noise considered in both passive and active simulations can be generated using a random number generator, or can come from samples of the actual Jovian noise. In either case, the noise amplitude and polarisation at each moon can be derived from [1]. The propagation through ionosphere can be modelled after the formulas presented in [4].

In the case of passive sounding with a long burst, where an acquisition contains both incident and reflected noise signals, range-compression is done through an autocorrelation of the signal. The resulting function contains two symmetric copies the echoes reflected from the target area, along with a central peak corresponding to the incoming wave. In the case of a short burst, a cross-correlation between the recorded incident signal and its non-overlapping reflections is performed, similarly to the active sounding case.



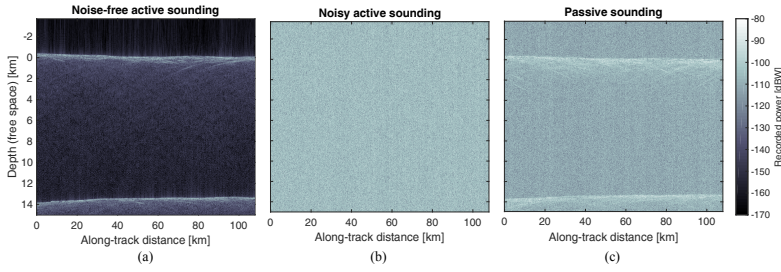


Figure 1: Example of simulations of RIME observing an Europa-like two-layer target area in presence of strong Jovian emissions: (a) active sounding with zero noise, (b) active sounding, (c) passive sounding.

### 3. Experimental results

Simulations were conducted with RIME as the considered instrument.

The central frequency of the radar was thus set  $f = 9$  MHz, its bandwidth  $B = 2.8$  MHz, and its sampling frequency at  $f_s = 12$  MHz. The platform altitude was set at  $h = 400$  km. The Jovian emissions were assumed to come from the anti-nadir direction.

The considered DEM was procedurally-generated and is composed of two layers: the space-ice interface (*i.e.*, the surface), and an interface modelling an hypothetical ice-ocean boundary. The surface was obtained with a fractional Brownian motion (fBm) process characterised by a Hurst's coefficient  $H = 0.6$  and an RMS height of 210 m. The second layer ("ice-ocean interface"), also generated with a fBm process using  $H = 0.8$ , has an RMS height of 80 m, and is placed at a depth of 8 km. The interlayer dielectric properties are set according to the European ice and ocean described in [6]:  $\epsilon_1 = 2.95$ ,  $\tan \delta_1 = 2 \cdot 10^{-4}$  for the space below the surface and  $\epsilon_2 = 80$  for the space below the second layer (*i.e.* the water ocean).

The noise we considered in these simulation is a band-limited white noise with a spectrum ranging from 7 MHz to 11 MHz. The noise amplitude was calculated from the European flux density of  $10^{-14}$   $\text{Wm}^{-2}\text{Hz}^{-1}$ [1]. No ionosphere was modelled in this preliminary test.

Results are shown in fig. 1. Comparing the noise-free (1-a) and noisy active sounding results (1-b), we observe that the echoes are completely overshadowed by the noise. When the same scene is observed with passive sounding (fig. 1-c), echoes from the surface and subsurface become apparent. However, this comes at a price of enhanced clutter echoes compared to noise-free active sounding. The surface we used in the example was relatively smooth, thus we expect clutter to overtake the subsurface echo when the surface is too rough. These observations obtained with the proposed simulator resemble those of [3].

### 4. Conclusion

The Jovian icy moons are the targets of two major planetary science missions carrying radar sounder instruments. However the active radio environment of Jupiter makes radar sounding a challenging objective. Preliminary results obtained with a purpose-made multilayer coherent simulator using band-limited white noise over a procedurally-generated DEM indicate that, in low-clutter environments, passive sounding is able to detect deep subsurface layers in situations where active sounding echoes are overtaken by Jupiter's noise.

### Acknowledgements

This work was supported by the Italian Space Agency under Contract ASI/INAF n.2013-056-R.O Partecipazione italiana alla fase A/B1 della missione JUICE.

### References

- [1] B. Cecconi et al. Natural radio emission of jupiter as interferences for radar investigations of the icy satellites of jupiter. *Planetary and Space Science*, 61(1):32–45, 2012.
- [2] A. Romero-Wolf et al. A passive probe for subsurface oceans and liquid water in jupiter's icy moons. *Icarus*, 248:463–477, 2015.
- [3] D. Schroeder et al. Assessing the potential for passive radio sounding of europa and ganymede with rime and reason. *Planetary and Space Science*, 134:52–60, 2016.
- [4] C. Grima et al. Radar signal propagation through the ionosphere of europa. *Planetary and Space Science*, 117:421–428, 2015.
- [5] C. Gerekos et al. A new technique for simulating radar echoes from layered subsurface targets. In *Geoscience and Remote Sensing Symposium (IGARSS)*, 2018, accepted for publication.
- [6] E. Heggy et al. Radar probing of jovian icy moons: Understanding subsurface water and structure detectability in the juice and europa missions. *Icarus*, 285:237–251, 2017.

# **JUICE: A European mission to explore the emergence of habitable worlds around gas giants**

O. Witasse (1), the JUICE Science Working Team and the JUICE Project Team

(1) European Space Agency, Noordwijk, The Netherlands (owitasse@cosmos.esa.int)

## **Abstract**

JUICE - JUPiter ICy moons Explorer - is the first large mission in the ESA Cosmic Vision 2015-2025 programme. The mission was selected in May 2012 and adopted in November 2014. The implementation phase started in July 2015, following the selection of the prime industrial contractor, Airbus Defense and Space (Toulouse, France). Due to launch in May/June 2022 and to arrive at Jupiter in October 2029, it will spend at least three ½ years making detailed observations of Jupiter and three of its largest moons, Ganymede, Callisto and Europa. The status of the important project milestones in 2018 are presented.

## **1. Science Objectives**

The focus of JUICE is to characterise the conditions that might have led to the emergence of habitable environments among the Jovian icy satellites, with special emphasis on the three worlds, Ganymede, Europa, and Callisto, likely hosting internal oceans [1,2]. Ganymede, the largest moon in the Solar System, is identified as a high-priority target because it provides a unique and natural laboratory for analysis of the nature, evolution and potential habitability of icy worlds and waterworlds in general, but also because of the role it plays within the system of Galilean satellites, and its special magnetic and plasma interactions with the surrounding Jovian environment. The mission also focuses on characterising the diversity of coupling processes and exchanges in the Jupiter system that are responsible for the changes in surface and space environments at Ganymede, Europa and Callisto, from short-term to geological time scales. Focused studies of Jupiter's

atmosphere and magnetosphere, and their interaction with the Galilean satellites will further enhance our understanding of the evolution and dynamics of the Jovian system. The overarching theme for JUICE is: The emergence of habitable worlds around gas giants. At Ganymede, the mission will characterise in detail the ocean layers; provide topographical, geological and compositional mapping of the surface; study the physical properties of the icy crusts; characterise the internal mass distribution, investigate the exosphere; study Ganymede's intrinsic magnetic field and its interactions with the Jovian magnetosphere. For Europa, the focus will be on the surface composition, understanding the formation of surface features and subsurface sounding of the icy crust over recently active regions. Callisto will be explored as a witness of the early solar system trying to also elucidate the mystery of its internal structure. JUICE will perform a multidisciplinary investigation of the Jupiter system as an archetype for gas giants. The Jovian atmosphere will be studied from the cloud tops to the thermosphere. The focus in Jupiter's magnetosphere will include an investigation of the three dimensional properties of the magnetodisc and in-depth study of the coupling processes within the magnetosphere, ionosphere and thermosphere. JUICE will study the moons' interactions with the magnetosphere, gravitational coupling and long-term tidal evolution of the Galilean satellites.

## **2. The Payload**

The JUICE payload consists of 10 state-of-the-art instruments plus one experiment that uses the spacecraft telecommunication system with ground-based instruments. This payload is capable of addressing all of the mission's science goals [1,2], from in situ measurements of the plasma environment, to remote observations of the surface and interior of the three icy moons, Ganymede, Europa and Callisto, and of Jupiter's atmosphere. A remote sensing package includes imaging (JANUS)

and spectral-imaging capabilities from the ultraviolet to the sub-millimetre wavelengths (MAJIS, UVS, SWI). A geophysical package consists of a laser altimeter (GALA) and a radar sounder (RIME) for exploring the surface and subsurface of the moons, and a radio science experiment (3GM) to probe the atmospheres of Jupiter and its satellites and to perform measurements of the gravity fields. An in situ package comprises a powerful suite to study plasma and neutral gas environments (PEP) with remote sensing capabilities via energetic neutrals, a magnetometer (J-MAG) and a radio and plasma wave instrument (RPWI), including electric fields sensors and a Langmuir probe. An experiment (PRIDE) using ground-based Very Long Baseline Interferometry (VLBI) will support precise determination of the spacecraft state vector with the focus at improving the ephemeris of the Jovian system.

### 3. The mission profile

The mission is due to launch from Kourou with an Ariane 5 ECA. The baseline launch is 1<sup>st</sup> of June 2022, which is in the middle of a 20 days launch window. There are backup launch slots two or three times per year. The interplanetary transfer sequence relies on gravity assist with Venus, the Earth and Mars. The Jupiter orbit insertion will be performed in October 2029. An initial Ganymede swing-by is performed just before the capture manoeuvre. The tour of the Jupiter system, as currently designed, starts with a series of three Ganymede swing-bys. The spacecraft is transferred to Callisto to initiate the Europa science phase, one year after the Jupiter insertion. This phase is composed of two fly-bys, separated by 15 days, with closest approach at 400 km altitude. The next phase is a 200-day period characterised by an excursion at moderate inclinations, in order to investigate regions of the Jupiter environment away from the equatorial plane. A series of resonant transfers with Callisto raise the inclination with respect to Jupiter's equator to a maximum value of about 28 deg. The spacecraft is then transferred from Callisto to Ganymede with a series of Callisto and Ganymede flybys, followed by a gravitational capture with the moon. The science phase around Ganymede is decomposed into a first elliptic subphase, a circular orbit at 5000 km altitude followed by a second elliptic subphase, and then a circular phase at 500 km altitude. The total duration of the Ganymede orbital phase is about nine months,

the end of mission being planned in September 2033. The spacecraft will eventually impact the surface.

## References

- [1] JUICE Definition Study Report, Reference ESA/SRE(2014)1, 2014. <http://sci.esa.int/juice/54994-juice-definition-study-report/>
- [2] Grasset, O., et al., Jupiter ICy moons Explorer (JUICE): An ESA mission to orbit Ganymede and to characterise the Jupiter system, Planetary and Space Science, Volume 78, p. 1-21, 2013

# Viscous tidal dissipation in Enceladus's ocean

Jérémy Rekier (1), A. Trinh (1,2), S. A. Triana (1) and V. Dehant (1,2)  
 (1) Royal Observatory of Belgium (2) Université Catholique de Louvain, Belgium  
 (jeremy.rekier@observatory.be)

## Abstract

We compute the energy dissipation inside Enceladus's ocean using a two step approach in which we first compute the displacement induced on the planet by the periodic tidal potential caused by its nearest companion (Saturn). We then use the value of the (periodic) displacement at the ocean's boundaries as a forcing for the momentum (Navier-Stokes) equation.

## 1. Introduction

Enceladus has a global ocean about 40kms deep (see e.g. [Beuthe et al., 2016]). Observations of its south pole reveals the presence of geysers. The source of energy that powers those geysers is still debated. one possible mechanism is viscous dissipation within the ocean induced by tidal forcing from Saturn. Previous estimations have relied on the thin layer approximation to model the ocean as a two-dimensional surface using the Laplace Tidal Equations [Matsuyama et al., 2018]. however, the thickness of the ocean amounts to 15% of Enceladus's radius. In addition, viscous dissipation estimated from boundary layer theory neglects the contribution of internal shear layers which are likely to fill the volume of the ocean. In the present study, we do away with this approximation as we solve for the linearised momentum equation numerically. We use a new efficient linearised spectral method which allows us to reach the a value of the viscosity parameter which matches the actual value inside Enceladus's ocean. We compare our results to those obtained within the thin layer approximation.

## 2. Method

### 2.1 Displacement due to tidal forcing

We model Enceladus's ocean as a spherical shell enclosed within solid impervious boundaries that constitute the core and the crust. Saturn's motion observed from Enceladus's reference frame induces a varying

gravity potential which, in turn, deforms the crust and the core, i.e, the boundaries of the ocean. The first step in our model consists in computing that motion by solving the gravito-elastic equations for a three-layer model. The resulting displacement is then imposed as a surface forcing in the next step of the model.

### 2.2 Momentum equation

The linearised Navier-Stokes equation in the reference frame tied to Enceladus's surface reads (in the frequency domain):

$$i\omega\vec{u} + 2(\vec{\Omega} \times \vec{u}) + \vec{\nabla}p - \text{Ek}\nabla^2\vec{u} = 0, \quad (1)$$

where  $p$  is the reduced pressure and includes the gravitational, centrifugal and tidal potentials. All the dynamical effects of the tidal forcing happen via the condition that the velocity field must be continuous across the fluid's boundary.

### 2.3 Numerical resolution

We assume that the fluid is incompressible,  $\vec{\nabla} \cdot \vec{u} = 0$ , this allows to decompose the velocity field as

$$\vec{u} = \vec{\nabla} \times \vec{\nabla} \times (P\vec{r}) + \vec{\nabla} \times (T\vec{r}). \quad (2)$$

We use a spectral decomposition in spherical harmonics and Chebyshev polynomials respectively in the angular and radial directions for the scalar functions  $P$  and  $T$ . We then solve simultaneously the radial projection of the curl and the double curl of Eq. (1). The discretised version of the resulting expressions together with the condition of continuity at the boundary form an algebraic problem of the type  $\mathbf{A}\vec{x} = \vec{b}$ . Fig. 1 shows a graphic representation of the matrix  $\mathbf{A}$  at low resolution. Once the algebraic problem is solved, one can reconstruct the velocity field which can then be used to compute the total viscous dissipation

$$D \equiv \text{Ek} \int_{\mathcal{V}} d\mathcal{V} \vec{u} \cdot \nabla^2 \vec{u}. \quad (3)$$

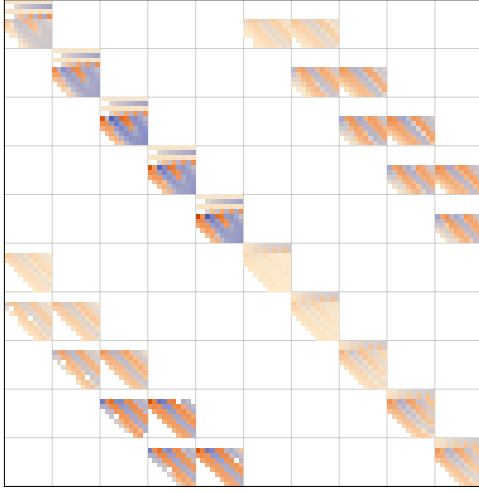


Figure 1: Low resolution illustration of the matrix used in the algebraic problem resulting from the discretisation of Eq. (1) and the condition that  $\vec{u}$  should be continuous at the physical boundary.

### 3. Discussion and remarks

The efficiency of the spectral method used in the present study allows to solve the momentum equations at very small values of the Ekman number,  $Ek$ , that correspond to the actual value relevant for Enceladus ( $Ek \sim 10^{-10}$ ). This is usually the most stringent limiting factor in numerical simulations of rotating fluids. In principle, it would be possible to extend our analysis to account for the non-spherical figure of Enceladus in which case it would be impossible to use such low values of  $Ek$ .

### Acknowledgements

This research has received funding from the European Research Council (ERC) under the European Union's Horizon 2020 research and innovation programme (Advanced Grant agreement No 670874).

### References

- [Beuthe et al., 2016] Beuthe, M., Rivoldini, A., and Trinh, A. (2016). Enceladus's and dione's floating ice shells supported by minimum stress isostasy. *Geophysical Research Letters*, 43(19).
- [Matsuyama et al., 2018] Matsuyama, I., Beuthe, M., Hay, H. C., Nimmo, F., and Kamata, S. (2018). Ocean tidal heating in icy satellites with solid shells. *Icarus*, 312:208 – 230.

# Heat and water generation in the vicinity of Europa's strike-slip faults

Kateřina Sládková (1), Ondřej Souček (2) and Klára Kalousová (1)

(1) Department of Geophysics, Charles University, Czech Republic (sladkova@karel.troja.mff.cuni.cz),

(2) Mathematical Institute, Charles University, Czech Republic

## Abstract

In this study, we investigate the onset of melting below Europa's recently active strike-slip faults and assess the stability of generated meltwater. We extend our previous study of water generation and its transport in the vicinity of strike-slip faults on Europa [3] by improving the model of internal heating due to frictional and bulk deformation. This is achieved through coupling of the original code with a model of tidally-induced deformation of a viscoelastic Maxwellian body. Our preliminary results indicate that the dissipation at the fault may be large enough to generate liquid water thus confirming the previous results. However, the new approach allows us to investigate the process of melting on the fault in a more self-consistent way.

## 1. Introduction

Jupiter's moon Europa has a very young surface with an abundance of unique terrains that indicate recent endogenic activity [2]. Morphological models and spectral observations suggest that it might possess shallow lenses of liquid water within its outer ice shell [5, 6]. We revisit our previous study on generation and transport of water below the strike-slip faults on Europa [3] where a constant heating amplitude was prescribed and improve the model of heat generation.

Following up the work of [4] we compute the response of a Maxwellian body subjected to shear motions that mimic the tidal forcing. As a result, bulk and frictional dissipation is calculated which provides a heat source in the two-phase convection model presented in our previous study [3]. Thermal evolution computed by the convection code in turn determines the parameters that govern the slip at the fault and thus the associated dissipative heating.

## 2. Numerical model

For the convection part of the model, the equations for two-phase flow of a compressible mixture of ice and liquid water [3] are employed. These allow us to consistently address melting of ice and the subsequent meltwater advection by Rayleigh-Taylor instabilities.

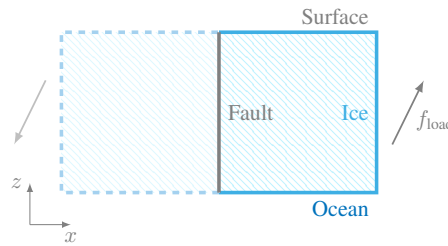


Figure 1: Sketch of the physical model. The arrows indicate the tidally-induced strike-slip forcing, the computational domain is represented by solid lines.

The response of a Maxwellian body is computed by solving the Stokes equation:

$$\text{div } \sigma = 0, \quad (1)$$

where  $\sigma$  is the Cauchy stress tensor described by incompressible Maxwell rheology:

$$\sigma = 2\mu\mathbb{D}_d(\mathbf{u}) - \frac{\mu}{\eta} \int_0^t \sigma(t') dt', \quad (2)$$

where  $\mathbb{D}_d(\mathbf{u})$  is a deviatoric part of the symmetric displacement gradient,  $\mu, \eta$  are shear modulus and viscosity, respectively, and  $t$  is time.

We can further simplify the previous equations by allowing the strike-slip motion only along the fault plane and by neglecting other than gravitational and tidal forces. Then, the problem can be rewritten in the form of a single vector equation:

$$\nabla_{x,z} \cdot (\mathcal{K} \Sigma) + \nabla_{x,z} \cdot (\mathcal{L} v) = 0, \quad (3)$$

where  $\mathcal{K}, \mathcal{L}$  are parameters dependent on viscosity, shear stress and time step according to the applied rheology (viscoelastic or the viscous/elastic limits),  $\Sigma = (\sigma_{xy}, \sigma_{yz})$  and  $v$  is the velocity. The tidal loading is then enforced through a boundary condition on the right side of the domain (cf. Figure 1).

On the left side, the fault is described through the Navier-slip boundary condition, where the slip velocity equals one half of the relative slip rate.

The fault behaviour is simulated through a pseudo-plastic stress-limiting viscosity dependent on the yield stress  $\sigma_Y$ , which, in our model, represents the friction coefficient and controls the depth of the fault:

$$\eta = \frac{\eta^\infty}{\left\{1 + \left(\frac{\eta^\infty |v|}{\sigma_Y}\right)^\alpha\right\}^{\frac{1}{\alpha}}}, \quad (4)$$

where  $\alpha$  is a parameter and  $\eta^\infty$  is a background viscosity.

Our model is implemented in the open-source finite element software package FEniCS [1], consequently we present equation (3) in the weak form and discretized in time:

$$\begin{aligned} & \int_{\Omega} \mathcal{L}^{k+1} \nabla_{x,z} v^{k+1} \cdot \nabla_{x,z} v' \, dx \\ &= - \int_{\Omega} \mathcal{K}^{k+1} \Sigma^k \cdot \nabla_{x,z} v' \, dx \\ &- \int_{\partial\Omega_L} 2v \frac{\eta^\infty}{\left(1 + \left(\frac{2\eta^\infty |v|}{\sigma_Y}\right)^\alpha\right)^{1/\alpha}} v' \, ds \\ &+ \int_{\partial\Omega_R} f_{\text{load}}(t^{k+1}) v' \, ds, \end{aligned} \quad (5)$$

where the indices  $k, k+1$  indicate the time step,  $\Omega, \partial\Omega_L, \partial\Omega_R$  denote the computational domain and its left and right boundary, respectively,  $f_{\text{load}}$  is the loading force and  $v'$  is the test function. In the numerical scheme, we employ a fixed point iteration to ensure better approximation of the slip velocity in the viscosity expression (4).

### 3. Preliminary results

In our reference simulation, the domain is strained by a force equivalent to  $3 \times 10^5$  Pa. Figure 2 shows the preliminary results for the slip velocity (left) and the temperature (right). In this setting, the fault propagates to approximately one third of the domain's depth. Deformation on the fault and the associated dissipation lead to substantial heating and increase in temperature at the fault tip. A parametric study and comparison

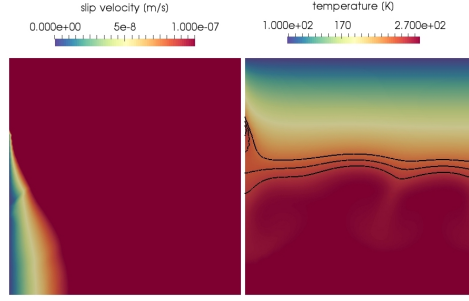


Figure 2: Preliminary results of simulation with the loading force equivalent to  $3 \times 10^5$  Pa prescribed on the right boundary: slip velocity (left) and temperature (right, contours mark 230, 240 and 250 K). Note the temperature increase in the vicinity of the fault tip.

with the previous results will be presented at the meeting.

### Acknowledgements

K.S. acknowledges support from Charles University through projects GA UK (project number 304217) and SVV-2018-260447. This work has been supported by the IT4Innovations Centre of Excellence project (project number OPEN-12-21) and by Charles University Research program No. UNCE/SCI/023 (O.S., K.K.).

### References

- [1] Alnaes, M. S., et al.: The FEniCS Project Version 1.5, Archive of Numerical Software, vol. 3, 2015.
- [2] Bierhaus, E. B., et al.: Europa's crater distributions and surface ages, in Europa, pp. 161–180, Univ. of Arizona Press, Tucson, 2009.
- [3] Kalousová, K., et al.: Water generation and transport below Europa's strike-slip faults, JGR-Planets, 121, 2444–2463, 2016.
- [4] Nimmo, F., and Gaidos, E.: Strike-slip motion and double ridge formation on Europa, JGR, 107, E45021, 2002.
- [5] Roth, L., et al.: Transient water vapor at Europa's south pole, Science, 343, 171–174, 2014.
- [6] Schmidt, B. E., et al.: Active formation of chaos terrain over shallow subsurface water on Europa, Nature, 479, 502–505, 2011.



# Onboard Detection of Thermal Anomalies for Europa Clipper

Gary Doran (1), **Ashley G. Davies** (1), Kiri L. Wagstaff (1), Saadat Anwar (2), Diana L. Blaney (1), Steve Chien (1), Phil Christensen (2), and Serina Diniega (1). (1) Jet Propulsion Laboratory, California Institute of Technology, Pasadena, CA, USA, (2) Arizona State University, Tempe, AZ, USA (Gary.Doran.Jr@jpl.nasa.gov)

## 1. Introduction

The *Europa Clipper* mission seeks to assess the habitability of Jupiter's moon Europa [6, 1]. *Europa Clipper*'s payload comprises nine instruments, including the Europa Thermal Emission Imaging System (E-THEMIS) for detecting thermal anomalies (e.g., hot spots) and the Mapping Imaging Spectrometer for Europa (MISE) for assessing composition. E-THEMIS can detect melting ice and other surface anomalies from 40,000 km above the surface. MISE covers the range 0.8–5.0  $\mu\text{m}$  and can distinguish between water ice phases, organics, salts, etc. [2].

*Europa Clipper* will conduct  $\sim 45$  flybys of Europa. The large Earth–Jupiter distance severely constrains the amount of data that can be downlinked from the spacecraft. To help maximize the scientifically valuable data returned by the mission, we are investigating approaches to perform basic data analysis onboard the spacecraft to identify the most relevant and valuable data to downlink with a higher priority.

Onboard science data analysis has been employed for Earth orbiters such as EO-1 to detect and prioritize biosignatures in Europa-analogue settings, such as biomediated sulfur deposits on glaciers [5]. The Mars Science Laboratory rover analyzes images as they are collected, then commands the ChemCam laser spectrometer to collect spectra of the most interesting rock

targets, without human intervention [4]. A previous study determined that the THEMIS instrument in Mars orbit could reliably detect thermal anomalies, aerosols, and ice features of interest [3].

Europa observations of high interest include those containing thermal and spectral anomalies that could signal the presence of hot spots, plumes, or deposits of organic materials at the surface. Any thermal anomalies detected in E-THEMIS data can also potentially inform prioritization of coincident MISE data during closer approach in the same flyby.

## 2. THEMIS Anomaly Detection

To develop and evaluate onboard thermal anomaly detection algorithms, we use data from analog instruments flown on previous missions. In particular, the THEMIS instrument on the Mars Odyssey spacecraft is a thermal imaging instrument and predecessor of the E-THEMIS instrument. We have applied an approach for onboard THEMIS anomaly detection [3] to THEMIS data observed since the original study in 2007. Our updated analysis encompasses 56,985 observations from the start of the mission through 2017 taken after midnight but before dawn local time between  $-60$  and  $60$  degrees latitude.

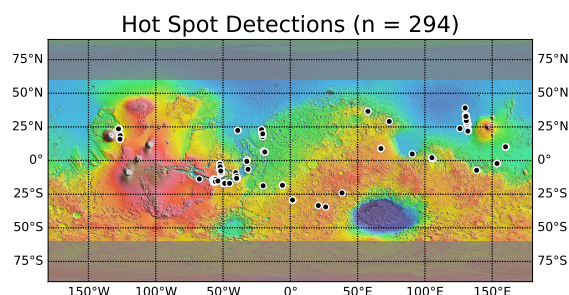


Figure 1: Hot spot detections ( $\geq 240$  K) from 14 years of THEMIS Mars data. Base map is MOLA elevation.

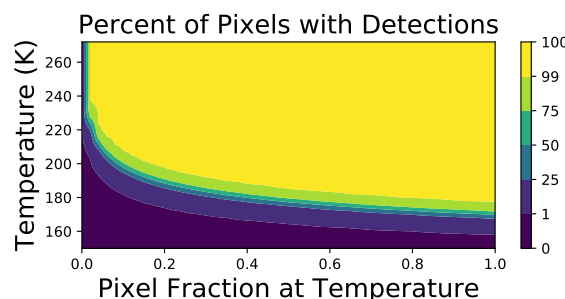


Figure 2: Characterizing the probability of detection across all pixels for injected thermal anomalies of various sizes and temperatures in NIMS observations at  $\alpha = 0.05$  significance.



The detection algorithm converts digital numbers to temperatures, then flags pixels  $\geq 240$  K as anomalous. If an observation contains too many pixels exceeding this threshold, it is discarded. After filtering these poorly calibrated observations, only a small fraction of pixels exceed this threshold, and no pixel exceeded 248 K. Adjacent pixels exceeding the 240 K threshold are clustered together into single “detections,” shown in Figure 1.

The detected hot spots occur in regions with high thermal inertia (e.g., exposed outcrop) that remain relatively warm during the night. A similar detection algorithm onboard *Europa Clipper* could be used to find endogenic heat sources on Europa (employing a lower temperature threshold).

### 3. NIMS Anomaly Detection

Observations of Europa by the Galileo NIMS instrument (0.7–5.2  $\mu\text{m}$ ) provide a good analogue for future MISE observations. We injected synthetic thermal anomalies into real NIMS data, then assessed our ability to detect those anomalies.

First, we compute a blackbody spectrum as observed by NIMS for a given temperature and viewing geometry with the original observation. We linearly combine this spectrum with each pixel in the observation, proportional to the intended anomaly size (we assume no existing thermal anomalies). Next, to detect the presence of a thermal anomaly, we compare the radiances in the 5–5.2  $\mu\text{m}$  range to the radiances in the 3.5–4.5  $\mu\text{m}$  range using Welch’s  $t$ -test. Finally, we compute the fraction of pixels for which the anomalies are detected, with a Bonferroni correction to account for the multiple hypothesis tests across every pixel in an observation.

Figure 2 shows the detection rate across all pixels in 14ENSUCOMP01A as the anomaly temperature and size is varied. For example, an anomaly at 190 K that comprises 50% of the 1.6  $\text{km}^2$  pixel is detected over 80% of the time.

We have also run the detection algorithm on the original observation with no anomalies injected. There are several pixels in the 14ENSUCOMP01A observation that have relatively low  $p$ -values, though not low enough to be significant under the threshold used in the previous analysis. The radiance curves for these pixels increase after 5  $\mu\text{m}$ , but it is difficult to determine whether the observed increase is evidence of a signal or due to noise. Nevertheless, these detections show that the algorithm identifies observations that merit further investigation.

## 4. Conclusion and Future Work

Our current results show that it is possible to use on-board methods to quickly flag data for high-priority downlink and investigation. Our next step is to investigate thermal anomaly detection algorithms using simulated data from the E-THEMIS instrument. We will use a Europa thermal model to simulate background temperatures, then inject synthetic thermal anomalies as above. We will also investigate the detection of spectral anomalies that indicate interesting minerals or deposits of organic materials on the surface.

## Acknowledgments

Part of this research was carried out at the Jet Propulsion Laboratory, California Institute of Technology, under a contract with the National Aeronautics and Space Administration.

## References

- [1] T. Bayer, B. Buffington, J. F. Castet, M. Jackson, G. Lee, K. Lewis, J. Kastner, K. Schimmels, and K. Kirby. Europa mission update: Beyond payload selection. In *2017 IEEE Aerospace Conference*, pages 1–12, 2017.
- [2] D. L. Blaney, R. N. Clark, J. B. Dalton, A. G. Davies, R. O. Green, M. M. Hedman, C. A. Hibbits, Y. Langevin, J. I. Lunine, T. B. McCord, C. Paranicas, S. L. Murchie, F. P. Seelos, and J. M. Soderblom. The Mapping Imaging Spectrometer for Europa (MISE) investigation: Exploring Europa’s habitability using compositional mapping. In *48th LPSC*, 2017.
- [3] R. Castano, K. L. Wagstaff, S. Chien, T. M. Stough, and B. Tang. On-board analysis of uncalibrated data for a spacecraft at Mars. In *13th Int’l Conf. on Knowledge Discovery and Data Mining*, pages 922–930, 2007.
- [4] R. Francis, T. Estlin, D. Gaines, G. Doran, O. Gasnault, S. Johnstone, S. Montañó, V. Mousset, V. Verma, B. Bornstein, M. Burl, S. Schaffer, and R. C. Wiens. AEGIS intelligent targeting deployed for the Curiosity rover’s ChemCam instrument. In *47th LPSC*, 2016.
- [5] L. Mandrake, U. Rebbapragada, K. Wagstaff, D. Thompson, S. Chien, D. Tran, R. Pappalardo, D. Gleeson, and R. Castañó. Surface sulfur detection via remote sensing and onboard classification. *ACM Transactions on Intelligent Systems Technology*, 3(4):Article 77, 2012.
- [6] R. T. Pappalardo, D. A. Senske, H. Korth, R. Klima, S. D. Vance, K. Craft, and the Europa Science Team. The Europa Clipper mission: Exploring the habitability of a unique icy world. In *European Planetary Science Congress*, 2017.

# Exploring Europa's Habitability: The Europa Clipper on the Path to Critical Design

**Haje Korth** (1), Robert T. Pappalardo (2), David A. Senske (2), Rachel L. Klima (1), Christina R. Richey (2), Kate L. Craft (1), and the Europa Science Team. (1) The Johns Hopkins University Applied Physics Laboratory, Laurel, MD, USA, (2) Jet Propulsion Laboratory, California Institute of Technology, Pasadena, CA, USA (haje.korth@jhuapl.edu).

## Abstract

By investigating the potential habitability of Jupiter's moon Europa, the Europa Clipper mission will aid understanding of habitability across the solar system. With passing of the Preliminary Design Review, the mission is on the path to enter full implementation. Here we present the mission's science objectives and an updated view of the scientific payload and mission design moving toward the final design and fabrication phase.

## 1. Mission Goal and Objectives

The overarching science goal of the Europa mission is to explore Europa to investigate its habitability. Following from this goal are three Mission Objectives: (1) characterize the ice shell and any subsurface water, including their heterogeneity, ocean properties, and the nature of surface-ice-ocean exchange; (2) understand the habitability of Europa's ocean through composition and chemistry; and (3) understand the formation of surface features, including sites of recent or current activity, and characterize high science interest localities. Folded into these three objectives is the desire to search for and characterize any current activity, notably plumes and thermal anomalies.

## 2. Exploring Europa Through Synergistic Investigations

To address the science questions of the Europa mission, NASA selected a scientific payload comprised of five remote-sensing instruments, which observe in the wavelength range from the ultraviolet through radio (radar), and four *in situ* instruments, which measure fields and particles. The capability of the science payload includes the following investigations: The *Europa Ultraviolet Spectrograph* (*Europa-UVS*) will measure the composition,

chemistry, structure, and variability of Europa's tenuous atmosphere. In addition, it will characterize the plasma environment and search for and characterize any active plumes to constrain surface composition and microphysics and relationships to endogenic and exogenic processes. The *Europa Imaging System* (*EIS*) will map Europa globally at 100 m resolution and image almost any point on the surface at better than 20 m resolution to provide constraints on the formation of surface features and insight into small-scale regolith processes, search for active plumes, and characterize the ice shell through modeling of the limb shape. The *Mapping Imaging Spectrometer for Europa* (*MISE*) will observe the distribution of surface compounds to identify and map the distributions of organics, salts, acid hydrates, water ice phases, altered silicates, radiolytic compounds, and warm thermal anomalies. The *Europa Thermal Imaging System* (*E-THEMIS*) will detect and characterize thermal anomalies that may indicate current or recent activity and provide information on thermal inertia to characterize regolith particle size, block abundance, and subsurface layering. The *Radar for Europa Assessment and Sounding: Ocean to Near-surface* (*REASON*) will map Europa's vertical crustal structure and search for shallow subsurface water and the deeper ice-ocean interface to provide insight into material exchange among the ocean, ice shell, surface, and atmosphere, and constrain the amplitude and phase of the tides. The *Interior Characterization of Europa using Magnetometry* (*ICEMAG*) investigation will measure magnetic fields generated by currents induced in Europa's subsurface ocean, ionized material ejected from any plumes, and electromagnetic coupling of the moon to Jupiter. The *Plasma Instrument for Magnetic Sounding* (*PIMS*) will measure ions and electrons in Europa's atmosphere to infer the contributions to the magnetic field from plasma currents and to understand the interaction and coupling of the plasma with the

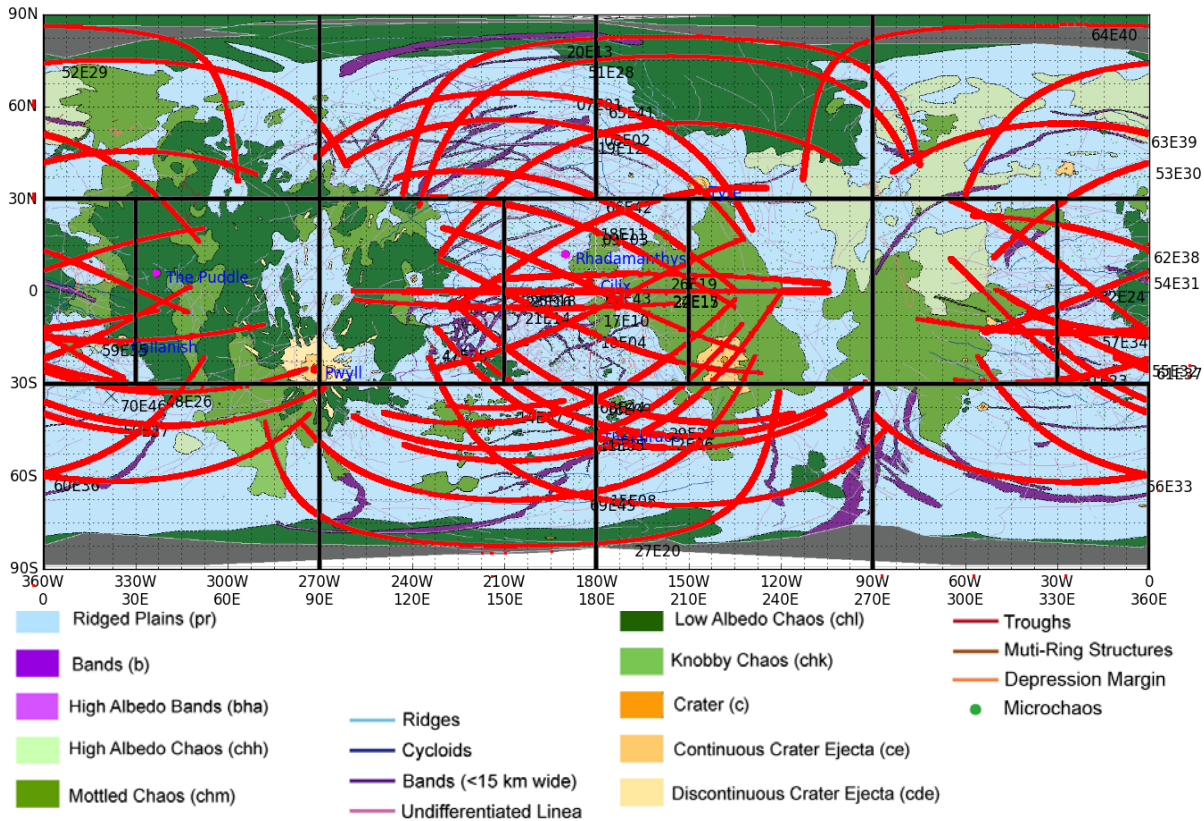


Figure 1: Planned Europa Clipper close approach ground tracks below 1000 km altitude (red) overlaid on the geologic map of Europa [1]. Blue areas are dominated by ridges. Purple areas are bands. Orange and yellow colors are associated with impact features. Chaos, pits, domes, and dark plains are most strongly concentrated in the green areas, but small examples are also found outside these regions.

moon's surface and with Jupiter. The *MASS Spectrometer for Planetary Exploration (MASPEX)* will measure trace neutral species to determine the composition in Europa's sputter-produced exosphere and potential plumes. Finally, the *Surface Dust Analyzer (SUDA)* will map the chemical composition of particles ejected from Europa's surface and identify the makeup of potential plumes by directly sampling microscopic particles originating from the surface, entrained in the plumes, or delivered from elsewhere within or outside the Jovian system. In addition, the spacecraft's telecommunication system in combination with radar altimetry will enable geodesy, and the spacecraft's radiation monitoring system will provide information on Europa's energetic particle environment.

The current tour consists of 46 Europa flybys below 1000 km numbered E01 through E46, shown in Figure 1 superposed on the geologic map of Europa [1]. The altitudes of closest approach

typically range from 25 km to 100 km. The tour is divided into two principal campaigns, visiting first the anti-Jovian hemisphere followed by observations of the sub-Jovian hemisphere. As seen in Figure 1, flybys occur over a rich variety of terrains, including ridges, bands, impact features, chaos, domes, pits, and plains.

Working together, the Europa mission's robust investigation suite can be used to test hypotheses and enable discoveries relevant to the interior, composition, and geology of Europa, thereby addressing the potential habitability of this intriguing ocean world.

## References

[1] Leonard et al., Updating the global geologic map of Europa, Lunar and Planetary Science Conference 48, #2357, 2017.

## Triton: Exploring a Candidate Ocean World

**Louise M. Prockter** (1), Karl L. Mitchell (2), David A. Bearden (2), William D. Smythe (2)

(1) Lunar and Planetary Institute, Universities Space Research Association, Houston, TX, USA

(2) Jet Propulsion Laboratory, Pasadena, CA, USA (prockter@lpi.usra.edu)

### Scientific background

Neptune's moon Triton was one of the most unusual and surprising bodies observed as part of the Voyager mission. During its distant flyby in 1989, Voyager 2 captured a series of images, mostly of the southern, sub-Neptune hemisphere, establishing Triton as one of a rare class of solar system bodies with a substantial atmosphere and active geology. Although Triton is, like many other bodies, subject to the tidal, radiolytic, and collisional environment of an icy satellite, its starting point and initial composition was that of a Dwarf Planet originating in the KBO. It is this duality as both captured dwarf planet and large icy satellite that has undergone extreme collisional and tidal processing that gives us a unique target for understanding two of the Solar System's principal constituencies and the fundamental processes that govern their evolution. Thus, comparisons between Triton and other icy objects will facilitate re-interpretation of existing data and maximize the return from prior NASA missions, including *New Horizons*, *Galileo*, *Cassini* and *Dawn*.

Triton has a remarkable but poorly understood surface and atmosphere that hint strongly at ongoing geological activity, suggesting an active interior and a possible subsurface ocean. Crater counts suggest a typical surface age of <10 Ma (Schenk and Zahnle, 2007), with more conservative upper estimates of ~50 Ma on more heavily cratered terrains, and ~6 Ma for the Neptune-facing cantaloupe terrain. These results imply that Triton almost certainly has the youngest surface age of any planetary body in the solar system, with the exception of the violently volcanic world, Io. The lack of compositional constraints obtained during Voyager, largely due to the lack of an infrared spectrometer, means that many of Triton's surface features have been interpreted as possibly endogenic based on comparative

photogeology alone. Candidate endogenic features include: a network of tectonic structures, including most notably long linear features which appear to be similar to Europa's double ridges (Prockter et al., 2005); several candidate cryovolcanic landforms (Croft et al., 1995), best explained by the same complex interaction among tidal dissipation, heat transfer, and tectonics that drives resurfacing on Europa, Ganymede, and Enceladus; widespread cantaloupe terrain, unique to Triton, is also suggested non-uniquely to be the result of vertical (diapiric) overturn of crustal materials (Schenk and Jackson, 1993); and several particulate plumes and associated deposits. Despite an exogenic solar-driven solid-state greenhouse effect within nitrogen ices being preferred initially (Kirk et al., 1990), some are starting to question this paradigm (Hansen and Kirk, 2015) in the context of observations of regionally-confined eruptive on the much smaller Enceladus.

The possibility of an endogenic heat source is considered more likely over the past few years, given recent studies that have suggested sufficient heat to maintain an internal ocean. Radiogenic heating alone may play an important role, possibly providing sufficient heat to sustain an ocean over ~4.5 Ga (Gaeman et al., 2012). Capture into orbit around Neptune (McKinnon, 1984; Agnor and Hamilton, 2006, and references therein) would have almost certainly resulted in substantial heating (McKinnon et al., 1995). The time of capture is not constrained, but if sufficiently recent some of that heat may be preserved. Finally, despite having a highly circular orbit, Triton's high inclination also results in significant obliquity, which should be sufficient to maintain an internal ocean if sufficient "antifreeze" such as NH<sub>3</sub> is present (Nimmo and Spencer, 2015). Confirmation of the presence of an ocean would establish Triton as arguably the most exotic and

probably the most distant ocean world in the solar system, potentially expanding the habitable zone. Even without the presence of an ocean and endogenic activity, Triton remains one of the most compelling targets in the solar system. Triton's atmosphere is thin,  $\sim 1$  Pa,  $10^{-5}$  bar, but sufficiently substantial to be a major sink for volatiles, and sufficiently dynamic to play a role in movement of surface materials. Its youthful age implies a highly dynamic environment, with surface atmosphere volatile interchange, and potentially dramatic climate change happening over obliquity and/or season timescales. An extensive south polar cap, probably mostly consisting of nitrogen which can exchange with the atmosphere, was observed. No north polar cap was detected, in part due to a lack of high northern latitude image coverage, but even so we would have expected to have observed the outer limits of such a structure, implying a dichotomy. The presence of methane in the atmosphere, and possibly on the surface, makes possible a wide range of "hot atom" chemistry allowing higher order organic materials to be produced in a similar albeit slower manner to Titan. The presence of such materials is of potential importance to habitability, especially if conditions exist where they come into contact with liquid water.

## Mission concept

We have identified an optimized solution to enable a New Horizons-like fast flyby of Triton in 2038 that appears at this preliminary stage to fit within the Discovery 2019 cost cap. The mission concept uses high heritage components and builds on the New Horizons concepts of operation. Our overarching science goals are to determine: (1) if Triton has a subsurface ocean; (2) why Triton has the youngest surface of any icy world in the solar system, and which processes are responsible for this; (3) the nature of Triton's plumes and their energy source; and (4) Triton's internal state and thermal history. If an ocean is present, we seek to determine its properties and whether the ocean interacts with the surface environment. To address these questions, we propose a focused instrument suite consisting of:

- (1) a magnetometer, primarily for detection of the presence of an induced magnetic field which would indicate compellingly the presence of an ocean;
- (2) a camera, for imaging of the mostly unseen anti-Neptune hemisphere, and repeat imaging of the sub-

Neptune hemisphere to look primarily for signs of change;

- (3) an infrared imaging spectrometer with spectral range up to 5  $\mu$ m, suitable for detection and characterization of surface materials at the scales of Triton's features.

In addition to the Triton science, opportunistic Neptune science data will also be acquired.

## Acknowledgments

Some of this research was carried out at the California Institute of Technology Jet Propulsion Laboratory under a contract from NASA.

## References

- Agnor C.B. and Hamilton D.P. (2006). Neptune's capture of its moon Triton in a binary-planet gravitational encounter. *Nature*, 441 (7090), 192.
- Croft, S. K., Kargel, J. S., Kirk, R. L., Moore, J. M., Schenk, P. M., & Strom, R. G. (1995). The geology of Triton. In *Neptune and Triton* (pp. 879-947).
- Gaeman, J., Hier-Majumder, S., & Roberts, J. H. (2012). Sustainability of a subsurface ocean within Triton's interior. *Icarus*, 220(2), 339-347.
- Hansen, C. J., & Kirk, R. (2015, March). Triton's Plumes---Solar-Driven Like Mars or Endogenic Like Enceladus?. In *Lunar and Planetary Science Conference* (Vol. 46, p. 2423).
- Kirk, R. L., Brown, R. H., & Soderblom, L. A. (1990). Subsurface energy storage and transport for solar-powered geysers on Triton. *Science*, 250(4979), 424-429.
- McKinnon, W. B. (1984). On the origin of Triton and Pluto. *Nature*, 311(5984), 355.
- McKinnon, W. B., Lunine, J. I., & Banfield, D. (1995). Origin and evolution of Triton. In *Neptune and Triton* (pp. 807-877).
- Nimmo, F., & Spencer, J. R. (2015). Powering Triton's recent geological activity by obliquity tides: Implications for Pluto geology. *Icarus*, 246, 2-10.
- Prockter, L. M., F. Nimmo, and R T. Pappalardo (2005). "A shear heating origin for ridges on Triton." *Geophysical research letters* 32.14.
- Schenk, P., & Jackson, M. P. A. (1993). Diapirism on Triton: A record of crustal layering and instability. *Geology*, 21(4), 299-302.
- Schenk, P. M., & Zahnle, K. (2007). On the negligible surface age of Triton. *Icarus*, 192(1), 135-149.



# Comprehensive high-pressure ices EoS for icy world interior

**Baptiste Journaux** (1,2), J. Michael Brown (1), Anna Pakhomova (3), Ines Colligns, (4), Sylvain Petitgirard (5), Jason Ott (1)

(1) University of Washington, Seattle, USA, (2) NASA Astrobiology Institute, (3) DESY, Hamburg, Germany, (4) ESRF, Grenoble, France, (5) Bayerisches Geoinstitut, Bayreuth, Germany.

## Abstract

New X-Ray diffraction (XRD) volume data on ice III, V and VI were collected in-situ in the 200-1800 MPa and 220-300 K range. The accuracy and density of the data allow to derive Mie-Gruneisen equations of state (EoS), providing other thermodynamic parameter such as their thermal expansion coefficient, bulk modulus or heat capacity as a function of pressure and temperature. These new comprehensive EoS enable accurate thermodynamic calculation of ice polymorphs in a framework directly usable for planetary interior modelling.

## 1. Introduction

Water is distinguished for its rich pressure (P) – temperature (T) phase diagram: currently, in which 17 polymorphs of ice have been experimentally identified. Some of these high-pressure forms are believed to be present in icy worlds like Europa, Ganymede, or Titan and newly discovered ocean exoplanets [1,2]. These icy satellites can be covered by a hydrosphere up to 900 km thick. These hydrospheres are probably separated into a sequence of concentric shells of high-pressure polymorphs depending on the depth and the temperature profile. In icy satellites like Titan or Ganymede, ice III, ice V and ice VI are likely to be major components [3]. Precise knowledge on elastic properties and thermodynamics of these ice phases as a function of P and T is essential to perform modelling of geological structure and evolution of these satellites.

Surprisingly, despite the high planetary relevance, there are very scarce compressibility data on ice III, V and VI. For ice III, only a few data points using volume measurements [4,5] exist and there is no *in-situ* single crystal refinement for pure H<sub>2</sub>O. Ice V appears to have been even less investigated: the only X-ray diffraction experiment has been performed on

recovered quenched sample at ambient pressure [6]. Ice VI has been also poorly investigated, and even if recent work has determined its compressibility above 300K [7], lower temperature data are still very sparse.

## 2. Experimental approach

To complete the lack of volume data for high pressure ices, we performed *in-situ* single-crystal and powder X-ray diffraction experiment on ices III and V and VI grown in a cryostat cooled diamond anvil cell (DAC) at the ID15B beamline of the European Synchrotron Research Facility. We were able to obtain many volume pressure-temperature data in the 200-1800 MPa and 220-300 K range for ice III, ice V and ice VI. This dataset surpasses in number and accuracy all of the combined data points previously published for each of these ice polymorphs, which allow to derive precise equations of states.

## 3. Data analysis and results

From our data and previously published PVT data, we derived complete Mie-Gruneisen EoS and thermodynamic properties as a function of P and T for ice III, V, and VI, such as their thermal expansion coefficient, bulk modulus or heat capacity. We combined those with liquid water local basis function Gibbs energy representation [8] to provide a comprehensive description of equilibriums of pure water, aiming at providing a solid thermodynamic framework for the description of ices and aqueous solutions when solutes are present.

The measured volumes are significantly lower than previous theoretical EoS by up to 8% for ice III and V, which results in a significant increase of their density, important to predict interior structure and buoyancy relations with salty brines. Other thermodynamic parameters such as the thermal expansion coefficient, bulk modulus, or heat capacity

are also obtained for the first time for ice III and V as function of pressure and temperature, as illustrated on figure 1 for ice V.

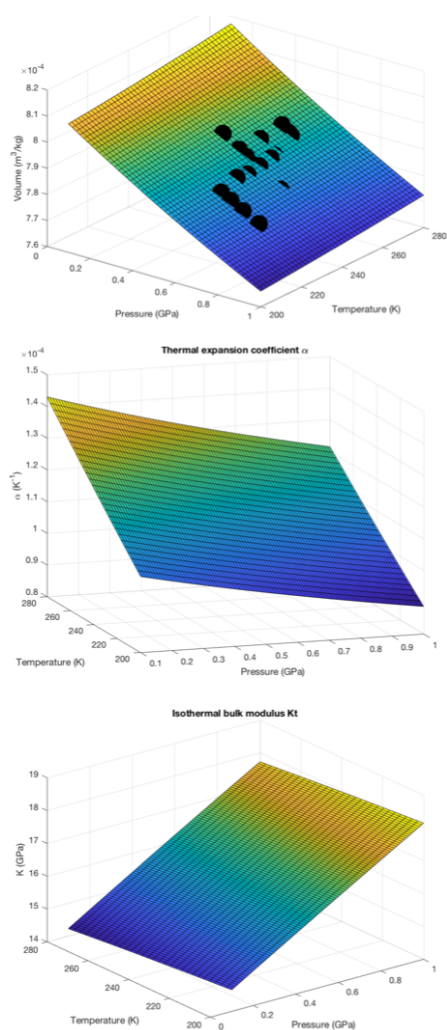


Figure 1: Top, fitted PVT equation of state for ice V, with the data represented as black dots. Middle and bottom, Thermal expansion coefficient and isothermal bulk modulus derived from the fitted PVT-EOS.

## 4. Summary and Conclusions

New volume data were collected in-situ for ice III, V and VI using single crystal and powder XRD. These data enable for the first time to derive accurate equations of states and subsequent thermodynamic parameters such as thermal expansion coefficient and the isothermal bulk modulus. This provide the most comprehensive thermodynamic representation to date

of ice III, V and VI, and will lead toward more realistic modelling of icy world interior, as well as water systems at high pressures.

## Acknowledgements

We thank Steve Vance, Evan Abramson, Olivier Bollengier and Tiziana Boffa-Ballaran for helpful discussion and comments on planetary implications, thermodynamic models and XRD measurements.

## References

- [1] Author, A., Author, B., and Author, C.: First example of a cited article title, First Example Journal, Vol. 1, pp. 1-100, 1999.
- [1] Léger, A, F Selsis, C Sotin, T Guillot, D Despois, D Mawet, M Ollivier, A Labèque, C Valette, and F Brachet. "A New Family of Planets?", *Icarus* 169, pp. 499-504, 2004.
- [2] Sohl, Frank, Mathieu Choukroun, Jeffrey Kargel, Jun Kimura, Robert Pappalardo, Steve Vance, and Mikhail Zolotov. "Subsurface Water Oceans on Icy Satellites: Chemical Composition and Exchange Processes.", *Space Science Reviews* 153, pp. 485-510, 2010.
- [3] Sotin, C, and G Tobie. "Internal Structure and Dynamics of the Large Icy Satellites." *Comptes Rendus Physique* 5, pp. 769-80, 2004.
- [4] Bridgman, P W. "Water, in the Liquid and Five Solid Forms, under Pressure." *Proceedings of the American Academy of Arts and Sciences* 47, no. 13, pp. 441-558, 1912.
- [5] Gagnon, R E, H Kieft, M J Clouter, and Edward Whalley. "Acoustic Velocities and Densities of Polycrystalline Ice Ih, II, III, V, and VI by Brillouin Spectroscopy." *The Journal of Chemical Physics* 92, no. 3, pp. 1909, 1990.
- [6] Kamb, B., A. Prakash, and C. Knobler. "Structure of Ice. V." *Acta Crystallographica* 22, no. 5, pp.706-15, 1967.
- [7] Bezacier, L., Journaux, B., Perrillat, J.P., Cardon, H., Hanfland, M., and Daniel, I. "Equations of State of Ice VI and Ice VII at High Pressure and High Temperature." *Journal of Chemical Physics* 141, no. 10, pp. 104505, 2014.
- [8] Brown, J. Michael. "Local Basis Function Representations of Thermodynamic Surfaces: Water at High Pressure and Temperature as an Example." *Fluid Phase Equilibria* 463, pp. 18-31, 2018.

## Enceladus' interior, tectonics, and evolution from tidal analysis

Alyssa R. Rhoden (1,2), Terry A. Hurford (3), Wade G. Henning (4), Joseph N. Spitale (5), Eric M. Huff (6)

(1) Arizona State University, Tempe, AZ (alyssa.rhoden@asu.edu), (2) Southwest Research Institute, Boulder, CO (3) NASA GSFC, Greenbelt, MD, (4) Univ. of Maryland, College Park, MD, (5) NASA JPL, Pasadena, CA.

### Abstract

Enceladus is a puzzling world. It has an extreme dichotomy in tectonic activity, with the south pole currently and spectacularly active and the north pole heavily cratered with relatively little tectonism. While tidal stresses have been proposed as a mechanism for controlling plume eruptions, few studies have assessed the role of tidal stress in the formation of the south polar fractures. With regard to Enceladus' interior structure, neither tidal heating models nor analyses of the timing of plume eruptions have matched the current estimates of a very thin shell at the south pole of 12 km or less. Here, we determine the thickness and rheology of Enceladus' ice shell that can best explain the north-south tectonic dichotomy and the orientations of the Tiger Stripe Fractures (TSFs). We compute and evaluate tidal stresses for a suite of interior structure models, and conduct a statistical analysis of each model's ability to reproduce the orientations of the TSFs. We find that the TSFs are strongly correlated with the tidal stresses, implying that tides played a key role in their formation. We further find that, at the time the TSFs formed, Enceladus most likely had a globally thick, convecting ice shell that was at least ~10 km thick at the south pole and ~20 km or thicker at the north pole. As the south polar terrain (SPT) is quite young, and the TSFs are among the youngest features in the region, we expect these conditions are indicative of the present day. We discuss additional constraints and implications, particularly on the failure process and the long-term changes in Enceladus' ice shell.

### 1. Introduction

Enceladus has an eccentric orbit that can drive daily-varying tidal stress, a global liquid water ocean, and a young, pervasively-fractured region at its south pole [1]. The south polar terrain (SPT) is made up of a background of densely-packed fractures, overlain by a more organized set of fractures [2]. The most prominent of these fractures are called the Tiger

Stripe Fractures (TSFs), which are roughly parallel but also have segments that deviate from the orientations of the main set [1]. Plumes emanate from both the main branches and some of these other segments [3][4][5]. The eruptive output of the plumes varies with Enceladus' tidal cycle [6], implying that tides control the eruptions [7][8]. The formation of the Tiger Stripe fractures (TSFs) has also been attributed to tidal stresses [e.g 7], although a non-tidal origin has also been suggested [9]. Curiously, Enceladus' north pole is heavily cratered and displays limited tectonic activity. As tides are a symmetric process, explaining the dichotomy in activity is a challenge.

The magnitude of tidal stress depends on the structure and responsiveness of Enceladus' interior. However, there is no consensus on the interior structure. Model fits to Enceladus' observed librations support a variable shell thickness that is ~12 km at the south pole and thicker at the north pole by ~10 km. Fits to the gravity data provide a range of values depending on the model assumptions, from roughly 10 km or thicker at the south pole [10][11] to a few km or less [12], with the north pole always being thicker than the south. To obtain constraints on Enceladus' interior structure, and better understand what governs tectonic activity on Enceladus, we conduct two related investigations: 1) we identify differences in interior structure that would promote tidally-driven fracturing near the south pole while inhibiting fracturing near the north pole, and 2) identify interior structures, and corresponding tidal stresses, that best match the observed orientations of fractures in the south polar terrain (SPT).

### 2. Approach

To compute tidal stresses in our layered models, we used the methods of [13], which we have previously applied to Charon [14] and Mimas [15]. We developed interior structure models with ice shell thicknesses of 500 m to 22 km, which spans the range of values inferred for the north and south poles



from Enceladus' libration, shape, and gravity [10-13]. We also varied the viscosity of the lower, ductile part of the ice shell and the fraction of the shell that behaves brittlely. Our past work has shown that these parameters have the largest impact on the resulting tidal stresses.

We used the magnitudes of tidal stresses produced with each model to determine the conditions by which tidal fractures would likely form in the south but not in the north, using Europa as a comparison point. We then computed the orientations at which tensile cracks would form, in response to tidal stress, at thousands of individual locations along the TSFs. We applied statistical tools to assess how well the model predictions fit the observed orientations and identified the model that produces the best overall fit.

### 3. Results

After testing 27 different interior structure models, we find that most models produce stresses comparable to, or greatly exceeding, the magnitude of tidal stress on Europa, which is globally fractured by tidal stress [e.g. 16]. Hence, it is more challenging to explain the limited fracturing at the north pole than the extensive fracturing at the south pole. We find that the north-south tectonic dichotomy can be explained in two ways: 1) a >10 km thick, convecting ice shell at the north pole and a ~5 km thick (or thinner), conducting shell at the south pole or 2) a globally thick, convecting ice shell that is at least 10 km thick in the south and at least 20 km in the north. In either case, to inhibit extensive fracturing in the north, we find that the viscosity of the convecting portion of the ice shell must be somewhat higher in the north ( $10^{14}$  Pa\*s or higher) than in the south.

When we compare the tidal stress orientations with the orientations of the TSFs, we find that models with a thick shell at the south pole, between 10 and 20 km, provide far superior fits to any of the thin shell models. We also find that, across all models, the TSF orientations are highly correlated with the tidal stress orientations, implying that tidal stresses did play a key role in their formation.

### 4. Discussion and Conclusions

Our analysis supports a tidal origin for the Tiger Stripe Fractures and an ice shell that is at least 10-20

km thick at the south pole. These results are consistent with interpretations of Enceladus' observed librations and gravity data [10][11], although some more recent studies suggest a much thinner shell at the south pole [12]. Our results are also compatible with the hypothesis that Enceladus' ice shell was thinner in the past, particularly at the south pole, and that it has thickened with time. We find that changes in ice shell thickness can lead to changes in the expected orientations of tidally-driven fractures. Hence, detailed analysis of older fracture sets in the SPT may provide more evidence of its evolution.

If the ice shell at the south pole is found to be less than a few km thick, it would suggest the TSFs were formed by a combination of stresses from tides and an additional, non-uniform source [e.g. 17], and that the exclusion of that stress in our models has led to a preference for a thick shell. We also note that our failure model is rather simplistic, and higher fidelity modeling may improve our understanding of the formation of fractures in the SPT.

### Acknowledgements

We wish to thank Michael Bland for helpful discussions about convection in ice shells and the Ocean Worlds Cooperative for their feedback and support.

### References

- [1] Porco, C. et al. (2006) *Science* 311, 1393-1401. [2] Patthoff, D. & Kattenhorn, S. (2011) *GRL* 38, 1-6. [3] Spencer et al. (2006) *Science*, 311, 1401-1405. [4] Spitale, J.N. and Porco, C.C. (2007) *Nature* 449, 695-697. [5] Spitale, J.N., et al. (2015) *Nature* 521, 57-60. [6] Hedman, M. et al. (2013) *Nature* 500, 182-184. [7] Nimmo, F. et al. (2007), *Nature* 447, 289-291. [8] Hurford, T. et al. (2007), *Nature* 447, 292-294. [9] Behounkova, M. (2015) *Nature Geoscience*, 8, 601-604. [10] Yin, A. and Pappalardo, R.T. (2015) *Icarus*, 260, 409-439. [11] Thomas, P. et al. (2016) *Icarus* 264, 37-47. [12] Iess, L. et al. (2014) *Science* 344, 78-80. [13] McKinnon, W. (2015) *GRL* 42, 2137-2143. [14] Cadek, C. et al. (2016) *GRL*, 43, 5653-5660. [15] Jara-Orue, H. and Vermeersen, B.L.A. (2011) *Icarus* 215, 417-438. [16] Rhoden, A.R. et al. (2015) *Icarus* 246, 11-20. [17] Rhoden, A.R. et al. (2017) *JGR-Planets* 122, 400-410. [18] Rhoden, A.R. et al (2010) *Icarus* 210, 770-784. [19] Johnston, S. and Montesi, L. (2017) *JGR-Planets* 122, 1258-1275.

# Structural map of the grooves of Ganymede

**Costanza Rossi** (1), Paola Cianfarra (1), Francesco Salvini (1), Olivier Bourgeois (2)  
(1) GeoQuTe Lab, Roma Tre University, Rome, Italy (costanza.rossi@uniroma3.it), (2) Laboratoire de Planétologie et Géodynamique, Université de Nantes, CNRS, France

## Abstract

Intense tectonic activity deforms most of the bodies of the inner and outer Solar System. The crust of the Jovian satellite Ganymede shows a great variety of kilometric-scaled morphotectonic features. These are the grooves and the furrows, developed within the light terrain and the dark, respectively. These structures represent the evidences of the past (and possibly the present) tectonic history of the satellite and their formation is a debated topic. In this contribution we investigate the grooves of Ganymede. Their geometry and crosscutting relationship represent a powerful mean to understand the global tectonic evolution of the satellite. We produced the structural map of Ganymede grooves where more than 6700 grooves were manually recognized and quantitatively analysed according the groove azimuth, length, sinuosity and spacing. Identified grooves were grouped into 5 structural systems and their remote sensing analysis allows to infer the stress field and the relative lithosphere rheology and thickness. The structural map of the grooves aims to identify the regional tectonic regime that affected Ganymede lithosphere. In this way we observed that groove systems are often organised as the terrestrial shear zones. This setting has been identified at local and regional scale. Two regions centered at 130°W-23°S and at 74°W-4°S suggest that strike-slip tectonics played a significant role in the formation of the recognized groove systems. Further investigations will be done to study the global tectonics of Ganymede with the aid of the obtained map.

## 1. Introduction

The crust of Ganymede is one of the most tectonized in the solar system. The younger light terrain covers the 65% of the surface and it is deformed by morphotectonic structures named grooves [1]. Ganymede grooved terrain is densely populated by

subparallel elongated landforms at the global and regional scale and well-defined morphology from straight to curvilinear. Grooves crosscut or intersect with each other with an arrangement not easily detectable. Ganymede groove tectonics was interpreted as mainly extensional [2], although strike-slip has been recently identified within several regions [3] and evidence of contraction has been recognized in transpressional environment [4]. The tectonic origin of these structures remains unclear. A global mapping of the grooves is required to unravel their tangled setting. As the other produced database of grooves [5], our map aims to analyse the different mechanisms for the grooved terrain formation and the construction of a global strain history. We manually mapped and quantitatively analysed grooves of Ganymede to produce a structural map to highlight their tectonic nature. The obtained map is represented by structural groove systems. This result indicates that it is possible to infer the stress field that produced them. By a preliminary structural analysis of several regions of the map we suggest that strike-slip has been the leading component on Ganymede global tectonic history. This map will be object of further investigation within several light terrain regions.

## 2. Mapping

In a GIS platform a total of 6765 groove structures were manually mapped within light terrain among 178°W-36°E and 60°N-66°S. The detection was performed on the USGS Ganymede Voyager and Galileo global mosaic with a resolution from 2000 m/pixel to approximately 400 m/pixel at the scale of 1:3.000.000. The recognized grooves represent approximately the 26% of the light terrain since about 50% of the light terrain images was not acquired with an acceptable resolution to manually resolve the structures. Identified grooves were quantitatively analysed according to their azimuth, sinuosity, length and spacing among adjacent features.

### 3. Results

The structural map of the grooves of Ganymede (detail in Fig.1) shows a total of 5 groove systems. These are globally distributed with orientations of N50°-90°W, N10°-50°W, N30°E-N10°W, N30°-60°E, N60°-90°E and their maximum length exceeds 300 km. The longer grooves often describe corridor regions delimited by two parallel boundaries inside which shorter groove systems with opposite azimuths are present. This setting resembles the strike-slip zones of the Earth.

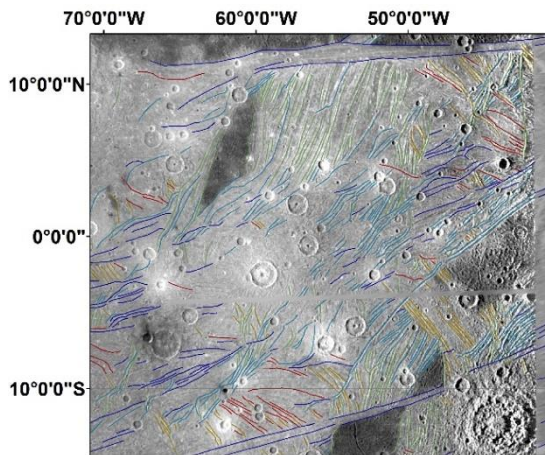


Figure 1: Structural map of the grooves of Ganymede detail. Babylon Sulci 74°W-4°S.

### 4. Conclusions

We produced a global map of the grooves of Ganymede where grooves are organised in structural systems. Their assemblage is compatible with strike-slip tectonics. We propose that the formation of the groove systems on Ganymede relates to the activity along regional shear corridors. The spatial arrangement of the recognized groove systems within these corridors is similar to the deformation associated to the regional strike-slip environments on the Earth. In this way we suggest a major role of the

strike-slip movement in the global tectonics of the satellite. This map is supposed to be an improvement of past studies and a support to understand the tectonic evolution of Ganymede. The structural analysis of the groove system will be further investigated by future studies.

### Acknowledgements

This research developed as a collaboration between Roma Tre University and the LPG (Laboratoire de Planétologie et Géodynamique) of the Nantes University and it is part of a PhD project funded by the University of Roma Tre and its GeoQuTe Lab.

### References

- [1] Patterson, G.W., Collins, G.C, Head, J.W., Pappalardo, R.T, Prockter, L.M, Lucchitta, B.K, and Kay, J.P.: Global geological mapping of Ganymede, *Icarus*, vol. 207, pp. 845–867, 2010.
- [2] Pappalardo, R.T., Head, J.W., Collins, G.C., Kirk, R. L., Neukum, G., Oberst, J., Giese, B., Greeley, R., Chapman, C.R., Helfenstein, P., Moore, J.M., McEwen, A., Tufts, B.R., Senske, D.A., Breneman, H.H. and Klaasen, K.: Grooved Terrain on Ganymede: First Results from Galileo High-Resolution Imaging, *Icarus*, vol. 135, pp. 276–302, 1998.
- [3] Seifert, F., Cameron, M. E., Smith-Konter, B. R., Pappalardo, R. T., and Collins, G. C. Global Morphological Mapping of Strike-Slip Structures on Ganymede. In *Lunar and Planetary Science Conference*, vol. 46, p. 2985. 2015.
- [4] Rossi, C., Cianfarra, P., Salvini, F., Mitri, G., and Massé, M. Evidence of transpressional tectonics on the Uruk Sulcus region, Ganymede. *Tectonophysics*, under review.
- [5] Collins, G. C., Head, J. W., Pappalardo, R. T., and Galileo SSI Team. A global database of grooves and dark terrain on Ganymede, enabling quantitative assessment of terrain features. In *Lunar and Planetary Science Conference*, vol. 31. 2000.

# Rhea's thermal properties and regional anomalies revealed by Cassini's Radar/radiometer

Léa E. Bonnefoy (1,2), Alice Le Gall (2), Emmanuel Lellouch (1), Cédric Leyrat (1), Michael A. Janssen (3) and the Cassini Radar team

(1) Laboratoire d'Etudes Spatiales et d'Instrumentation en Astrophysique (LESIA), Observatoire de Paris-Meudon, LESIA (Bât. 18), 5, place Jules Janssen, 92195 Meudon Cedex, France (2) Laboratoire Atmosphères, Milieux, Observations Spatiales (LATMOS), UVSQ /CNRS/Paris VI, UMR 8190, 78280 Guyancourt, France (3) Jet Propulsion Laboratory, California Institute of Technology, Pasadena, CA 91109, USA  
(lea.bonnefoy@latmos.ipsl.fr)

## 1. Introduction

The Cassini Radar/radiometer was primarily designed to study Titan's surface, but also observed other Saturn satellites on multiple occasions. Operating at a wavelength of 2.2 cm, the Radar/radiometer is able to probe up to several meters into the subsurface, deeper than any other instrument on board Cassini, and thus provides a unique insight into the composition and structure of the subsurface. On Enceladus and Iapetus, this dataset allowed the identification of thermal [1], structural [2], and compositional [3] anomalies. Spatially-resolved Radar and passive radiometry data were also acquired over Rhea: we perform a similar analysis as on Iapetus and Enceladus. Rhea is Saturn's largest icy satellite, and is the furthest of Saturn's satellites thought to have formed from the rings, which may be very young [4,5]. We use a thermal model described in Le Gall et al. (2014, 2017) to simulate the brightness temperature, which we compare to observations to constrain thermophysical properties and anomalies [1, 3]. Understanding the origin of such anomalies can help us to investigate the formation and evolution of Rhea, and to place new constraints on its age.

## 2. Dataset and Methods

Microwave radiometry scans were conducted on 11 instances, during 7 different flybys, as reported in Table 1. On March 2<sup>nd</sup>, 2010, concurrent active Radar and passive radiometry data were taken at resolutions of down to 0.11 times the diameter of Rhea (~85 km). This Radar observation was calibrated and corrected to an incidence angle of 32° by Wye (2011); the resulting Real Aperture Radar (RAR) image is shown in Fig. 1B [6]. We calibrate the radiometry data using the method described in [7],

and map it using an iterative deconvolution method as described in [8].

Table 1: Cassini radiometry data of Rhea

| Observation ID | Beam size (diameter) | Sub-spacecraft point (°) | Sub-solar point (°) |
|----------------|----------------------|--------------------------|---------------------|
| RH11           | 0.79                 | (-48, -75)               | (175, -20)          |
| RH18           | 0.74                 | (-22, 0)                 | (157, -19)          |
| RH22-1         | 0.51                 | (-136, 1)                | (52, -18)           |
| RH22-2         | 0.64                 | (-153, 1)                | (46, -18)           |
| RH45           | 0.84                 | (-58, -44)               | (-158, -12)         |
| RH49           | 0.51                 | (15, 0)                  | (-114, -11)         |
| RH127-1        | 0.47                 | (-160, 0)                | (19, 3)             |
| RH127-2        | 0.35                 | (-162, 0)                | (17, 3)             |
| RH127-4        | 0.11-0.24            | (-167, 1)                | (12, 3)             |
| RH177-1        | 0.40                 | (-102, -76)              | (-12, 17)           |
| RH177-2        | 0.33                 | (-92, -77)               | (13, 17)            |

While studying the deconvolved maps of the brightness temperature can help us identify anomalies, a thermal model is necessary to determine whether they are due to compositional or structural variations or to diurnal and seasonal temperature variations. We therefore simulate brightness temperatures by using a combination of a thermal model, a radiative transfer model, and an emissivity model, as described in Le Gall et al. (2014) [3].

## 3. Preliminary results

The thermal model assumes uniform properties over the surface, and therefore highlights anomalies that cannot be explained simply with diurnal or seasonal temperature variations. All resolved radiometry data (RH22, RH49, RH127, and RH177) covering the Inktomi crater region were taken during the night and consistently show the Inktomi crater ejecta region as colder than its surroundings (e.g. Fig. 1D), a pattern which the model is unable to duplicate (Fig. 1C). Using Cassini's Composite and Infrared



Spectrometer (CIRS), Howett et al. (2014) found an anomalously high thermal inertia in this region, which should lead to higher temperatures during the night [9]. This contradiction can be resolved by the existence of a lower emissivity anomaly, which is consistent with the high Radar return (Fig. 1B). A low emissivity in Inktomi crater and its ejecta blanket can be explained by a high water ice purity at depth,

as detected on the surface by VIMS [10], and/or by increased volume scattering, due likely to the cm-scale structure of the fresh ice. Preliminary results also point to a lower emissivity in the leading hemisphere as opposed to the trailing hemisphere, and to possible differences between the poles, maybe indicative of regional variations in the degree of compaction of Rhea's regolith.

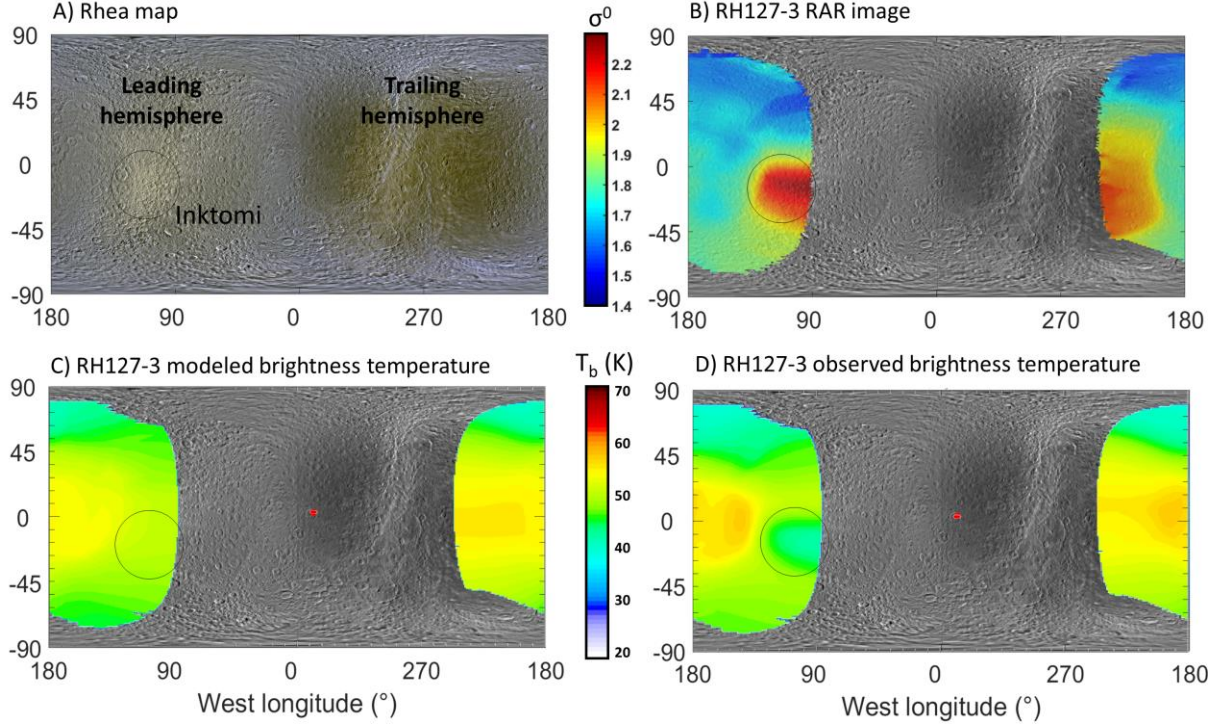


**Figure 1: RH127-3 spatially-resolved Cassini Radar and radiometry data. A) Color mosaic made from Cassini IR, UV, and visible data (credit: NASA/JPL-Caltech/SSI/LPI). B) Real Aperture Radar (RAR) image [5]. C) Deconvolved map of the best fit model temperature. D) Deconvolved map of the observed brightness temperature. The sub-solar point is indicated in red, and the Inktomi crater ejecta region is circled. Note that the thermal model is unable to explain the low temperatures in Inktomi crater.**

## Acknowledgements

This work was funded by DIM-ACAV and CNES. The authors wish to thank the Cassini-Huygens (NASA/ESA/ASI) team for the design, development, and operation of the mission.

## References

- [1] A. Le Gall et al. (2017), *Nature Astronomy*, Vol. 1, 0063.
- [2] P. Ries and M.A. Janssen (2015), *Icarus*, Vol. 257, pp. 88-102.
- [3] A. Le Gall et al. (2014), *Icarus*, Vol. 241, pp.221-238.
- [4] S. Charnoz et al. (2011), *Icarus*, Vol. 216, pp.535-550.
- [5] J. Cuzzi (2018), LPSC #2083.
- [6] L.C. Wye (2011), PhD thesis.
- [7] M.A. Janssen et al. (2009), *Icarus*, Vol. 200, pp. 222- 239.
- [8] Z. Zhang et al. (2017), *Icarus*, Vol. 281, pp. 297-321
- [9] C.J.A. Howett et al. (2014), *Icarus*, Vol. 241, pp. 239-247.
- [10] F. Scipioni et al. (2014), *Icarus*, Vol. 234, pp. 1-16.

# Modelling the Rock-Water Interface on Enceladus

**R. E. Hamp**, K. Olsson-Francis, S.P. Schwenzer, N. K. Ramkissoon and V.K. Pearson  
Faculty of Science, Technology, Engineering and Mathematics, The Open University, Milton Keynes  
([rachael.hamp@open.ac.uk](mailto:rachael.hamp@open.ac.uk))

## Abstract

Understanding the potential reactions occurring at the rock-water interface within Enceladus is crucial for establishing that environment's viability as habitable. We are developing methodology to both model and simulate this environment and present preliminary results from this work.

## 1. Introduction

The detection of plumes emerging from the South Polar Region (SPR) on Enceladus [1] and a high heat flux in the same location [2] have provided evidence of a sub-surface ocean and potential ongoing hydrothermal activity [3, 4]. This, coupled with the presence of bio-essential elements (such as carbon, nitrogen and hydrogen) within the plumes [5], raises the possibility that Enceladus' sub-surface could be a potentially habitable environment.

To understand this environment fully, and to ascertain if it can support life, the biogeochemical cycles occurring at the rock-water interface need to be constrained. Using the data provided by Cassini [6, 7], we aim to model the processes occurring at the rock-water interface. This modelling requires a definition of both silicate and ocean chemistry and an understanding of the physical parameters anticipated to occur at this interface.

Our initial focus will be to model the internal environment at the rock-water interface, then using the results from this, we will simulate these conditions in a laboratory, using a high temperature high pressure reactor. We will present preliminary results of the modelling and its implications for the experimental work.

## 2. Defining Silicate Chemistry

Cassini detected  $\text{SiO}_2$  nanoparticles within the plumes [4], most likely produced through rock-water interactions. This infers Enceladus has a silicate

interior [4], but its precise composition is not yet confirmed.

Analysis of the plumes has provided identification of carbon species, including methane, short chain hydrocarbons and carbon dioxide [6, 7]. In addition, nitrogen species were detected in the form of ammonia, molecular nitrogen and hydrogen cyanide [6, 7]. Analysis of the particles within Saturn's E-ring by the Cassini Dust Analyzer [7, 8] suggests that the silicate contains Mg-rich, Al-poor minerals. The inferred composition is one equivalent to a carbonaceous chondrite [3].

For our experiments, we have devised a simulant, basing the silicate on the average composition of a CI chondrite. An average elemental composition was calculated using data available from the Alais, Orgueil and Ivuna meteorites. Using minerals that have been detected previously within CI chondrites, the same chemistry was replicated as closely as possible (Table 1). In addition to the silica component, we will also incorporate the organic components that have been detected in CI chondrites.

Table 1: Initial mineralogy for the silicate interior of Enceladus

| Mineral             | Weight % |
|---------------------|----------|
| Olivine (9:1 Fo:Fa) | 15       |
| Magnetite           | 15       |
| Serpentine          | 15       |
| Almandine           | 10       |
| Diopside            | 5        |
| Talc                | 5        |
| Quartz              | 5        |
| Pyrite              | 3        |
| Anhydrite           | 1        |
| Apatite             | 1        |
| Dolomite            | 1        |
| Magnesite           | 0.15     |
| Calcite             | 0.02     |



### 3. Ocean Chemistry

We will be using a theoretical starting composition for the ‘initial’ sub-surface ocean, based upon the chemistry of the ice shell, assuming the ocean originated from the melting of this. The composition will be based upon previous research by Neveu et al., [9] using C, N, S-bearing cometary fluids, proposed to be the materials initially accreted by icy worlds [9].

### 4. Modelling

The modelling will focus on the interaction of the ‘initial’ ocean chemistry with the defined silicate simulant – mimicking the interaction of the sub-surface ocean with the silicate interior, specifically focusing on the movement of carbon species.

We will initially use CHIM-XPT [10], used previously to model martian water-rock interaction [11-13], at a temperature range of 273-373 K [4]. These temperatures were chosen based on the assumption that the concentration of salt and ammonia is insufficient to have an effect on the freezing/melting point of water. We will explore a pressure range suggested by Hsu et al., of 10-80 bar [4], which will allow us to better constrain the pressure to be used for the simulation experiments. Based upon the plume chemistry, the expected pH of the sub-surface ocean would be alkaline, with an estimated range from 8.5-12 [14]. This would also be consistent with our martian models that contain many of the same minerals [12,13]. We expect phyllosilicates and oxides to form, potentially zeolites [13].

The CHIM-XPT database contains hydrocarbons (e.g. CH<sub>4</sub>, C<sub>2</sub>H<sub>6</sub>, C<sub>3</sub>H<sub>8</sub>), ammonia, and C-N-S-bearing compounds. This will allow us to establish a baseline mineralogy before incorporating the full set of organics into the models. The modelling will lead to a theoretical ‘modern’ ocean composition, which can be compared to the composition of the plumes, analysed by Cassini [6, 7]. Since these plumes are expected to originate from the sub-surface ocean, it can be considered that the plume composition reflects that of the ocean.

### 5. Summary

We plan to model the rock-water interface on Enceladus using the chemistry of a CI chondrite to represent the silicate interior. Using both Cassini data

and preliminary modelling of an early sub-surface ocean, we will acquire a theoretical composition for the current sub-surface ocean. Subsequently, modelling the interaction between the ocean and silicate we aim to acquire a better knowledge of what reactions are occurring at their interface. We plan to use the results of this modelling work to underpin laboratory simulations of the rock-water interface.

### Acknowledgements

RH would like to thank STFC and The Open University’s Space Strategic Research Area for the funding for this project.

### References

- [1] Porco, C., et al., Cassini Observes the Active South Pole of Enceladus, *Science*, 311, 1393-1401, 2006. [2] Howett, C. J. A., Spencer, J. R., Pearl, J., and Segura, M., High heat flow from Enceladus’ south polar region measured using 10-600 cm<sup>-1</sup> Cassini/CIRS data, *Journal of Geophysical Research*, 116, 2011. [3] Sekine, Y., et al., High temperature water-rock interactions and hydrothermal environments in the chondrite like core of Enceladus, *Nature Communications*, 6, 2015. [4] Hsu, H. W., et al., Ongoing hydrothermal activities within Enceladus, *Nature*, 519, 207-210, 2015. [5] McKay, C. P., Anbar, A. D., Porco, C., and Tsou, P., Follow the Plume: the Habitability of Enceladus, *Astrobiology*, 14, 352-355, 2014. [6] Waite, J. H., et al., Liquid water on Enceladus from observations of ammonia and 40Ar in the plume, *Nature*, 460, 487-490, 2009. [7] Bouquet, A., Mousis, O., Waite, J. H., and Picaud, S., Possible evidence for a methane source in Enceladus’ ocean, *Geophysical Research Letters*, 42, 1334-1339, 2015. [8] Postberg, F., et al., The E ring in the vicinity of Enceladus II. Probing the moons interior-The composition of the E-ring particles, *Icarus*, 193, 438-454, 2008. [9] Neveu, M., Desch, S. J., and Castillo-Rogez, J. C., Aqueous geochemistry in icy world interior: Equilibrium fluid, rock and gas compositions, and fate of antifreezes and radionuclides, *Geochimica et Cosmochimica Acta*, 212, 324-371, 2017. [10] Reed, M. H., Spycher, N. F., Palandri, J., User guide for CHIM-XPT, University of Oregon, Oregon, 2010 [11] Bridges, J. C., Schwenzer, S. P., *EPSL*, 359-360: 117-123, 2012 [12] Schwenzer, S. P., Abramov, O., Allen, C. C., Clifford, S. M., Cockell, C. S., Filiberto, J., Kring, D. A., Lasue, J., McGovern, P. J., Newsom, H. E., Treiman, A. H., Vaniman, D. T., Wiens, R. C., Puncturing Mars: How impact craters interact with the Martian cryosphere, *Earth and Planetary Science Letters* 335-336, 9-17, 2012b [13] Schwenzer, S. P. and Kring, D. A., Alteration minerals in impact-generated hydrothermal systems – exploring host rock variability, *Icarus*, 226: 487-496, 2013 [14] Glein, C. R., Baross, J. A., and Waite, J. H., The pH of Enceladus’ ocean, *Geochimica et Cosmochimica Acta*, 162, 202-219, 2015.

# Long-term stability of Enceladus' ice shell

Ondřej Čadek (1), Ondřej Souček (1), Marie Běhouňková (1), Gaël Choblet (2) and Gabriel Tobie (2)  
 (1) Charles University, Prague, Czech Republic, (2) Université de Nantes, UMR 6112, France (ondrej.cadek@mff.cuni.cz)

## Abstract

We present a new model of Enceladus' ice shell based on shape and gravity information and we investigate its long-term stability by computing the flow of ice induced by variations in hydrostatic pressure on the ice/water interface. We demonstrate that the ice shell is stable if the viscosity of ice at the melting temperature is equal to or higher than  $3 \times 10^{14}$  Pa s and the heat flux coming from the ocean varies by tens of mW/m<sup>2</sup> laterally.

## 1. Introduction

In the last few years, several models of Enceladus' internal structure based on the shape [1], gravity [2] and libration [3] data collected by Cassini have been presented [3-6]. All these models show that the thickness of the ice shell significantly varies, from probably less than 10 km in the south polar region to more than 30 km near the equator. This suggests that the base of the ice shell is subjected to large variations in hydrostatic pressure which induce flow in the ice shell tending to restore the hydrostatic equilibrium. For the shape of the bottom boundary of the ice shell to be stable in time, the flow in the ice shell must be counterbalanced by the phase change on the ice/water interface, i.e. the normal velocity of ice flow on the ice/water interface must be the same as the rate of melting/freezing [e.g. 7]:

$$\vec{n} \cdot \vec{v} = \frac{\vec{n} \cdot (\vec{q}_i - \vec{q}_w)}{L\rho_i}, \quad (1)$$

where  $\vec{n}$  is the normal vector to the boundary,  $\vec{v}$  is the velocity of ice flow at the base of the shell,  $L$  is the latent heat,  $\rho_i$  is the density of ice, and  $\vec{q}_i$  and  $\vec{q}_w$  are the heat flux in the ice shell and in the ocean, respectively.

In this study, we derive a new model of Enceladus ice shell and we use it to determine the conditions under which the ice shell is stable on a geological time scale. This requires the computation of viscous flow in the ice shell with strongly irregular boundaries and large viscosity contrasts. Because of this complexity, the computation cannot be performed by a standard

spectral code but requires the use of a finite element method which is able to capture the irregular shape of the ice shell.

## 2. Structural model of Enceladus

The model of the internal structure is based on the low-degree model of Enceladus' gravity [2], the measurement of physical libration [3] and the recent model of Enceladus' shape [8]. Assuming that the core is homogeneous and in hydrostatic equilibrium, we first develop a set of structural models that accurately reproduce the main characteristics of Enceladus' gravity field. In order to reduce this set to a single model, we impose the additional constraint that the topographic anomalies described by low-degree spherical harmonic coefficients are equally compensated. We find that the degree of compensation (ratio of the surface to the bottom topographic load) is 0.9–1, and we use this information to determine the shape of the ice/water interface for harmonic degrees that are not constrained by gravity data. Inclusion of density anomalies in the core that are compatible with the numerical simulations of hydrothermal circulation [9] results in an increase of the mean degree of compensation. For some simulations, the degree of compensation is found very close to 1 and the formal error of the solution is smaller than that corresponding to a homogeneous core. The derived model of the ice shell thickness (Fig. 1a) is similar in basic features to previous models [cf. 5, 6]. The ice shell thickness ranges from about 5 to 35 km and the best-fitting radius of the core is about 190 km.

## 3. Stability of the ice shell

Using the model shown in Fig. 1a, we compute the viscous flow in the ice shell generated by variations in pressure acting on the ice/water interface. The computation is performed using FEniCS software package (<http://fenicsproject.org>) for a temperature dependent viscosity corresponding to diffusion creep with a grain size of 1 mm. Substituting the flow velocity to Eq. (1)

and estimating  $\vec{q}_i$  from a conductive temperature profile, we determine the heat flux anomalies ( $\vec{n} \cdot \vec{q}_w$ ) on top of the ocean (Fig. 1b) that are required to maintain the ice shell thickness variations.

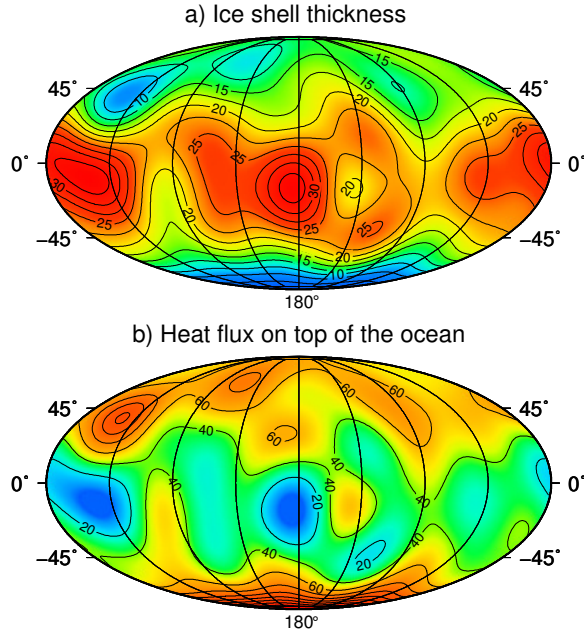


Figure 1: a) Thickness of Enceladus’ ice shell in km. b) Normal component of the heat flux on top of the ocean in  $\text{mW/m}^2$  computed from Eq. (1). Ice velocity  $\vec{v}$  in Eq. (1) is evaluated for diffusion creep with a grain size of 1 mm, corresponding to viscosity of  $3 \times 10^{14}$  Pa s at the melting point.

The heat flux reaches the minimum near the equator where it decreases to zero. If viscosity at the ice/water interface was lower than  $3 \times 10^{14}$  Pa s, the heat flux on top of the ocean would be negative, leading to a contradiction with the assumption that the bottom boundary of the ice shell separates the solid and liquid phases. The pattern of the heat flux anti-correlates with the ice thickness and it is consistent with the numerical simulations of hydrothermal circulation in the core predicting sea floor spots of hot water outflow in the polar regions [9].

## 4. Conclusions

Our analysis of the gravity and topography data suggests that Enceladus’ ice shell is close to equilibrium and the data are compatible with the model of hydrothermal activity in the core recently proposed by Choblet and co-workers [9]. The large variations in

ice shell thickness predicted by previous studies and confirmed by our model are maintained by heat flux anomalies on top of the ocean which are of the order of tens of  $\text{mW/m}^2$ . A physically acceptable (non-negative) heat flux is obtained only if the viscosity of ice at the melting point is equal to or higher than  $3 \times 10^{14}$  Pa s. Our study provides a constraint on the thermal state of Enceladus’ ocean that is needed for the ice shell to be stable. Strikingly large variations of the heat flux predicted by our model should be verified by future simulations of thermal convection in Enceladus’ ocean.

## Acknowledgements

O.S. acknowledges support from the Charles University research program No. UNCE/SCI/023.

## References

- [1] Nimmo, F., Bills, B. G. and Thomas, P. C.: Geophysical implications of the long-wavelength topography of the Saturnian satellites, *J. Geophys. Res.-Planets*, 116, E11001, 2011.
- [2] Iess, L. et al.: The gravity field and interior structure of Enceladus, *Science*, 344, 78–80, 2014.
- [3] Thomas, P. C. et al.: Enceladus’s measured physical libration requires a global subsurface ocean, *Icarus*, 264, 37–47, 2016.
- [4] Van Hoolst, T., Baland, R. M. and Trinh, A.: The diurnal libration and interior structure of Enceladus, *Icarus*, 277, 311–318, 2016.
- [5] Čadež, O. et al.: Enceladus’s internal ocean and ice shell constrained from Cassini gravity, shape and libration data, *Geophys. Res. Lett.*, 43, 5653–5660, 2016.
- [6] Beuthe, M., Rivoldini, A. and Trinh, A.: Enceladus’s and Dione’s floating ice shells supported by minimum stress isostasy, *Geophys. Res. Lett.*, 43, 10,088–10,096, 2016.
- [7] Kvorka, J. et al.: Does Titan’s long-wavelength topography contain information about subsurface ocean dynamics? *Icarus*, 310, 149–164, 2018.
- [8] Tajeddine, R. et al.: True polar wander of Enceladus from topographic data, *Icarus*, 295, 46–60, 2017.
- [9] Choblet, G. et al.: Powering prolonged hydrothermal activity inside Enceladus, *Nat. Astr.*, 1, 841–847, 2017.

## The large bright ray crater Osiris on Ganymede: its age, role as a potential time-stratigraphic marker, and target for detailed imaging by the JUICE/JANUS Camera

**Roland J. Wagner** (1), Katrin Stephan (1), Nico Schmedemann (2), Stephanie C. Werner (3), Harald Hoffmann (1), Thomas Roatsch (1), Elke Kersten (1), Ralf Jaumann (1), and Pasquale Palumbo (4).  
(1) DLR, Institute of Planetary Research, Berlin, Germany, (2) Max Planck Institute for Solar System Research, Göttingen, Germany, (3) CEED, University of Oslo, Norway, (4) Università degli Studi di Napoli Parthenope, Naples, Italy.

### 1. Introduction

Bright ray craters are known from more or less any major planetary body which represent comparably young geological units on their surfaces. On, e.g., the Moon, Mercury, or dwarf planet (1) Ceres, a major ray crater was identified as a marker horizon to define the youngest time-stratigraphic system, or chronologic period, on these bodies, termed Copernican (Moon, [1] and ref's therein), Kuiperian (Mercury, [2]), and Azaccan (Ceres, [3] and ref's therein). Ganymede, the largest icy Jovian satellite, features several large bright craters with extended ray systems, e.g., Hershef, Tros, Tashmetum, and Osiris. Unfortunately, these craters could not be imaged by Galileo SSI due to technical reasons [4]. In this study we use reprocessed Voyager images and focus on Osiris, its stratigraphic position in the context of dark and bright materials, try to constrain its age, and propose a new candidate time-stratigraphic system for Ganymede's young geologic history. Also, Osiris is an important candidate target area for detailed imaging (high-resolution; color data) by ESA's JUICE spacecraft to orbit Ganymede in 2030 – 2033.

### 2. Procedure

**Image processing:** In a previous study [5], relative and absolute model ages, henceforth termed AMAs, of Osiris and other large bright ray craters could only be estimated with a high degree of uncertainty in a global Voyager and SSI basemap at a resolution of 1 km/pxl. Since the spatial resolutions of Voyager images during the two Jupiter encounters in 1979 varied considerably, we reprocessed Voyager (and Galileo SSI Voyager gap fill) images to produce a global basemap at a resolution of 700 m/pxl. The images were high-pass filtered to enhance fine detail. From the basemap, 15 quadrangle mosaics were

derived following the U. S. G. S. quadrangle scheme for Ganymede. **Geologic mapping:** Geologic units were mapped based on the global geologic map by [6]. Units were modified locally to account for suitable crater count areas. The authors [6] proposed the following time-stratigraphic systems and chronologic periods for Ganymede, from oldest to youngest: *Nicholsonian* (based on dark cratered plains in Nicholson Regio); *Harpagian* (based on bright tectonically resurfaced materials in Harpagia Sulcus), and *Gilgameshan* (impact of the youngest large crater/basin Gilgamesh). **Crater counts and cratering chronologies:** We used recent improvements of the method of crater counting and age dating, including buffered crater counting [7] and the Poisson timing analysis [8] to obtain AMAs from measurements of the crater size distribution on a geologic unit. AMAs in units of  $10^9$  (Ga) or  $10^6$  (Ma) years were derived from two model chronologies, one assuming a lunar-like time scale, henceforth termed LDM [9], and one derived from the impacts of Jupiter-family comets, termed JCM [10]. Geologic mapping and crater counts were carried out with *ESRI/ArcGIS* and a *CraterTool* plug-in, and crater statistics analysis was performed with the program *craterstats2* ([7][8], and ref's therein).

### 3. Results

Osiris (107 km, lat.  $38^\circ$  S, long.  $193.69^\circ$  E) and part of its extended bright ray system of discontinuous ejecta are shown in **Fig. 1**. The age of Osiris is constrained by the identification of a single small crater (1.4 km, close to the resolution limit) superimposed on its floor (**Fig. 1**, left, red arrow). In addition, an age can also be estimated from the area of bright ejecta material superimposed on older terrain (**Fig. 1**, right) (see procedure described in [5]). Both data points can very well be fitted by the crater

production function of Ganymede [9][this study], shown in **Fig. 2**. By this procedure we obtain AMAs of **750 Ma** (1.4 Ga / 300 Ma upper/lower uncertainty) (LDM [9]), versus **80 Ma** (240 / 30 Ma) (JCM [10]), rendering a good estimation of Osiris' formation age in the currently available image data. For the bases of the three time-stratigraphic systems of Ganymede [6], we found AMAs of  $3.75 \pm 0.05$  Ga (LDM, [9]) versus  $1.47$  Ga (3.14 Ga / 550 Ma) (JCM [10]) for the *Gilgameshan Period* (**Fig. 2**, green symbols),  $3.85 \pm 0.06$  Ga (LDM [9]) versus  $2.26$  Ga (3.97 Ga / 930 Ma) (JCM [10]) for the *Harpagian Period* (**Fig. 2**, blue symbols), and  $4.1 \pm 0.02$  Ga (LDM [9]) versus  $4.33$  Ga (4.56 / 2.87 Ga) for the *Nicholsonian Period* (**Fig. 2**, red symbols). The crater distribution measured in the dark cratered plains surrounding Osiris also show a *Nicholsonian* age (**Fig. 2**, dark brown symbols). Craters measured within the bright rays, however, as those indicated by the yellow arrows in **Fig. 1** (right), give an approximately *Harpagian* age inferring they were formed prior to Osiris and are not superimposed on its ejecta (not included in **Fig. 2**).

## Summary and Future Work

Osiris represents a prominent impact feature on Ganymede characterized by water ice as a major constituent in its floor and ejecta material [11], resurfacing a large surface area. Taking an AMA of 750 Ma as an upper limit, our results reveal that bright, ice-rich crater rays may remain stable on Ganymede's surface for  $\sim 1$  Ga, comparable to bright rays on, e.g., rocky bodies such as the Moon. Osiris represents a stratigraphic marker horizon which we choose to propose a base for a time-stratigraphic system termed *Osirian*, characterizing a period where erosional processes are not effective enough to completely remove thin deposits such as bright crater rays. Osiris should be envisaged as an important target for detailed observations by the JANUS camera aboard ESA's JUICE Mission [12], involving image coverage at resolutions at least of 400 m/pxl (or better) in four colors, and local hi-res imaging.

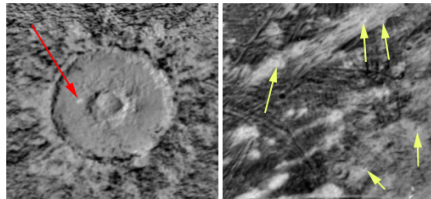


**Figure 1:** Crater floor and continuous ejecta close to the rim of Osiris (*left*), and part of the bright ray system (*right*). *Red arrow*: small post-Osiris crater on its floor. *Yellow arrows*: craters within the bright ray system, most likely pre-dating Osiris.

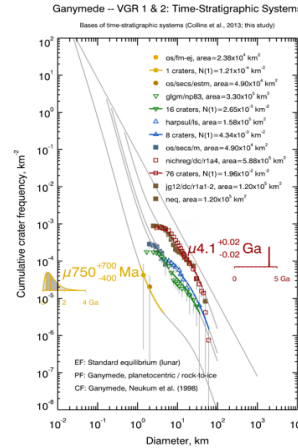


**Figure 2:** Cumulative crater diagram showing Osiris' age (yellow symbols) within the context of Ganymede's time-stratigraphic system (further explanation given in text). Curve shown is the crater production function of Ganymede [9]. The straight line represents an equilibrium distribution, indicating that crater distributions on Ganymede in general are below the saturation limit for craters in the diameter range shown here.

## References

- [1] Wilhelms, D. E., : U. S. G. S. Professional Paper #1348, 302p., 1987. [2] Spudis, P. D. and Guest, J. E.: in F. Vilas, C. R. Chapman, and M. S. Matthews (Eds.), Mercury, Univ. of Arizona Press, Tucson, Az., p. 118-164, 1988. [3] Stephan, K., et al.: Icarus, in press, 19p., 2017. [4] Carr, M. H., et al.: J. Geophys. Res. 100 (E9), 18,935-18,955, 1995. [5] Wagner, R., et al.: LPSC XXX, abstr. #1818, 1999. [6] Collins, G. C., et al.: U. S. G. S. Sci. Inv. Map #3237, 2013. [7] Kneissl, T., et al.: Icarus 277, 187-195, 2016. [8] Michael, G. G., et al.: Icarus 277, 279-285, 2016. [9] Neukum, G., et al.: LPSC XXIX, abstr. #1742, 1998. [10] Zahnle, K., et al.: Icarus 163, 263-289, 2003. [11] Stephan, K.: FU Berlin, Online Dissertations, [http://www.diss.fu-berlin.de/diss/receive/FUDISS\\_thesis\\_000000002224](http://www.diss.fu-berlin.de/diss/receive/FUDISS_thesis_000000002224), 2006. [12] Della Corte, V., et al., Proc. SPIE 9143, doi:10.1117/2056353.



## Core-ocean-ice exchange processes in Europa, Ganymede and Callisto

**Gabriel Tobie** (1), Ludvine Harel (1), Klara Kalousova (2), Jakub Kverka (2), Marie Behounekova (2), Olivier Bollengier (3), Michael Brown (3), Ondrej Cadek (2), Gaël Choblet (1), Caroline Dumoulin (1), Olivier Grasset (4), Baptiste Journaux (3), Frank Postberg (5), Christophe Sotin (6), Ondrej Soucek (7) and Steve Vance (6).

(1) Laboratoire de Planétologie et Géodynamique, Université de Nantes, UMR-CNRS 6112; (2) Charles University, Faculty of Mathematics and Physics, Department of Geophysics, Praha, Czech Republic; (3) Earth and Space Sciences, University of Washington, Seattle, United States; (4) Présidence, University of Nantes, France; (5) Institut für Geowissenschaften, Universität Heidelberg, Germany; (6) Jet Propulsion Laboratory, Caltech, Pasadena, USA; (7) Charles University, Mathematical Institute, Praha, Czech Republic.

(gabriel.tobie@univ-nantes.fr)

Magnetic data gathered by the Galileo spacecraft [1, 2] along with the observations of time-varying auroral emissions [3] provide evidences for deep salty water oceans within Jupiter's moons, Europa, Ganymede and Callisto. However, the composition and the depth of these internal oceans remain very poorly constrained. Identifications of magnesium-bearing and sodium-bearing salts at the surface of Europa [4] provides some indications about the possible oceanic composition. For Ganymede and Callisto, unfortunately, no compositional clues exist yet. The thickness of the outer ice shell is also unconstrained. Based on thermal evolution models, Europa's ice shell thickness is estimated between 10 to 40 km, while Ganymede and Callisto may have an ice shell as thick as 100 km. Due to their large volume of H<sub>2</sub>O compared to Europa, Ganymede and Callisto are expected to have a high-pressure ice mantle separating the ocean base from the rock core. However, the thickness of this high-pressure mantle remains unconstrained. Future geophysical and compositional measurements by the NASA Europa Clipper mission [6] and the ESA JUpiter ICy moon Explorer (JUICE) mission [5] will provide crucial constraints on the hydrosphere structure, the ocean composition and the deep interior structure of these bodies [7].

In preparation of the future measurements, we model the possible present-day internal structure of these three icy ocean worlds and the exchange processes between their internal layers. A first step is to develop structural models consistent with available experimental and geophysical constraints. In order to predict accurately the density profile and the ice-ocean interfaces, we use a thermodynamical representation

based on local basis functions [8]. Different oceanic compositions are considered in order to test their influence on the hydrosphere structure and the potential signature of oceanic composition in the future geophysical measurements. For the moment, only the global shape and the degree-two component of the static gravity field are known, with significant uncertainties. Future measurements will give access to both gravity and topography data at much higher degree together with time variations due to tides. First estimates based on NaCl and MgSO<sub>4</sub> oceanic compositions [7] indicate that tidal fluctuations are sensitive to the oceanic composition in addition to ice shell thickness. Similar to the approach developed for the interpretation of Cassini data at Titan [9, 10], the joint interpretation of gravimetric and altimetric data may provide constraints on ice shell thickness variations, providing indirect informations on the thermal state of the ice shell and on heat flux anomalies at the ocean-ice interface. New models of ice shell dynamics including composite rheology are developed in order to better characterize the thermal structure of the outer ice shell and the efficiency of heat transfer from the ocean to the surface.

The present-day structure and composition of the ice-covered ocean worlds results from a complex interplay between heat production and transfer, water-rock interactions, and melting/crystallization processes. Since their formation, each moon has followed a unique evolutionary path, characterized by various degree of rock-water-ice interactions. For Ganymede and Callisto, massive water-rock interactions may have occurred during their differentiation stage, while on Europa direct contact between the



ocean and the rock core promotes efficient water-rock interactions all along its history. However, using 2D and 3D numerical simulations of thermal convection in the high-pressure ice mantle [11, 12], we show that efficient transport of volatiles and salts from the rock core to the ocean may have also occurred in Ganymede, at least in the past, and possibly in Callisto. The ocean crystallization/melting varies as a function of time depending on the heat production mostly due to radiogenic and tidal heating and on the efficiency of heat release to space. Tidal heating, which is a main driver of Europa's evolution, is likely negligible at present on Ganymede, but could have played a role in the past. Based on models, the present-day tidal dissipation at present in Europa is expected to be larger than the radiogenic heating and may have been even larger in the past depending on its orbital evolution, which is intimately linked to Io and Ganymede through the Laplace resonance. Therefore, understanding the evolution of these icy ocean worlds requires a simultaneous description of their evolution and their tidal interactions. A detailed model incorporating these various processes and their coupling is under development. The ultimate goal is to provide a theoretical framework to interpret the future data and to assess their implications in terms of thermal history and habitability of these icy ocean worlds.

**Acknowledgements** The research leading to these results received financial support from the CNRS-INSU PNP program, the ANR OASIS project, and from CNES for the Europa Clipper and JUICE project. Work by CS and SDV was partially supported by the Jet Propulsion Laboratory, Caltech, and by the "Icy Worlds" and "Titan and Beyond" nodes of NASA's Astrobiology Institute (13-13NAI7-2-0024 and 17-NAI8-2-0017).

## References

- [1] Khurana, K. K. et al. *Nature*, 397, 777-780 (1998)
- [2] Kivelson, M. G. et al. *Icarus*, 157, 507-522, (2002).
- [3] Saur, J. et al. *J. Geophys. Res.*, 120, 1715-1737 (2015).
- [4] Ligier, N. et al. *Astrophys. J.* 151:163 (2016).
- [5] Grasset, O. et al. *Planet. Space Sci.*, 78, 1-21 (2013).
- [6] Europa Study Team, JPL Internal Document D -71990 (2012).
- [7] Vance, S. D. et al. *J. Geophys. Res.*, 123, 180-205 (2017)
- [8] Brown, J. M., *Fluid Phase Equilibria*, 463, 18-31 (2018).
- [9] Lefevre, A. et al. *Icarus*, 237, 16-28 (2014).
- [10] Kverka, J. et al. *Icarus*, in press (2018).
- [11] Choblet, G. et al. *Icarus*, 285, 252-262 (2017).
- [12] Kalousova, K. et al. 299, 133-147 (2018).

# The Ganymede Laser Altimeter (GALA) for ESA's Jupiter Icy Moons Explorer (JUICE) Mission

Hauke Hussmann (1), Kay Lingenauber (1), Reinald Kallenbach (1), Jürgen Oberst (1), Keigo Enya (2), Masanori Kobayashi (3), Noriyuki Namiki (4), Jun Kimura (5), Nicolas Thomas (6), Luisa Lara (7), Gregor Steinbrügge (1,8), Alexander Stark (1), Christian Hüttig (1), Fabian Lüdicke (1), Horst-Georg Lötze (1), Thomas Behnke (1), Christian Althaus (1), Simone Del Togo (1), Belinda Wendler (1), Harald Michaelis (1)

(1) DLR Institute of Planetary Research, Rutherfordstr. 2, 12489 Berlin, Germany ([hauke.hussmann@dlr.de](mailto:hauke.hussmann@dlr.de)), (2) ISAS/JAXA, (3) Chiba Institute of Technology, Japan, (4) National Astronomical Observatory of Japan, (5) Osaka University Japan, (6) Physikalisches Institut, University of Bern (UBE), Sidlerstrasse 5, 3012 Bern Switzerland, (7) CSIC, Instituto de Astrofísica de Andalucía (IAA), Glorieta de la Astronomía s/n, 18008 Granada, Spain, (8) Institute for Geophysics, University of Texas at Austin, Austin, TX, USA

## Abstract

The Ganymede Laser Altimeter (GALA) is one of ten instruments selected for ESA's Jupiter Icy Moons Explorer (JUICE) mission. The scientific goals of the GALA instrument cover a wide range of questions in the areas of geology, geophysics and geodesy of the icy satellites of Jupiter, Ganymede, Europa and Callisto. Here we will present an overview on the scientific goals as well as on the status of the instrument development, operational concepts and the current performance analysis.

## 1. Introduction

In 2013 ESA selected the Jupiter Icy Moons Explorer (JUICE) as the first L-class mission within the Cosmic Vision Program. This mission will explore Jupiter, its magnetosphere and satellites first in orbit around Jupiter before going finally into polar orbit around Ganymede the largest of the Galilean moons [1]. Ganymede is a typical icy moon containing mainly H<sub>2</sub>O ice at the surface and about up to 40% H<sub>2</sub>O by mass in its interior. Ganymede is unique in having an intrinsic magnetic dipole field and the satellite has undergone phases of intense geological activity during its evolution. This is most evident in the so-called bright terrain characterized by extension and tectonism covering roughly two thirds of the surface. The bright terrain is distinct from the heavily cratered and older dark terrain. The Ganymede Laser Altimeter (GALA) is one of ten payloads onboard the spacecraft and is developed under responsibility of the DLR Institute of Planetary Research in collaboration with industry and institutes from

Germany, Japan, Switzerland and Spain. Its major objectives are to measure the surface topography and the tidal deformation of the satellite.

## 2. The JUICE Mission

JUICE will be the first orbiter around a moon (other than Earth's moon) in solar system exploration. Its launch is currently planned for June 2022 followed by an interplanetary cruise of 7.6 years. Jupiter orbit insertion will take place by the end of 2029. The spacecraft will perform a 3-years Jupiter-orbiting tour including two flybys of Europa at 400 km altitude and multiple flybys at Ganymede and Callisto with a minimum altitude of 200 km. Finally, JUICE will enter into a near-polar orbit around Ganymede. After Ganymede orbit insertion the initial highly elliptical orbit will naturally evolve into a 5000-km circular orbit followed again by a highly elliptical (500 x 10,000 km) phase due to perturbations by Jupiter. During one of the pericenter passages an orbit maneuver will bring the spacecraft into a 500-km circular orbit in which it will be staying for at least 132 days until end of nominal mission. The latter phase will be the main period for GALA taking data. In addition data will be taken at Europa, Ganymede, and Callisto at closest approaches of flybys in the Jupiter orbiting phase.

## 3. GALA Science

GALA has two main objectives: (1) by range measurements it shall obtain Ganymede's topography on global, regional and local scales. This will reveal how surface features have formed and how they are

connected with the shallow interior ice shell. Global shape measurements will tell us whether the satellite is in hydrostatic state with respect to rotational and tidal forces. (2) Obtaining range measurements distributed in time along the orbital cycle, tidal variations of surface elevations will be measured. The tidal amplitudes are indicative for the presence of a subsurface ocean and would (together with complementary measurements) constrain the ice-I shell thickness [2]. In addition, GALA will provide surface roughness maps on global, regional and local scales that will be set into context with the geological surface record. With GALA the orientation of the polar axis can be determined and rotational models, including possible longitudinal librations, will be improved. GALA will use a digital filter but will also be capable of transmitting digitized return signals. With the latter, a better separation of albedo, surface roughness and local slopes can be expected. An important objective is to relate the surface roughness to different terrain types on Ganymede. To characterize surface roughness at Ganymede laser footprints of 50 m and high shot frequencies will be used in the Ganymede orbit phases. Analysis of the digitized sample of the return pulse by GALA provides the data-sets for surface roughness. Furthermore, surface roughness measurements will be used to characterize possible landing sites for future landers. A laser altimeter can obtain data on surface albedo at the corresponding laser wavelength, in this case 1064 nm. The icy satellites all show high reflectivities in the 1-micron range. As the altimeter carries its own light source, the albedo measurements do not depend on corrections of photometric (illumination) effects. Hence, more controlled measurements of albedo –though restricted to the narrow bandwidth of the laser– are possible. Laser altimeter observations become particularly important in areas of permanent shadow, where camera observations are not at all possible. Such measurements will complement the data sets from the near-infrared spectrometers. Correlation of albedo with geological units and the relation to Ganymede's magnetic field and interaction with the Jovian magnetosphere will be searched for.

## 4. The Instrument

GALA is a single-beam altimeter: a laser pulse (at 1064 nm wavelength) is emitted by using an actively Q-switched Nd:YAG laser firing at 30 Hz in nominal

operation. A small fraction of the pulse is guided through fiber optics onto the detector characterizing the outgoing pulse and time of emission. After about 3 msec (assuming 500 km altitude) the Lambertian reflection of the pulse from the surface of Ganymede is received by a 26-cm aperture telescope and transferred to the detector, an Avalanche Photo Diode (APD). The signal is digitized at a sampling rate of 200 MHz and transferred to the range finder module, which determines (a) the time of flight between the emission and receiving of the pulse (b) the pulse shape, in particular the pulse-width, and (c) the energy of the received pulse. From the time of flight of the wave-package and the spacecraft position and attitude, the distance for each shot can be converted into height above a reference surface in post-processing of the data. The pulse-width is a measure of the surface roughness and slope at the scale of the laser footprint (50 m diameter at 500 km altitude orbit). An estimate of the albedo is obtained by comparing the energy of the emitted pulse with the one of the received pulse. Here we will report on the overall status of the technical development of GALA.

## References

- [1] Grasset, O. and 17 colleagues (2013), JUpiter ICy moons Explorer (JUICE): an ESA mission to orbit Ganymede and to characterise the Jupiter system, *Planet. Space Sci.*, 78, 1-21.
- [2] Steinbrügge, G., A. Stark, H. Hussmann, F. Sohl, and J. Oberst (2015), Measuring tidal deformations by laser altimetry. A performance model for the Ganymede Laser Altimeter, *Planet. Space Sci.*, 117, 184-191.

# Modeling the Interior Evolution of Water-Rich Bodies: From Dust Aggregates to Ocean Worlds

**Wladimir Neumann**<sup>1,2</sup>, <sup>1</sup>Institute of Planetology, University of Münster (wladimir.neumann@dlr.de), <sup>2</sup>German Aerospace Center, Institute of Planetary Research, Berlin

## Abstract

The properties and structures of small planetary bodies are greatly diverse. These objects can be subdivided into rocky asteroids with ordinary chondritic bulk composition and icy bodies that have a substantial amount of water (carbonaceous chondritic objects, dwarf planet (1) Ceres, icy satellites). The water is either bound in minerals, or is available as a free phase within the planetesimal. Several thermal evolution models for ice-silicate planetesimals were developed and applied to the dwarf planet Ceres (assuming both a CI/CM chondrite-like composition without free water and a water-rock composition with a free water phase), to ice-silicate planetesimals in general, and to Enceladus, the sixth-largest moon of Saturn. A review of the results of these models, the implications for planetesimals in general as well as for some prominent bodies will be presented.

## 1. Introduction

Small bodies are potential proxies for the building blocks of the Earth. Most of them are clustered in belts, but some of them move on distinct orbits (e.g. NEAs, comets) or are satellites (icy moons). Small bodies cover a spectrum of compositions in terms of H<sub>2</sub>O content, ranging from dry objects (Vesta) to those that contain a high H<sub>2</sub>O fraction in a distinct layer (Ceres, Enceladus). Both types (e.g. Vesta, Ceres) are found in the asteroid belt; bodies of the second type are also found in the outer solar system (e.g. Enceladus, Charon).

Large variation of their surface properties is observed, ranging from dry, basaltic surfaces produced by igneous processes, over primordial ones, to surfaces characterized by water bearing minerals (Ceres) or silicates that are low in iron and water (Pallas). There is geochemical evidence for silicate melting and even magma oceans (Vesta, Lutetia) on some small bodies, and for ice melting and water-rock differentiation on the others (e.g., Ceres, Enceladus). To understand the formation and evolution of the planets it is essential to know by which mechanism, how, and when this diversity

emerged. The insights gained from the interior evolution models for small bodies bring planetary science closer to the understanding of the evolution of the Solar System as a whole and of the planets in particular.

Here, an overview over some recent modeling results and the implications for icy planetesimals in general as well as for some prominent bodies (e.g. Ceres, Enceladus, Charon) will be presented.

## 2. Model

Several numerical models for rocky and icy planetesimals and planetary embryos were developed previously<sup>[1-5]</sup> in order to study the formation and evolution of asteroids, moons and dwarf planets. The models consider processes relevant for the interior evolution of small icy objects, such as accretion, accretional heating, closure of the dust porosity, melting of ice, water-rock separation by matrix compaction, and convection (solid/liquid-state ice/water convection and hydrothermal circulation). The investigations performed using these models provide constraints on the timing and duration of the formation of rocky core and icy mantle, as well as the present-day state of icy bodies. The scientific goal is to find likely evolution scenarios and interior structures of such objects depending on their composition, formation time, and accretion duration, and to reproduce features observed by space missions.

## 3. Selected Results

Specific objects of the very diverse set of icy bodies that were observed by space missions are the dwarf planet Ceres, the icy moon Enceladus and various KBOs (e.g. Charon). The water-rock separation on Ceres and the stability of the crust, as well as the hypothesized present-day porosity in Enceladus' core were investigated by calculating the thermal evolution and the differentiation of these bodies. Calculations that assume a free H<sub>2</sub>O fraction of  $\approx 25$  vol% in the initially homogeneous interior for Ceres produce a partially differentiated structure with a more dense undifferentiated ice-silicate crust at top of

a less dense (possibly “muddy”) H<sub>2</sub>O layer and a silicate core (Fig. 1). Such potentially gravitationally unstable configuration can develop further by subduction and overturn, attended by mixing of the crustal material with the H<sub>2</sub>O layer. However, a stiff crust with a viscosity that is higher than the “critical” viscosity for the development of the Rayleigh-Taylor instabilities will not overturn and remain stable on a geological timescale.

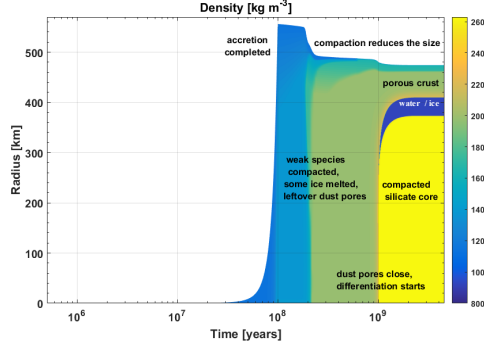


**Figure 1.** Evolution of the density assuming accretion of Ceres in the Kuiper belt within 100 Ma and migration into the asteroid belt after the late heavy bombardment. Due to the sluggish compaction of the rock, water separates very slowly on a time scale of several hundred Ma. The differentiation is not completed because a porous undifferentiated crust is retained. Free water is present in the ocean, while in the undifferentiated crust and in the porous outer core interaction between the liquid water and the rock results in aqueous alteration if the precursor material contained dry silicates.

The evolution of the viscosity at the base of the crust and of the critical viscosity for the stability of the crust (Fig. 2) implies that in case that Ceres retained a largely undifferentiated crust in the course of the water-rock separation in the interior, this crust could have remained stable as a separate layer until present.

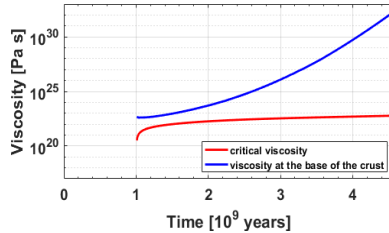


**Figure 2.** Crust Stability: Comparison of the viscosity at the base of the undifferentiated crust with the critical viscosity for the body from Fig. 1 indicates survival of the crust if Ceres formed late.

A much higher H<sub>2</sub>O fraction of > 45 vol% suggested for Enceladus implies a rapid water-rock separation after the onset of ice melting. Rock particles that settle by Stokes flow in a liquid layer form a grain agglomerate with water-filled pores. Calculations of core compaction for different core compositions (dry/wet olivine, antigorite) indicate that a porous layer can be retained for a suitable choice of

parameters for both dry and wet olivine rheologies. By contrast, if the core material is dominated by antigorite, the compaction is efficient and no porosity remains for any reasonable choice of parameters. Figure 3 shows porosity profiles for a core with a wet olivine rheology obtained for several successful models that produced a porous outer core layer.

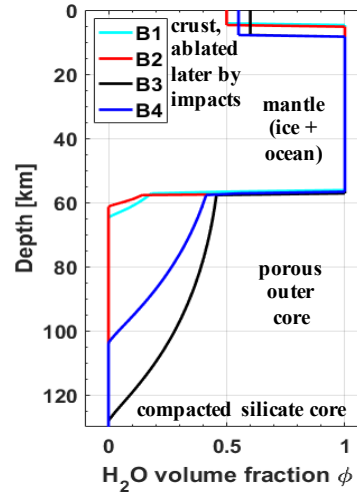


**Figure 3.** Final porosity profiles in the outer 130 km of Enceladus after differentiation and compaction assuming “wet” olivine rock rheology. Models B1-B4 correspond to different values of parameters (accretion time, H<sub>2</sub>O fraction, creep activation energy, grain size, water fugacity) and they result in a different thickness of the porous layer.

## 4. Summary and Conclusions

The initial amount of ice is the main criterion that determines the mechanism and the timing of the differentiation of small icy planetesimals (quasi-instantaneous or not). If the ice fraction is small and differentiation occurs slowly in the matrix compaction regime, the composition of the rock determines the timing of the differentiation and the stability of the crust. This is initially not the case for a high ice fraction. However, when a rocky core forms the structural evolution is highly dependent on the compaction rate, and, thus, on the composition of the core.

A highly viscous rock component can extend the time of the differentiation of Ceres to up to  $\approx 1$  Ga and ensure crust stability on this time scale. In the case of Enceladus, modeling confirms the conjecture of a porous core for an olivine-like core composition, but not for a core that is dominated by antigorite.

## References

- [1] Kruse, A. (2016) Bachelor thesis, University of Potsdam. [2] Neumann, W. et al. (2014) EPSL 395, 267-280. [3] Neumann, W. et al. (2015) A&A 584, A117, 16pp. [4] Neumann, W., et al. (2016) Joint 48<sup>th</sup> DPS and 11<sup>th</sup> EPSC, Pasadena, USA. [5] Neumann, W. et al. (2018) JGR 123.

# Report on JUICE 3GM gravity experiment performance

**P. Cappuccio**, M. Di Benedetto, G. Cascioli and L. Iess

University La Sapienza of Rome, Department of Mechanical and Aerospace Engineering, Italy, Rome, Via Eudossiana 18  
(paolo.cappuccio@uniroma1.it)

## Abstract

The ESA's JUICE mission will provide a multi-disciplinary investigation of Jupiter and its Galilean moons through a suite of eleven different experiments. JUICE will perform 2 Europa flybys, more than 10 Callisto flybys, and will orbit about Ganymede in the last 9 months of the mission. The 3GM (Geodesy and Geophysics of Jupiter and the Galilean Moons) experiment will use accurate Doppler and range measurements to infer the moons' internal structure by measuring their gravity field and, for Ganymede and Callisto, their tidal Love number  $k_2$ . This work presents the attainable 3GM gravity experiment performances with the latest trajectory kernels and the High Accuracy Accelerometer (HAA) to remove the dynamical noise induced by propellant sloshing.

## 1. Introduction

JUICE -Jupiter ICy moons Explorer- is an ESA L-class mission devoted to study the Jovian system. The nominal launch date is in September 2022, with arrival at Jupiter foreseen in July 2029.

After the JOI maneuver, JUICE will use multiple gravity assists of the Galilean satellites to shape a comprehensive orbital tour over 3.5 years. The mission includes Europa, Callisto and Ganymede flybys and it will culminate in a dedicated, nine-month orbital phase around Ganymede. It consists of a 5 months elliptical phase, with a periapsis at about 1000 km and an apoapsis at about 10000 km, and a final circular orbit phase at an altitude of 500 km (named Ganymede Circular Orbit - GCO500). This will be the first time that a moon beyond our own will be orbited by a spacecraft [1].

The 3GM experiment is one of the eleven investigations that JUICE will perform (one has no HW onboard as it will rely on ground-based observations). The 3GM gravity experiment performances are addressed in this work. In particular, we investigate one of the 3GM main scientific goals, namely the determination of Galilean moons' gravity

fields and the spacecraft orbital accuracy relative to those moons. The latter goal is important to provide a precise reference to the onboard laser altimeter.

## 2. 3GM instruments

The KaT is the core of the gravity experiment, providing a two-way coherent Ka/Ka link supporting range and range-rate data as accurate as 20 cm (two-way) and  $3 \mu\text{m/s}$  @ 1000s integration time. Radio metric measurements will enable a precise orbit determination of the JUICE spacecraft and the estimation of Europa, Ganymede and Callisto's gravity fields. Such accuracies are attainable thanks to the simultaneous use of the KaT and the onboard DST (Deep Space Transponder) providing the two additional X/X and X/Ka links. Such multi-frequency scheme will allow a nearly complete calibration of the dispersive plasma noise, while the use of advanced Microwave Radiometers (MWRs) on ground will allow the calibration of the non-dispersive tropospheric noise. This corresponds to an expected end-to-end link frequency stability at an Allan Deviation of  $\sim 10^{-14}$ . The high accuracy radio link will permit also an improvement of the solar system ephemerides thanks to the 24 Mcps PN ranging system. It will guarantee a 20 cm two-way accuracy after 10 s integration time.

All the three ESTRACK stations (New Norcia, Cebreros, Malargüe) are considered capable of Ka-band uplink at the time of the experiment; thus, radio tracking data are simulated from all of them, without permitting overlapping in time.

In addition to that, 3GM will make use also of data from the onboard HAA to calibrate out the non-gravitational disturbances, mainly due the propellant sloshing. The HAA selected for JUICE is identical in design to the Italian Spring Accelerometer (ISA) already mounted onboard the ESA's BepiColombo mission.



3GM science package comprises another instrument, the Ultra Stable Oscillator (USO), which will be used to carry out an occultation experiment.

### 3. 3GM gravity experiment

JUICE will perform only 2 Europa flybys that will allow the independent estimation of the  $J_2$  and  $C_{22}$  gravity parameters, which are sufficient to test the hydrostatic equilibrium hypothesis ( $J_2/C_{22} = 10/3$ ). The 12 Callisto flybys will provide enough data to infer its gravity field at least up to degree and order 3. Concerning Ganymede only the circular phase at 500 km altitude will be considered for the gravity experiment. It will allow the estimation of the  $10 \times 10$  (or higher) gravity field and rotation parameters. Measurements of Callisto and Ganymede gravity fields at different moons mean anomalies will allow also the estimation of the tidal Love number  $k_2$ , this parameter will let us to infer the presence or absence of a liquid ocean under the superficial icy shell. The estimation of the complex  $k_2$  will allow not only to prove (or disprove) the presence of an internal ocean, but also to measure the tidal phase lag and ice viscosity.

Preliminary simulations carried out by 3GM team with the initial baseline trajectory envisioned in the JUICE Announcement of Opportunity (AO) showed an attainable accuracy of 0.06 for Callisto  $k_2$  Love number, and for Ganymede an accuracy of about  $10^{-3}$  for the complex  $k_2$  [2]. However, because of some stringent mass constraints reducing the available propellant onboard the spacecraft, the number of Callisto flybys has decreased from 20 to 12 while the old GCO200 phase is no more baselined, turning out into an extended GCO500. Therefore, this work does not consider a GCO200 phase, also if there are good chances to recover it in the future. The accuracy at which it is possible to compute Callisto's  $k_2$  is the main concern because of the reduced amount of data available. An additional concern comes from the dynamical stability of the platform, which is subject to unpredictable accelerations due to propellant sloshing during flybys.

### 4. Conclusions

The estimation of the accuracies at which is possible to recover the gravity fields of Europa, Callisto and Ganymede, and the orbit of the spacecraft relative to those moons are investigated in this work. The estimation of these parameters is obtained from refined simulations of 3GM gravity experiment,

taking into account the latest available JUICE baseline trajectory (141a of the CReMA 3.2) and the inclusion of the HAA data into the orbit determination software.

### Acknowledgements

This research was carried out at the Radio Science Laboratory of Sapienza University of Rome under the sponsorship of the Italian Space Agency.

### References

- [1] A. Boutonnet and G. Varga, *JUICE - Jupiter Icy moons Explorer Consolidated Report on Mission Analysis (CReMA)*, JUI-ESOC-MOC-RP-001, Issue 3, Revision 2, 25/04/2017
- [2] M. Parisi, L. Iess and S. Finocchiaro, *The gravity fields of Ganymede, Callisto and Europa: how well can JUICE do?*, EGU General Assembly, 2014

## The effect of Ganymede's exosphere on JUICE's determination of the moon's gravity field

A. Hickey (1), D. Durante (1), L. Iess (1), C. Plainaki (2), A. Mura (3), A. Milillo (3)

(1) Sapienza University of Rome, Department of Mechanical and Aerospace Engineering, Rome, Italy  
([anne.hickey@uniroma1.it](mailto:anne.hickey@uniroma1.it))

(2) ASI – Italian Space Agency, Rome, Italy

(3) INAF-IAPS, Rome, Italy

### Abstract

ESA's Jupiter ICy moons Explorer (JUICE) is planned to be launched in 2022 with arrival at Jupiter in 2029. The spacecraft will spend approximately 3 years observing the Jupiter System, performing flybys of the moons, ending the mission with a tour around Ganymede, the largest moon in our solar system.

One of the instruments on board the JUICE spacecraft is the 3GM experiment, devoted to revealing the moons' gravity fields. An orbit determination code will use Doppler measurements to determine a spacecraft's position, velocity and dynamical model parameters that affect the spacecraft's trajectory, including gravity field coefficients which relate to the interior structure of a planetary body. Additionally, a spacecraft experiences the effect of drag in the presence of an atmosphere/exosphere.

Ganymede's exosphere consists of  $O_2$  and  $H_2O$  which is generated by ongoing processes of sputtering, sublimation and radiolysis on the moon's icy surface. This generation of the exosphere is complicated by the fact that Ganymede has its own magnetic field which is imbedded within Jupiter's magnetosphere and results in preferred regions of ion precipitation on the moon's surface. Recently, a model of this complex interaction has been developed [1].

This work aims to incorporate this exospheric model for Ganymede in our orbit determination code, in order to simulate and assess the effect experienced by JUICE during the final phase around Ganymede and

to determine the feasibility of using an onboard accelerometer to calibrate and estimate this effect.

### Acknowledgements

This research was carried out under the sponsorship of the Italian Space Agency.

### References

- [1] Plainaki, C., Milillo, A., Massetti, S., Mura, A., Jia, X., Orsini, S., Mangano, V., De Angelis, E. and Rispoli, R. (2015). *The  $H_2O$  and  $O_2$  exospheres of Ganymede: The result of a complex interaction between the jovian magnetospheric ions and the icy moon*. Icarus, 245, pp.306-319.

# Macromolecular organic compounds emerging from the Enceladus ocean

**Frank Postberg**<sup>1,6</sup>, Nozair Khawaja<sup>1</sup>, Christopher R. Glein<sup>2</sup>, Hsiang-Wen Hsu<sup>3</sup>, Sascha Kempf<sup>3</sup>, Fabian Klenner<sup>1</sup>, Lenz Nölle<sup>1</sup>, Juergen Schmidt<sup>4</sup>, Gabriel Tobie<sup>5</sup>, J. Hunter Waite<sup>2</sup>

<sup>1</sup> University of Heidelberg, Heidelberg, Germany, <sup>2</sup> Southwest Research Institute, San Antonio, Texas, United States, <sup>3</sup> University of Colorado at Boulder, Boulder, Colorado, United States, <sup>4</sup> University of Oulu, Oulu, Finland, <sup>5</sup> University of Nantes, Nantes, France, <sup>6</sup> Freie Universität, Berlin, Germany

## Abstract

We present the detection of macromolecular organic compounds in ice grains ejected by Enceladus plume into Saturn's E ring. The evaluation is based on data obtained by Cassini's Cosmic Dust Analyser (CDA) and the Ion and Neutral mass spectrometer (INMS). We infer key properties of the macromolecules and link these to possible subsurface processes in the ocean of Enceladus and its hydrothermally active rock core.

## 1. Introduction

Saturn's icy moon Enceladus harbors a global subsurface ocean, which is thickest (50 km) below the south polar region. There, through warm fractures in the less than 5 km thick ice crust [1,2], jets of vapor and nanometer to micrometer-sized ice grains emerge from the ocean into space. Two mass spectrometers aboard the Cassini spacecraft frequently carried out compositional in situ measurements of material emerging from the subsurface of Enceladus. These measurements were made inside both the plume and the E ring. The Cosmic Dust Analyser (CDA) showed that a large fraction of the ice grains are direct samples of subsurface alkaline ocean water with mild salinity [3,4].

The CDA also uncovered the first evidence of hydrothermal activity taking place at the interface of the moon's rocky core and its ocean [5]. The detection of molecular hydrogen in the plume by the Ion and Neutral Mass Spectrometer (INMS) provided further support for fluid-rock interactions, most consistent with exothermic serpentinization reactions [6], similar to certain alkaline hydrothermal systems

of Earth's oceans, such as Lost City in the Atlantic Ocean. Because of the relatively low density (2500 kg/m<sup>3</sup>) of the moon's core it is likely porous and percolated by ocean water [7]. Hydrothermal reactions thus probably take place deep inside the core and are likely powered by tidal dissipation [8].

## 2. Results

Previous CDA and INMS measurements showed that the plume emits organic material of low molecular weight both, in the gas phase and in about 25% of the ice grains, so-called Type 2 grains [3,9] but complex organics emerging from Enceladus oceans have not been reported before. Here we will present spectra of emitted ice grains containing concentrated, macromolecular organic material with molecular masses clearly above 200u. The data provides key constraints on the macromolecular structure and is suggestive of thin a organic-rich film on top of the oceanic water table [10]. We suggest that it originates from Enceladus' rocky core and might be a product of hydrothermal rock/water interaction.

Furthermore, we suggest a large-scale ocean convection mechanism that, together with bubbles of volatile gases, transports these and other materials from the moon's core up to the ocean surface. There, organic nucleation cores - generated by bubble bursting and subsequently coated with ice from vapour freezing - are ejected into space [10]. This mechanism shows similarities to the formation of ice clouds from sea spray on Earth [11] and allows probing of Enceladus' organic inventory in drastically enhanced concentrations.

## References

- [1] Čadež, O. et al. Enceladus's internal ocean and ice shell constrained from Cassini gravity, shape, and libration data. *Geophysical Research Lett.* 43, Issue 11, 5653-5660 (2016)
- [2] Le Gall, A. et al. Thermally anomalous features in the subsurface of Enceladus's south polar terrain. *Nat. Astron.* 1, 0063 (2017).
- [3] Postberg, F. et al. Sodium salts in E-ring ice grains from an ocean below the surface of Enceladus. *Nature* 459, 1098–1101 (2009)
- [4] Postberg, F., Schmidt, J., Hillier, J., Kempf, S. & Srama, R. A salt-water reservoir as the source of a compositionally stratified plume on Enceladus. *Nature* 474, 620–622 (2011)
- [5] Hsu, S. et al. Ongoing hydrothermal activities within Enceladus. *Nature* 519, 207-210 (2015)
- [6] Waite, Jr J. H. et al. Cassini finds molecular hydrogen in the Enceladus plume: Evidence for hydrothermal processes. *Science* 356, 155-159 (2017)
- [7] Iess, L. et al. The Gravity Field and Interior Structure of Enceladus. *Science* 344, 78-80 (2014)
- [8] Choblet, G. et al. Powering prolonged hydrothermal activity inside Enceladus. *Nature Astronomy* 1, 841 - 847 (2017).
- [9] Postberg, F. et al. The E ring in the vicinity of Enceladus. II. Probing the moon's interior—the composition of E-ring particles. *Icarus* 193, 438–454 (2008)
- [10] Postberg, F. *et al.* Macromolecular organic compounds from the depths of Enceladus. *Nature*, in press (2018)
- [11] Wilson, T. W. et al. A marine biogenic source of atmospheric ice-nucleation particles. *Nature* 525, 234-238 (2015)